

A Thesis Submitted for the Degree of PhD at the University of Warwick

Permanent WRAP URL:

<http://wrap.warwick.ac.uk/87867>

Copyright and reuse:

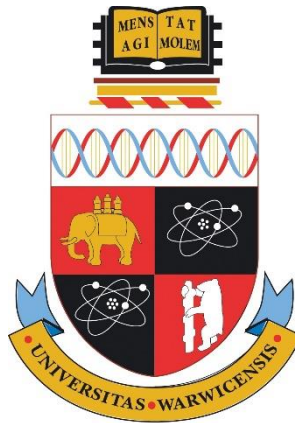
This thesis is made available online and is protected by original copyright.

Please scroll down to view the document itself.

Please refer to the repository record for this item for information to help you to cite it.

Our policy information is available from the repository home page.

For more information, please contact the WRAP Team at: wrap@warwick.ac.uk



A Discrete Model for Patterning of Tensile Fabric Structures

Stuart Gale MEng

Thesis submitted to the University of Warwick
for the degree of Doctor of Philosophy in Engineering

School of Engineering
University of Warwick

May 2016



Table of Contents

Table of Contents	I
List of Figures	VIII
List of Tables.....	XVI
Acknowledgements.....	XVII
Declaration	XVIII
Abstract	XIX
List of Symbols.....	XX
List of Abbreviations.....	XXVI
1 Introduction	1
1.1 Introduction to tensile fabric structures	1
1.1.1 Design process.....	3
1.2 Form-finding.....	4
1.2.1 Minimal surfaces	5
1.3 Patterning.....	5
1.4 Architectural fabrics, types and composition	6
1.4.1 Numerical modelling	8
1.5 Problem statement and scope	9
1.6 Scope, research objectives and contributions	9
1.7 Structure of Thesis	11
1.8 Publications arising from the research.....	12

2	Literature review.....	13
2.1	Patterning.....	13
2.1.1	Mathematical basis of patterning	13
2.1.2	Computational patterning – the 5-step process	14
2.1.3	Subdivision of the membrane	15
2.1.4	Flattening	15
2.1.5	Stress reduction.....	17
2.1.6	Compensating for pre-stress	20
2.1.7	Assembly of cutting patterns	21
2.1.8	Integrated approaches, optimisation and genetic algorithms.....	22
2.1.9	Patterning – research objectives identified	22
2.2	Numerical modelling	24
2.2.1	Behaviour of architectural fabrics.....	24
2.2.2	Continuum models and Finite Elements	28
2.2.2.1	Continuum models	28
2.2.2.2	Implementation by Finite Elements	30
2.2.2.3	Drawbacks of continuum modelling	31
2.2.3	Discrete models.....	32
2.2.3.1	Deformation modes in discrete models.....	34
2.2.4	Numerical modelling for patterning - research objectives identified.....	36
2.3	Summary	37

2.4	Identified gaps in knowledge	38
2.5	Research objectives and consequent direction of this thesis	39
2.6	Research methodology	40
2.7	Contributions to knowledge.....	41
3	Development of discrete element model	42
3.1	Proposed discrete element model	43
3.1.1	Treatment of tensile deformation.....	44
3.1.1.1	Strain calculation	45
3.1.1.2	Stress calculation.....	46
3.1.1.3	Element width calculation.....	47
3.1.1.4	Non-rectangular edge geometries	49
3.1.1.5	Force from stress and width.....	50
3.1.1.6	Forces applied to nodes	50
3.1.2	Treatment of shear deformation	51
3.1.2.1	Remarks on methods of modelling shear in discrete models.....	51
3.1.2.2	Shear strain between elements	53
3.1.2.3	Shear stress	54
3.1.2.4	Shear forces and fabric response	54
3.1.3	Examination of the proposed shear model - shear forces for a simple square	
	56	
3.1.3.1	Calculation of corner forces by treating the patch as a continuum.....	57

3.1.3.2	Calculation of the corner forces using the proposed discrete model.....	59
3.1.3.3	Comparison of approaches	65
3.2	Analysis by Dynamic Relaxation	66
3.2.1	Dynamic relaxation with kinetic damping.....	66
3.2.1.1	Governing equation of motion and iterative procedure.....	66
3.2.1.2	Kinetic damping by identification of kinetic energy peaks	69
3.3	Computational implementation.....	73
3.4	Summary	77
4	Proposed patterning method.....	79
4.1	Method of determining the cutting pattern	80
4.1.1	Subdivision of the form-found membrane shape	81
4.1.2	Flattening	84
4.1.2.1	Geodesic meshing of the 3D panels.....	84
4.1.2.2	Flattening methods	87
4.1.2.3	Flattening by direct projection.....	87
4.1.2.4	Flattening by unrolling with a single spine of elements.....	88
4.1.2.5	Flattening by unrolling with two spines of elements	91
4.1.3	Integrated stress reduction and compensation by dynamic relaxation ...	95
4.2	Proposed method of cutting pattern assembly and evaluation	97
4.2.1	Orthogonal re-meshing of planar panels	98
4.2.1.1	Construction of the orthogonal mesh.....	99

4.2.1.2	Factors affecting the suitability of the orthogonal mesh.....	100
4.2.2	Assembly of orthogonally meshed panels	103
4.2.2.1	Mapping the panels.....	104
4.2.2.2	Joining the panels.....	107
4.2.3	Equilibrium finding of the assembled mesh by dynamic relaxation	110
4.3	Summary	110
5	Application of the method to examples and results.....	113
5.1	Introduction	113
5.2	Flattening, stress reduction and compensation results.....	114
5.2.1	Specification for geometry from Linhard et al. [6].....	114
5.2.1.1	Method used by Linhard et al. [6]	115
5.2.1.2	Patterning conducted by the author.....	115
5.2.2	Stresses incurred through flattening for geometry from Linhard et al. [6].....	116
5.2.2.1	Axial stresses incurred.....	117
5.2.2.2	Shear stresses incurred	120
5.2.2.3	Comparison of flattening methods	122
5.2.3	Residual stresses after stress reduction and compensation for geometry from Linhard et al. [6]	123
5.2.3.1	Residual stresses excluding the shear stiffness of the fabric.....	123
5.2.3.2	Residual stresses including the shear stiffness of the fabric.....	126
5.2.4	Final cutting pattern shapes for the geometry from Linhard et al. [6] ...	131

5.2.4.1	Cutting patterns generated without including the shear stiffness of the fabric	131
5.2.4.2	Cutting patterns generated including the shear stiffness of the fabric	132
5.2.4.3	Comparison of cutting patterns	134
5.2.5	Specification for the geometry from Moncrieff & Topping [4]	135
5.2.5.1	Method used by Moncrieff & Topping [4]	135
5.2.5.2	Patterning conducted by the author	135
5.2.6	Residual stresses after stress reduction and compensation, and final cutting pattern shapes for Moncrieff & Topping [4]	136
5.2.6.1	Residual stresses without including the shear stiffness of the fabric	136
5.2.6.2	Residual stresses including the shear stiffness of the fabric	137
5.2.6.3	Comparison of cutting patterns	139
5.3	Pattern assembly results	139
5.3.1	Comparison with pattern assembly results from Linhard et al. [6]	140
5.3.2	Comparison with pattern assembly results from Moncrieff & Topping [4]	143
5.4	Conditions affecting the analyses of the pattern assembly	146
5.4.1	The effect of including the shear stiffness of the fabric throughout patterning	147
5.4.2	Ill conditioning of shear elements	151
5.4.3	Necessity for the triangulation of the mesh at the boundary	156
5.5	Summary	166
6	Summary, conclusions and future work	168

6.1	Summary of thesis.....	168
6.2	Conclusions	169
6.2.1	Limitations of the work	172
6.3	Future work and implications for engineering practice.....	173
7	References.....	177

List of Figures

Figure 1.1 – Example of a tensile fabric structure. Santa Fe Opera Cantina, California	1
Figure 1.2 - Surfaces with anticlastic and synclastic curvature.....	2
Figure 1.3 – Woven fabric structure	7
Figure 2.1 - Unfolding of a panel to the plane. Note that across the width, the panel is represented by just a single triangular element	16
Figure 2.2 - Reduction of stresses using the structural solution - adapted from Linhard et al. [6]	19
Figure 2.3 - Stress reduction problem formulations, solution methods and the relationship between them.....	20
Figure 2.4 – Distinct vs integrated methods for stress reduction and compensation.....	21
Figure 2.5 - Illustration of shear deformation resulting from the tensioning of a planar net into doubly curved geometry – adapted from Wagner [18].....	28
Figure 2.6 - Numerical models and their relation to base fabric	33
Figure 3.1 – Proposed discrete element mesh, comprising tensile elements, shear elements, and nodes.....	44
Figure 3.2 - Deformation of a single tensile element in 3D space	45
Figure 3.3 - Area of fabric represented by a given element	47
Figure 3.4 – Areas bound by other elements, adjacent to the element for which the width is being calculated	48
Figure 3.5 - Calculation of area by splitting a quadrilateral into four triangles	49
Figure 3.6 - Omission of part of the fabric from the material response, if only half of the area is used to define the width for elements adjacent to non-parallel boundaries.....	49
Figure 3.7 – Relevant areas when calculating width for element A-B	50
Figure 3.8 - Shear forces producing shear strain on quadrilateral piece of fabric.....	52

Figure 3.9 - Shear strain represented as angle change between warp and weft elements	54
Figure 3.10 - Shear forces, resolved shear force, and resistance force for shear deformation in Figure 3.9.....	55
Figure 3.11 - Square of fabric, dimensions $L \times L$, with shear action forces, and corner reactions	57
Figure 3.12 - Equivalent representation with proposed discrete elements	59
Figure 3.13 - Free body diagram of node A.....	60
Figure 3.14 - Free body diagram of node B.....	62
Figure 3.15 - Free body diagram of node C.....	63
Figure 3.16 - Free body diagram of node D.....	64
Figure 3.17 - Trace of kinetic energy around peak.....	70
Figure 3.18 - Screenshot of the discrete element model implemented using VB.Net	74
Figure 3.19 - Pseudocode describing the set up process for running dynamic relaxation	75
Figure 3.20 – Dynamic Relaxation pseudocode	76
Figure 3.21 - Dynamic Relaxation pseudocode continued.....	77
Figure 4.1 (a) - Interpolation of a catenoid shape by revolving a radial line of element edges around the centre axis. The original mesh is shown in green.....	83
Figure 4.1 (b) - Interpolated surface with geodesic seams defined.....	83
Figure 4.1 (c) - Surface split into individual panels, which can now be flattened.....	83
Figure 4.2 - Comparison of different mesh constructions. The red circle indicates the longer elements in mesh (a), not present in mesh (b).....	85
Figure 4.3 - Meshing a panel by constructing geodesics in two directions	86
Figure 4.4- Meshing a panel using geodesics in one direction. These geodesics are then divided into equal segments that dictate the node positions. Elements in the second direction are then interpolated.....	86

Figure 4.5 - Flattening of a panel by direct projection, showing projection of nodes to the plane	88
Figure 4.6 (a) - Definition of the 'spine' of elements on the panel to be flattened	89
Figure 4.6 (b) - Unrolling of the spine of elements to the plane.....	90
Figure 4.6 (c) - Unrolling of the elements (including boundary elements) approximately perpendicular to the spine.....	90
Figure 4.6 (d) - Interpolation of the elements (including boundary elements) approximately parallel to the spine, thus completing the unrolling of the mesh.....	91
Figure 4.7 - Construction of a point C on a surface S that is distance L_1 from a point A and distance L_2 from a point B.....	92
Figure 4.8 (a) - Definition of two spines on the mesh.....	93
Figure 4.8 (b) - Mapping of the spines to the plane.....	94
Figure 4.8 (c) - Mapping of the first line of nodes using the intersection of two circles in the plane	94
Figure 4.8 (d) – Mapping of the next line of nodes using the intersection of two circles in the plane.....	95
Figure 4.9 - Typical restraints for a flattened panel. Nodes in red are restrained in the directions indicated by the arrows. All nodes are additionally restrained perpendicular to the plane of the panel.....	97
Figure 4.10 - Intersection of orthogonal lines with defined cutting panel boundary.....	99
Figure 4.11 - Misrepresentation of boundary due to poor choice of orthogonal grid lines	100
Figure 4.12 - Portions of triangulated and non-triangulated meshes.....	102
Figure 4.13 - Conditions for joining of panels	104
Figure 4.14 (a) - Planar pattern in relation to original 3D panel geometry	105

Figure 4.14 (b) - Re-orientation of 3D panel geometry, and subsequent mapping of boundary nodes (steps 1 & 2).....	105
Figure 4.14 (c) - Rotation and translation of mapped panel to appropriate location in assembled structure (step 3).....	106
Figure 4.15 - Multiple panels arranged appropriately, to allow joining of adjacent panels (due to symmetry one quarter of this structure is sufficient for performing analyses).....	106
Figure 4.16 – Elements along a common edge	108
Figure 4.17 – Elements A-B and C-D become element P-Q	108
Figure 4.18 - Joined mesh representing portion of structure (due to symmetry one quarter of this structure is sufficient for performing analyses)	109
Figure 5.1 – Form-found Catenoid geometry from Linhard et al. [6]	115
Figure 5.2 – Axial stresses incurred by direct projection	117
Figure 5.3 – Axial stresses incurred through unrolling with one spine	118
Figure 5.4 – Axial stresses incurred through unrolling with two spines	118
Figure 5.5 - Gaussian curvature across the panel for the geometry from Linhard et al. [6].....	119
Figure 5.6 – Shear stresses incurred through flattening by direct projection	121
Figure 5.7 - Shear stresses incurred through unrolling with one spine	121
Figure 5.8 – Shear stresses incurred through unrolling with two spines.....	122
Figure 5.9 – Residual stresses after stress reduction and compensation without including the shear stiffness of the fabric, after direct projection flattening.....	124
Figure 5.10 – Residual stresses after stress reduction and compensation without including the shear stiffness of the fabric, after flattening by unrolling with one spine.....	125
Figure 5.11 – Residual stresses after stress reduction and compensation without including the shear stiffness of the fabric, after flattening by unrolling with two spines	125

Figure 5.12 – Residual stresses after stress reduction and compensation, including the shear stiffness of the fabric, after direct projection flattening	127
Figure 5.13 – Residual stresses after stress reduction and compensation, including the shear stiffness of the fabric, after flattening by unrolling with one spine	127
Figure 5.14 – Residual stresses after stress reduction and compensation, including the shear stiffness of the fabric, after flattening by unrolling with two spines.....	128
Figure 5.15 – Residual shear stresses after stress reduction and compensation, including the shear stiffness of the fabric, after flattening by direction projection.....	128
Figure 5.16 – Residual shear stresses after stress reduction and compensation, including the shear stiffness of the fabric, after flattening by unrolling with a single spine.....	129
Figure 5.17 – Residual shear stresses after stress reduction and compensation, including the shear stiffness of the fabric, for flattening by unrolling with two spines	129
Figure 5.18 - Resultant cutting pattern boundaries for each flattening method, after stress reduction and compensation is conducted without shear	132
Figure 5.19 - Resultant cutting pattern boundaries for each flattening method when stress reduction and compensation is conducted with shear.....	133
Figure 5.20 - Comparison of cutting patterns resulting from unrolling with one spine, after stress reduction and compensation is conducted with and without shear	134
Figure 5.21 – Residual stresses after stress reduction and compensation, without including the shear stiffness of the fabric, for the geometry from Moncrieff & Topping [4].....	137
Figure 5.22 – Residual stresses after stress reduction and compensation, including the shear stiffness of the fabric, for the geometry from Moncrieff & Topping [4]	138
Figure 5.23 – Residual shear stresses after stress reduction and compensation, including the shear stiffness of the fabric, for the geometry from Moncrieff & Topping [4].....	138

Figure 5.24 - Comparison of cutting patterns for the geometry from Moncrieff & Topping [4]	139
Figure 5.25 - Plan view of node restraints for the analysis of $\frac{1}{4}$ of the geometry from Linhard et al. [6]	141
Figure 5.26 - Warp stress deviation after assembly of the cutting patterns for the geometry from Linhard et al. [6], without including shear in the analysis	141
Figure 5.27 - Weft stress deviation after assembly of the cutting patterns for the geometry from Linhard et al. [6], without including shear in the analysis	142
Figure 5.28 – Principal stresses after pattern assembly – reproduced from Linhard et al. [6]	142
Figure 5.29 - Warp stress deviation after assembly of the cutting patterns for the geometry from Moncrieff & Topping [4], without including shear in the analysis	144
Figure 5.30 - Weft stress deviation after assembly of the cutting patterns for the geometry from Moncrieff & Topping [4], without including shear in the analysis	145
Figure 5.31 – Stress deviation after pattern assembly – original results from Moncrieff & Topping [4]	145
Figure 5.32 - Warp stress deviation after assembly of the cutting patterns for the geometry from Linhard et al. [6], including shear in the analysis	148
Figure 5.33 - Weft stress deviation after assembly of the cutting patterns for the geometry from Linhard et al. [6], including shear in the analysis	148
Figure 5.34 – Shear stresses after assembly of the cutting patterns for the geometry from Linhard et al. [6], including shear in the analysis	149
Figure 5.35 - Warp stress deviation after assembly of the cutting patterns for the geometry from Moncrieff & Topping [4], including shear in the analysis	151
Figure 5.36 - Weft stress deviation after assembly of the cutting patterns for the geometry from Moncrieff & Topping [4], including shear in the analysis	152

Figure 5.37 – Shear stresses after assembly of the cutting patterns for the geometry from Moncrieff & Topping [4], including shear in the analysis	152
Figure 5.38 - Close up of warp stresses near lower boundary for results shown in Figures 5.35 – 5.37.....	153
Figure 5.39 - Close up of shear stresses near lower boundary for results shown in Figures 5.35 – 5.37.....	154
Figure 5.40 – Differing shear triangle sizes around a node and their effect on the forces apportioned to that node	155
Figure 5.41 - Triangulated and non-triangulated mesh configurations for cutting patterns generated for the geometry from Linhard et al. [6], with shear included in the analysis	157
Figure 5.42 - Warp stress deviation after assembly of a non-triangulated mesh, for the geometry from Linhard et al. [6], including shear in the analysis	158
Figure 5.43 - Weft stress deviation after assembly of a non-triangulated mesh at the seam lines, for the geometry from Linhard et al. [6], including shear in the analysis.....	158
Figure 5.44 - Deviation of the boundary from its expected position, after assembly of a non-triangulated mesh, for the geometry from Linhard et al. [6], including shear in the analysis .	159
Figure 5.45 – Boundary forces after assembly of the triangulated mesh, for the geometry from Linhard et al. [6], including shear in the analysis.....	160
Figure 5.46 – Boundary forces after assembly of the non-triangulated mesh, for the geometry from Linhard et al. [6], including shear in the analysis	161
Figure 5.47 – Gross shear deformations after assembly of the non-triangulated mesh, for the geometry from Linhard et al. [6], including shear in the analysis.....	164
Figure 5.48 – Shear stresses after assembly of the triangulated mesh, for the geometry from Linhard et al. [6], including shear in the analysis.....	165

Figure 5.49 - Restriction of node movement due to connectivity of elements, and resulting control of shear deformations 166

Figure 6.1 - 3D form-found panel with two different meshes – (a) current, rectilinear mesh, (b) suggested, non-rectilinear mesh..... 175

List of Tables

Table 1.1 – PVC coated polyester fabric classifications and relevant material properties – adapted from [12] (originally [13,14])..... 8

Table 1.2 - PTFE coated glass fabric classifications and relevant material properties – adapted from [12] (originally [13,14])..... 8

Table 5.1 – Maximum and minimum incurred stresses for all flattening methods..... 122

Acknowledgements

I would like to express gratitude to a number of people who have made this thesis possible.

I would first and foremost like to thank my supervisor, Professor Wanda J Lewis, for her enthusiasm, patience and guidance over the last four years.

Secondly I would like to thank Dr Thomas Li and Peter Debney of Arup, whose insights, discussion and comparison of methods and results strengthened and expanded the direction of this research.

Furthermore I would like to thank the Rhino Developer community, and Dale Fugier of Robert McNeel & Associates, whose assistance with troubleshooting program code was most valuable in completion of this work.

Thanks go to the members of the Civil Research Group at the University of Warwick for their probing questions, which have strengthened this research.

Further thanks go to the admin staff and members of the IT department at the School of Engineering, University of Warwick, particularly Kerrie Hatton, for their patience and assistance.

Finally, the greatest thanks of all go to my partner, Leanne Dew, for her encouragement, patience, and support, and for the many sacrifices she has made over the last four years.

Declaration

This thesis is submitted to the University of Warwick in support of my application for the degree of Doctor of Philosophy. It has been composed by myself and has not been submitted in any previous application for any degree.

The work presented was carried out by the author, except where indicated otherwise in the text.

Parts of this thesis have been published by the author, in the following journal and conference papers:

1. Gale S, Lewis WJ. Patterning of tensile fabric structures with a discrete element model using dynamic relaxation. *Comput Struct* 2016;169:112–21.
2. Gale S, Lewis WJ. Computational patterning methods for tensioned fabric structures. Use of a discrete element model. *Proc. Int. Assoc. Shell Spat. Struct. Symp.* 2015, Amsterdam, Amsterdam: 2015.

Abstract

Tensile fabric structures are efficient and cost effective structural systems for covering large areas. The performance of such structures is highly dependent on their geometry, and for this reason they must be doubly curved. However, doubly curved surfaces may not be formed from flat fabric without incurring distortions. The process of patterning is employed to determine the planar configuration of panels, such that after assembly, these distortions are minimised. However, patterning is sensitive to the numerical models and processes employed. Shear of the fabric is required for it to adopt a doubly curved shape, but this has been overlooked in the numerical models used currently for the patterning of tensile fabric structures.

On this basis, a discrete element model for numerical representation of the fabric, during the patterning process, is proposed and examined in this thesis. Further to this, the computational process of patterning is examined thoroughly, and improvements to sub-processes within patterning form part of a proposed patterning method.

This thesis reviews the literature relating to tensile fabric structures, patterning, and numerical modelling. The discrete model is described, along with its implementation in the proposed patterning method. Comparison with published results is included to evaluate the suitability of the proposed model and patterning method.

It is shown that the proposed discrete element model offers an alternative model for architectural fabrics at the patterning stage. Conditions for successful use of the model are stated and explored. In addition to this, the proposed improvements to the patterning process are examined.

List of Symbols

Symbol	Quantity
κ_G	Gaussian curvature
κ_1	First principal curvature
κ_2	Second principal curvature
L_0	Element reference length
L	Element current length
ε	Element strain
\underline{r}_A	Node A position vector (current configuration)
\underline{r}_B	Node B position vector (current configuration)
\underline{r}_{A_0}	Node A position vector (reference configuration)
\underline{r}_{B_0}	Node B position vector (reference configuration)
σ	Element tensile stress
$E_{(w/f)}$	Fabric tensile modulus in either the warp or weft direction
$\sigma_{P(w/f)}$	Prescribed pre-stress in either the warp or weft direction
w	Fabric width represented by an element
A_1	First adjacent area
A_2	Second adjacent area
F	Element tensile force
\underline{d}	Element direction unit vector
γ	Shear strain

F_u	Applied shear force 1
F_v	Applied shear force 2
F_1	Resolved force 1
F_2	Resolved force 2
ϕ_0	Rest angle between two elements (reference configuration)
ϕ	Current shear angle between two elements
\underline{r}_C	Node C Position Vector
τ	Shear stress
G	Fabric shear modulus
\underline{F}_{AB}	Shear force along side AB
\underline{F}_{AC}	Shear force along side AC
\underline{v}_{BA}	Vector from node B to node A
\underline{v}_{CA}	Vector from node C to node A
\underline{u}	Arbitrary vector
\underline{F}	Resolved shear force
\underline{R}	Resolved shear reaction force
\underline{R}_A	Resolved shear reaction force at node A
\underline{R}_B	Resolved shear reaction force at node B
\underline{R}_C	Resolved shear reaction force at node C
\underline{R}_D	Resolved shear reaction force at node D

$\underline{r_D}$	Position vector of node D
$\underline{F_A}$	Resolved shear force at node A
$\underline{F_{AD}}$	Force along side AD
$\underline{v_{AB}}$	Vector from node A to node B
$\underline{v_{AD}}$	Vector from node A to node D
$\underline{F_B}$	Resolved shear force at node B
$\underline{F_{BA}}$	Force along side AB
$\underline{F_{BC}}$	Force along side BC
$\underline{v_{BC}}$	Vector from node B to C
$\underline{v_{CD}}$	Vector from node C to D
$\underline{v_{CB}}$	Vector from node C to B
$\underline{F_C}$	Resolved shear force at node C
$\underline{F_{CB}}$	Force along side BC
$\underline{F_{CD}}$	Force along side CD
$\underline{v_{DA}}$	Vector from node D to A
$\underline{v_{DC}}$	Vector from node D to C
$\underline{F_D}$	Resolved shear force at node D
$\underline{F_{DA}}$	Force along side AD
$\underline{F_{DC}}$	Force along side CD

$\underline{R}_A(\textit{continuum})$	Resolved shear reaction force at node A from continuum model
$\underline{R}_B(\textit{continuum})$	Resolved shear reaction force at node B from continuum model
$\underline{R}_C(\textit{continuum})$	Resolved shear reaction force at node C from continuum model
$\underline{R}_D(\textit{continuum})$	Resolved shear reaction force at node D from continuum model
$\underline{R}_A(\textit{discrete})$	Resolved shear reaction force at node A from discrete model
$\underline{R}_B(\textit{discrete})$	Resolved shear reaction force at node B from discrete model
$\underline{R}_C(\textit{discrete})$	Resolved shear reaction force at node C from discrete model
$\underline{R}_D(\textit{discrete})$	Resolved shear reaction force at node D from discrete model
N_{ji}	Node residual force for node j , direction i
m_{ji}	Node mass for node j , direction i
a_{ji}	Node acceleration for node j , direction i
C	Damping factor
v_{ji}	Node velocity for node j , direction i
P_{ji}	Forces applied at node j , in direction i
K_{EL}	Element stiffness
δ	Nodal displacement
\underline{N}	Node residual force vector
m	Node mass (scalar)
\underline{a}	Node acceleration vector
$\underline{v}^{k+\frac{1}{2}}$	Node velocity vector at iteration $k + \frac{1}{2}$

$\underline{v}^{k-\frac{1}{2}}$	Node velocity vector at iteration $k - \frac{1}{2}$
Δt	Time interval
k	Iteration number
$\underline{\delta}^{k+1}$	Nodal displacement at iteration $k + 1$
$\underline{\delta}^k$	Nodal displacement at iteration k
K	Nodal stiffness for iteration k
\underline{X}^{k+1}	Nodal position for iteration $k + 1$
\underline{X}^0	Nodal position for iteration 0 (reference configuration)
$KE^{k+\frac{1}{2}}$	Kinetic Energy at iteration $k + \frac{1}{2}$
$KE^{k-\frac{1}{2}}$	Kinetic Energy at iteration $k - \frac{1}{2}$
t	Iteration number
a	Quadratic coefficient of t^2
b	Quadratic coefficient of t
c	Quadratic constant
t_{\max}	Iteration corresponding to maximum KE
KE_1	Kinetic Energy at iteration $t - \frac{3}{2}$
KE_2	Kinetic Energy at iteration $t - \frac{1}{2}$
KE_3	Kinetic Energy at iteration $t + \frac{1}{2}$
β	Adjustment factor for displacements due to KE peak
$\underline{\delta}^{k+1}_{corrected}$	Corrected nodal displacement at iteration $k + 1$
$\underline{X}^{k+1}_{corrected}$	Corrected nodal position at iteration $k + 1$

S	A given surface
L₁	Distance from point A to point C on S
L₂	Distance from point B to point C on S
P₁	Sphere with radius L ₁
P₂	Sphere with radius L ₂
C₁	Circle with radius L ₁
C₂	Circle with radius L ₂

List of Abbreviations

2D	Two Dimensional <i>or</i> Two Dimensions
3D	Three Dimensional <i>or</i> Three Dimensions
DR	Dynamic Relaxation
KE	Kinetic Energy
NURBS	Non-Uniform Rational B-Spline
PTFE	Polytetrafluoroethylene
PVC	Polyvinyl Chloride
RO	Research Objective
WG	Working Group

1 Introduction

1.1 Introduction to tensile fabric structures

Tensile fabric structures comprise a fabric membrane, tensioned within a boundary comprising rigid structural elements and/or flexible cables. The tension in the fabric may be introduced through installation of the fabric in the boundary, or by the additional use of air pressure. Fabric structures supported by air pressure are referred to as pneumatic tensile fabric structures.

Figure 1.1 shows an example of a tensile fabric structure:



Figure 1.1 – Example of a tensile fabric structure. Santa Fe Opera Cantina, California¹

Tensioned fabrics have in-plane stiffness only, thus out-of-plane loads must necessarily result in large displacements and a consequent change in the surface stress field. This change is then resisted by tension in flexible cables, in turn transferred to rigid supports, or through compression and/or bending in supporting rigid beam elements. Large out-of-plane displacements are the main contributor to geometrically nonlinear behaviour.

¹ Source: http://www.fabritecstructures.com/sites/default/files/styles/juicebox_medium/public/SantaFeOperaCantina_MastSppt_PTFESFIIHT_1_CC.jpg?itok=Kv1APi4L

To prevent excessive deformation, that is to give sufficient stiffness to the membrane, the surface curvature should be high [1]. In particular, pneumatic tensile structures should be *synclastic* (dome-shaped), and non-pneumatic structures should be *anticlastic* (saddle-shaped) (Figure 1.2). Pre-stressing is employed, with the intention of ensuring the fabric remains in tension under external loads over the life span of the structure.

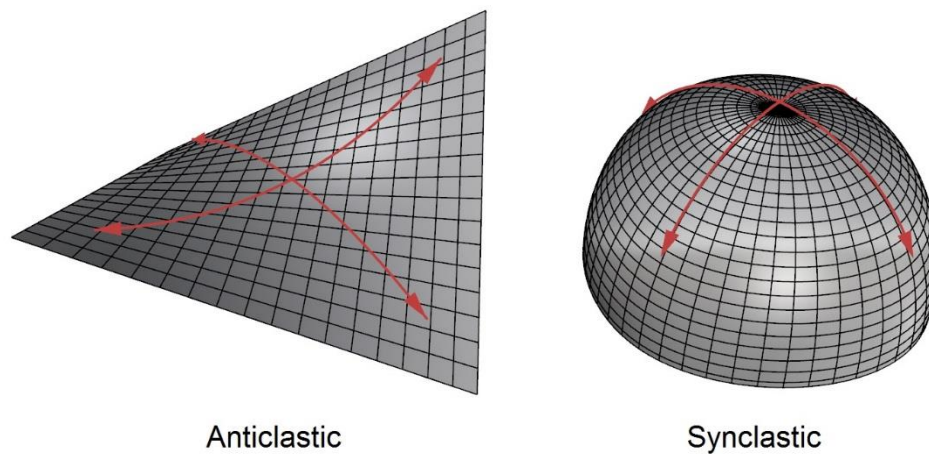


Figure 1.2 - Surfaces with anticlastic and synclastic curvature

The shape of the membrane surface cannot be defined by the design engineer [2], because fabric will adopt its own shape within a given boundary under pre-stress. Consequently, fabric structures require *form-finding* [2,3], a process, historically conducted using physical models [4], but now most commonly conducted computationally, that finds the equilibrium geometry of a structure within a prescribed boundary and for a given stress state. Form-finding is the first phase in the design process of tensile fabric structures.

Both *synclastic* and *anticlastic* shapes are doubly curved – they have non-zero principal curvature in both directions. Doubly curved surfaces cannot be flattened into the plane without distorting [5], that is, they are not developable [6], but fabrics are flat in their unstressed state, prior to the construction of the 3D surface. Architectural fabrics have a typical width of 2-3m [5], and a maximum width of 5m [7].

Such constraints are imposed by the size of the manufacturing apparatuses, and this leads to larger structures requiring multiple fabric panels to make up the 3D membrane surface. The configuration of the panels that are assembled into the final structure affects the membrane form and stress distribution. The effects of pattern shape on structural performance necessitate a further process in the design of fabric structures, *Patterning*, be conducted to define the planar shape of the panels which form the final surface.

1.1.1 Design process

The design process incorporates the two processes of form-finding and patterning, in addition to analysis of the structure under load. Historically, in the design process the analyses were conducted in the following order:

1. Form-finding – finding the 3D shape of the membrane surface under pre-stress
2. Load Analysis – finding the stresses and deflections of the form-found structure, due to environmental loading such as rain or snow
3. Patterning – determining the shape of the planar panels, which will be cut from the fabric and assembled to form the final membrane surface

However, given the effect of the cutting pattern on the membrane surface stress field, as demonstrated through this work, it is advisable to conduct patterning before load analysis. In this way, the assembled cutting pattern is analysed for performance under load, accommodating variations in the surface stress field due to the patterning process. Consequently, the design process should be conducted in the following order:

1. Form-finding
2. Patterning
3. Load Analysis

Form-finding and patterning are now discussed briefly. A more detailed discussion of patterning is presented in chapter 2.

1.2 Form-finding

As mentioned, fabrics sustained by a boundary will adopt their own unique shape in response to load. In the case of tensile fabric structures, the boundary is defined at the design stage, but the fabric membrane shape cannot be specified simply.

In the design of structures composed of traditional materials such as steel or concrete, the engineer specifies the geometry of a structural component and evaluates its maximum stress capacity. The capacity of the component is compared with the expected stress state to indicate its suitability. In this manner, the geometry of the structural component is a free choice variable, and the capacity is a calculated value.

In the process of form-finding, however, the nature of these quantities is reversed, and the intended stress state is specified. Form-finding is then used to generate the geometry of the structure - for a certain boundary - that has the prescribed stress state. It then remains only to specify the correct material to ensure the structure's capacity to cope with the prescribed stress and further imposed loads, such as those arising from wind or snow. For tensile fabric structures, the prescribed stress state is the pre-stress desired in the membrane. (Typical pre-stresses are specified in section 1.4).

Hence, the exact objective of form-finding is to determine the form of a membrane structure, with specified boundary conditions and pre-stress, such that that resulting form is in equilibrium [6] under the prescribed pre-stress. The nature of membrane structures provides the opportunity to generate efficient structural forms, in particular, those of minimal surfaces. Where a uniform membrane stress is specified during the form-finding process, the structure adopts a form close to that of a stable minimal surface, or soap film [2].

1.2.1 Minimal surfaces

Minimal surfaces are defined as surfaces with zero mean curvature at every point [8], and are well documented in the field of mathematical geometry [9]. Of specific interest, however, is the property that when considering the area functional of a surface, the extremals correspond to minimal surfaces [9]. In particular, the minima of the area functional correspond to stable minimal surfaces – surfaces that minimise their surface area.

Where membrane surfaces adopt the form of a stable minimal surface, they can be considered to represent optimal structures. The prescription of a uniform stress field during form-finding results in a structure of minimal area [10] – in this structure, stress concentrations are eliminated (no portion of the structure is under-utilised), and the quantity of material used to achieve this is minimal. The physical realisation of these structures is however a challenge, necessitating careful patterning.

1.3 Patterning

The mathematical condition of non-developability for membrane surfaces necessitates the process of patterning (see section 2.1.1). Patterning is now conducted using computational methods, and comprises the following 4-5 steps:

1. **Subdivision** of the membrane to define the panels which will make up the final structure. The panels are defined by the position of the seams on the surface. These seams are present in the final, built structure, and comprise an overlap of fabric between adjacent panels, which is then sewn or welded [11].
2. **Flattening** of the resulting panels from 3D to 2D. Flattening incurs distortions on account of the non-developability of the surface.
3. **Stress reduction**, applied to the flattened panels, to reduce as much as possible the stresses from flattening. Owing to the non-developability of the doubly curved

membrane surface, complete nullification of the stresses induced by flattening is not possible. Stress reduction methods tend to be iterative.

4. **Compensation** to reduce the 2D panel in size, to account for pre-stressing. The membrane surface represents a stressed geometry, and the fabric from which the planar panels will be cut is not stressed. Because of this, the panels are reduced in size, such that the act of installing the panels in the boundary of the final, built structure gives rise to the intended pre-stress. Steps 3 & 4 may be performed in one process [6].

An additional fifth step is included in some, but not all, analyses:

5. **Panel assembly** to evaluate the cutting pattern, by comparison with the intended stress state and geometry. Because stress reduction cannot give completely stress-free panels, residual stresses will be present in the final membrane. Thus, the cutting pattern determined by steps 1 – 4 may be evaluated by finding the equilibrium geometry of the assembled panels – stresses after erection are thus calculated.

1.4 Architectural fabrics, types and composition

Architectural fabrics comprise woven fibres with a polymer topcoat (Figure 1.3). The two most commonly used fabrics are PVC coated polyester, and PTFE coated glass fibre [12,13]. PVC coated polyester is the more common of the two, and has a lifespan of around 15 years, compared with PTFE coated glass fibre, which can have a lifespan of 30+ years, though manufacturers guarantee only 15 years [12]. The fibres in the fabric run in two directions, the stiffer warp direction, and the weft (or in North America, the fill) direction. The fibres are approximately orthogonal in planar fabrics, in either a *plain weave* (as in Figure 1.3) or *Panama bond* configuration. Panama bond is similar to that of plain weave, but multiple fibres are interwoven, rather than single fibres [12].

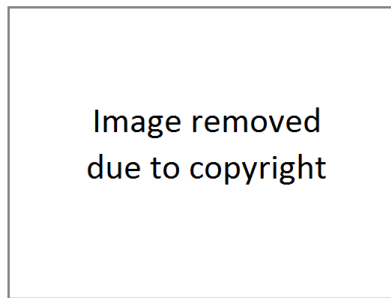


Figure 1.3 – Woven fabric structure²

Fabrics come in a variety of weights and strengths, and are classified as such, though no standardised classifications are available. The classifications for PVC were proposed by the working group (WG) for architecture at Messe Frankfurt, and a French design guide, as stated in [13]. PVC coated polyester fabrics are grouped within the classifications Type 1 to Type 5, and PTFE coated glass fabrics are categorised as Type G1 to G7 [12]. Tables 1.1 and 1.2 show these classifications, and relevant material properties. It is seen in tables 1.1 and 1.2 that the material properties relating to stress are given in units of kN/m, not kN/m². The same applies to elastic properties (e.g. modulus of elasticity). This is because the small thickness of architectural fabrics can magnify errors when dividing the force per width by this small thickness [12]. The tensile strength of the fabric is measured using a *strip tensile test*, and the tear strength of the fabric through a *trapezoidal test* [12].

² Source: <https://armijos.files.wordpress.com/2011/02/fabric-close-up-001.jpg>

Table 1.1 – PVC coated polyester fabric classifications and relevant material properties – adapted from [12] (originally [13,14])

PVC coated polyester fabrics					
	Type 1	Type 2	Type 3	Type 4	Type 5
Surface Weight (g/m²)					
French design guide	720	1000	1200	1400	2000
WG Messe Frankfurt	800	900	1050	1300	1450
Tensile strength (kN/m)					
French design guide (warp)	60	84	110	120	160
French design guide (weft)	60	80	104	130	170
WG Messe Frankfurt (warp)	60	88	115	149	196
WG Messe Frankfurt (weft)	60	79	102	128	166
Trapezoidal test (tear strength test) (N)					
WG Messe Frankfurt (warp)	310	520	800	1100	1600
WG Messe Frankfurt (weft)	350	580	950	1400	1800
Minimum pre-stress (kN/m)	0.7	0.9	1.3	1.6	2

Table 1.2 - PTFE coated glass fabric classifications and relevant material properties – adapted from [12] (originally [13,14])

PTFE coated glass fabrics							
	Type G1	Type G2	Type G3	Type G4	Type G5	Type G6	Type G7
Surface Weight (g/m²)	500	420	800	1000	1200	1500	1600
Tensile strength (Warp) (kN/m)	26	43	70	90	124	140	170
Tensile strength (Weft) (kN/m)	22	28	70	72	100	120	158
Trapezoidal test (Warp & Weft) (tear strength test) (N)	-	-	300	300	400	500	450

Typical pre-stresses for the two materials are 0.7 kN/m to 2.0 kN/m for PVC coated polyester [12,14], and 2.0 kN/m to 5.0 kN/m for PTFE coated glass fibre [14]. Alternatively, the following heuristics may be used: for PVC coated polyester, the pre-stress should be greater than 1.3% of the average tensile strip capacity in both directions [14]; for PTFE coated glass fibre, the pre-stress should be between 2.5% and 6% of the average tensile strip capacity in both directions [12,14].

1.4.1 Numerical modelling

Architectural fabrics resist external forces through increased tension in the fibres, and shear stresses in the polymer topcoat. The main load carrying directions of the fabric are defined by the weave [15], which is approximately orthogonal when the fabric is in an unstressed configuration. For a flat fabric to adopt a doubly curved shape (required for suitable performance under load), this weave must shear [15–18], becoming non-orthogonal. The stiffness properties of architectural fabrics thus change through the assembly of the cutting patterns, but this phenomenon is not currently accounted for. As will be explored in later sections, numerical modelling that accounts for this behaviour is required. Further to this, since the shear stiffness of architectural fabric is low in comparison with the tensile modulus [19], it is frequently ignored [20].

1.5 Problem statement and scope

Whilst methods for patterning have been developed, the focus of these methods has been to reduce distortions between the plane and doubly curved shapes, based on orthogonal mechanical models. That shear of the weave is necessary for the fabric to adopt a doubly curved shape has been mostly ignored, yet it affects the ultimate accuracy of the generated cutting patterns. Such shear dependent mechanical behaviour has the greatest impact on membranes of higher curvature. Thus to analyse and design structures of increasingly complex shape requires a mechanical model that accommodates this behaviour of architectural fabrics.

Further to this, a thorough examination of patterning, and its individual sub-processes, has not been previously presented. There remains to be made some improvements to individual sub-processes, and these are discussed further in chapter 2. Additionally, the inclusion or exclusion of the shear stiffness throughout patterning merits investigation.

1.6 Scope, research objectives and contributions

In light of the problem stated above (which is further elaborated in chapter 2), the research presented in this thesis was undertaken to fulfil the following aim and research objectives (ROs):

Aim: The investigation and advancement of the computational process of patterning

RO 1: The development, application and examination of a discrete model

- (a)** To develop and implement a discrete model for patterning
- (b)** To examine the model's suitability for patterning
- (c)** To identify conditions and guidance for the successful use of discrete models in patterning

RO 2: The advancement of the computational process of patterning

- (a)** To develop improved flattening methods and investigate their application
- (b)** To investigate the effect, on the cutting pattern shape and final stress distribution, of including shear stiffness throughout patterning

The main contribution of this work is thus the development and application of a discrete element model for patterning of tensile fabric structures, and the examination of this model. The proposed model reflects the nature of the fabric weave, and thus accounts for the phenomenon of weave shear highlighted previously. The development of such a model is timely and relevant on the basis of sections 1.3 to 1.5 above. It is shown, through comparison with published work, that the proposed model is simple in application and gives results within the expected range of stress deviation. Conditions for the successful use of discrete models, elaborated through the research, are detailed in chapters 5 & 6.

In addition to the development and application of the discrete model, further contributions were made through the development of geometric flattening methods, aimed at reducing distortions prior to iterative stress reduction and compensation processes. The relevance of

these is discussed in chapter 2, and the developed methods and their application are detailed in chapters 4 & 5.

1.7 Structure of Thesis

In presenting the research outlined above, this thesis is structured in the following way:

In **chapter 2**, a review of the literature and key concepts pertaining to the numerical modelling and patterning of tensile fabric structures is presented. Form-finding, and the consequent doubly curved surface shapes are briefly discussed as the basis for patterning. Patterning is then explored in detail, starting with the mathematical basis of patterning, before each phase of the computational process is examined. Numerical modelling is then explored. The behaviour of architectural fabrics, and the use of finite element and discrete element models are discussed. The use of discrete models is advocated, based on the challenges identified, and provides the basis for the proposed discrete model.

Chapter 3 presents the proposed discrete model, and solution by the dynamic relaxation method with kinetic damping. The modelling of tensile behaviour is presented, including methods for overcoming limitations in models proposed by other authors. Modelling of the shear resistance of the fabric is shown next. A brief review of the dynamic relaxation method is presented, to illustrate the solution of problems posed for various stages of the proposed patterning method. The computational implementation of the discrete model within the dynamic relaxation method is explained, with the inclusion of pseudocode.

Chapter 4 details the proposed patterning method. The method employs the discrete model together with the solution by the dynamic relaxation method presented in chapter 3. In the first part of chapter 4, the proposed method for determining the cutting pattern is presented, including methods for each of the patterning steps identified in chapters 1 & 2. The proposed method for assembling the generated patterns is shown, including the additional step of re-

meshing the panel with an orthogonal mesh, and final equilibrium finding by dynamic relaxation is mentioned.

Chapter 5 presents results from the application of the proposed patterning method using the discrete element model. Cutting patterns generated using the methods outlined in chapter 4 are shown for two examples taken from the literature. Comparisons of cutting patterns generated with different methods, including the one proposed in this thesis, are presented and discussed. The assembly of the generated cutting patterns is shown, facilitating comparison with published work. It is shown that the discrete element model gives results within the expected ranges quoted in literature. Conditions for successful use of the discrete model are presented using the examples.

Chapter 6 presents the summary and conclusions drawn from the work, including conditions for successful use of the discrete model, together with reflections on the effectiveness of the developed patterning method. Suggested further work is then presented.

1.8 Publications arising from the research

This research resulted in two publications:

1. **Journal paper:** "Patterning of tensile fabric structures with a discrete element model using dynamic relaxation", in Computers & Structures 2016 [21].
2. **Conference paper:** "Computational patterning methods for tensioned fabric structures. Use of a discrete element model.", IASS Symposium on Future Visions 2015 [22].

2 Literature review

This chapter presents in depth explorations of patterning and numerical modelling, and the literature relating to these topics. The general design process and form-finding were explored in sufficient detail in chapter 1 and are not explored further. The key points of the review are presented in the summary of this chapter.

2.1 Patterning

As mentioned, suitable shapes for tensile fabric structures are doubly curved. Such doubly curved surfaces cannot be formed from planar fabric panels without incurring distortions. The magnitude and distribution of these distortions, and their consequent stresses across the membrane surface, are dependent on the method by which the planar panels were determined.

Patterning was historically conducted with the aid of physical models [4]. Now it is mainly conducted as a computational process. The general computational process comprises a number of distinct sub-processes. These are discussed below, after a brief review of the mathematical conditions necessitating patterning.

2.1.1 Mathematical basis of patterning

It is relevant at this point to discuss the necessity of patterning from a mathematical point of view. One surface may be mapped to another isometrically, that is, in such a way that preserves all lengths on the surface, if and only if they have identical first fundamental forms [23]. Such a requirement equates to the two surfaces having equal Gaussian curvature at corresponding points. Since tensile fabric structures should be doubly curved to resist external loads, they have non-zero Gaussian curvature (κ_G). Gaussian curvature is defined as the product of the two principal curvatures at a point on the surface [8]:

$$\kappa_G = \kappa_1 \kappa_2 \quad (2.1)$$

Where κ_1 & κ_2 are the first and second principal curvatures respectively. For pneumatic tensile fabric structures, $\kappa_G > 0$ and for non-pneumatic tensile fabric structures, $\kappa_G < 0$. Plane surfaces have $\kappa_G = 0$. Positive Gaussian curvature indicates a synclastic surface, negative Gaussian curvature indicates an anticlastic surface. Zero Gaussian curvature indicates a flat surface.

Isometric mappings are mappings that preserve *all* lengths between the original and mapped geometry, giving rise to no stresses, and are equivalent to the combination of conformal and equiareal mappings [23]. These mappings are in turn defined thusly: conformal mappings confer no changes in angles between the original and mapped geometry; equiareal mappings confer no changes in areas between the original and mapped geometry [23]. In an engineering context, conformal mappings result in zero shear stress as a result of the mapping.

It is not possible to fully nullify the stresses induced by non-developability – an isometric mapping is not possible, as explained above. Thus, in defining the cutting pattern for tensile fabric structures, the mapping between the doubly curved form-found surface, and the plane, must accommodate a trade-off between shear stresses and tensile stresses.

2.1.2 Computational patterning – the 5-step process

The mathematical condition of non-developability for membrane surfaces necessitates the process of patterning. Patterning is now conducted using computational methods, and comprises the following 4-5 steps, as previously mentioned in chapter 1, section 1.3. The 5-step process is presented in short here:

1. **Subdivision** of the membrane by defining seams on the form-found surface
2. **Flattening** of the resulting panels from 3D to 2D
3. **Stress reduction** to reduce the stresses induced by flattening

4. **Compensation** to scale the 2D panel to account for pre-stressing

An additional fifth step is included in some, but not all, analyses:

5. **Panel assembly** to visualise the final 3D form and calculate stresses

Steps 1-4 concern the *method of determining the cutting pattern*. Step 5 concerns the simulation of the *assembly of the cutting pattern* to determine its suitability.

The above five steps are discussed separately, in detail, in the following sections.

2.1.3 Subdivision of the membrane

The form-found shape represents an idealised surface geometry for the given boundary conditions. This surface must be divided into a series of sub-surfaces representing the panels from which the structure will be fabricated. This sub-division is achieved by defining the positions of the *seams* that will be present in the assembled structure. Seams in the physical structure are constructed from overlapping, and welding (or less commonly sewing), the edges of adjacent panels [11].

When defining the positions of the seams on the surface, it is generally accepted that the seams should follow geodesics [5,15,24]. Geodesics represent the path that a cable adopts when stretched across the surface with constant stress [25]. Errors, such as wrinkling in the fabric, may be introduced during the welding of the seams, when fabricating and assembling the membrane. For this reason, seams should run through the regions of lowest curvature.

The seams dictate the size of the individual panels, and consequently the curvatures across each panel. The subdivision of the membrane by seams thus affects the subsequent processes of flattening, stress reduction and compensation, and the suitability of the final cutting pattern.

2.1.4 Flattening

The form-found surface, and its constituent panels after subdivision, are doubly curved. To produce a pattern suitable for cutting from planar cloth, the planar configuration of the constituent panels must be found, and the first step is to flatten the 3D panels into the plane.

Historically, so called “cloth unfolding” [26] (Figure 2.1) was employed to flatten the membrane. Individual panels were represented by a developable polyhedral strip which was unfolded into the plane [4,20,26] in a procedural manner. The polyhedral representation tended to use only a single row of elements for each panel, representing a significant misrepresentation of the original panel geometry, and non-seam panel edges [26]. It has similarly been noted, owing to this use of a single row of elements, that a triangular polyhedral representation of a panel does not offer an accurate representation for smaller structures [20]. For two structures of similar geometry, but different size, where the maximum panel width is the same for both structures, the smaller structure requires fewer panels. Thus, the panels in the smaller structure represent surfaces of higher curvature, and the error in the approximation of the surface by a single row of elements is particularly acute.

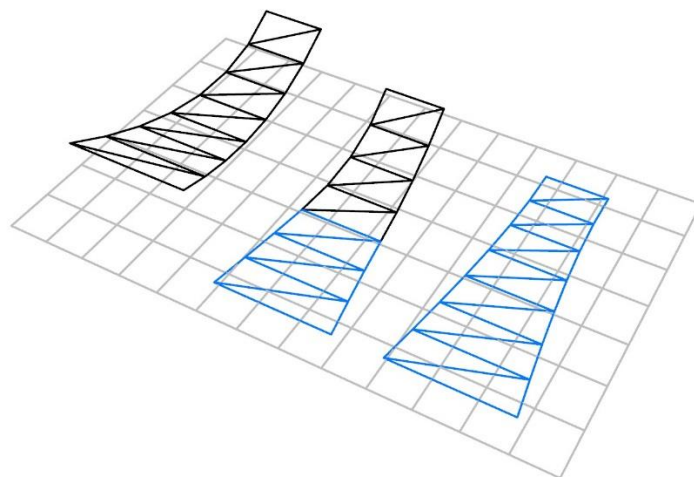


Figure 2.1 - Unfolding of a panel to the plane. Note that across the width, the panel is represented by just a single triangular element

Cloth unfolding was, in the past, the sole method used to account for the distortions due to double curvature, when determining the planar cutting patterns. Cloth unfolding was accompanied only by compensation, to reduce the cutting pattern in size, in light of the pre-stress. In view of the drawbacks highlighted above, recent methods of patterning employ further computational methods to reduce the stresses from flattening [20], as discussed in the following section. An adaptation of cloth unfolding does, however, offer a computationally efficient method of minimising the stresses due to flattening, before computationally intensive iterative methods are employed. Use of such a method in the flattening process is often overlooked, and simple projection of the panel to the plane is used. Methods for flattening, that minimise distortions through simple geometrical algorithms, are presented in chapter 4.

2.1.5 Stress reduction

Flattening, whether using cloth unfolding or not, results in distorted patterns. Distortions in the pattern must be reduced. The problem of reducing distortions in the mapping of a doubly curved surface to a planar surface is a mathematical one, having been explored in a number of other fields, including cartography [23]. The equivalent engineering problem is formulated by considering the reduction of the *stresses* that these distortions incur.

The reduction of stresses in the determination of the cutting pattern is approached both as a mathematical problem and an engineering one. In this thesis, formulation of the problem as a reduction of the distortions is termed the *geometrical problem formulation*, and formulation of the problem as a stress reduction problem is termed the *mechanical problem formulation*. These two problem formulations are in essence separated by the exclusion or inclusion of the material properties. It has been mentioned in [27] that excluding material properties results in a purely geometrical problem.

A number of solutions to these problem formulations have been proposed, and these solutions can be further categorised. Two main solution methods are used; the more common, termed the '*minimisation solution*', formulates the reduction of the distortions, or stresses, as an optimisation problem. In the case of the *geometrical problem formulation*, the description of the distortions constitutes an objective function. In the case of the *mechanical problem formulation*, the description of the stresses, or the deviation of the stresses from the intended design pre-stress, constitute an objective function. Solution by the *minimisation solution* has been achieved by methods such as least squares, applied to geometrical [28], and mechanical [3,26] problem formulations.

The second solution is termed the '*structural solution*'. The distorted, flattened geometry represents a configuration of the subsurface which is not in equilibrium, in the absence of sufficient restraints. With careful selection of the restraints, the panel can be equilibrated using a solution method, such as dynamic relaxation [5] or Newton-Raphson [6]. This equilibration process has the effect of *releasing the stresses*, and yields a subsurface geometry with reduced stresses (Figure 2.2):




Image removed
due to copyright

Figure 2.2 - Reduction of stresses using the structural solution - adapted from Linhard et al. [6]

In Figure 2.2 (a), the 3D surface is flattened into the plane. The method of flattening incurs distortions, such that under relaxation (Figure 2.2 (b)), the left hand pinned support remains stationary, and the right hand roller support, and other nodes on the 2D surface, move in plane. This movement is what permits the release of the stresses, providing sufficient restraints are employed to prevent rigid body transformations.

Because the structural solution models a physical process, material properties are required. Thus, the structural solution is applicable only to the mechanical problem formulation. Figure 2.3 shows the relationship between the problem formulations and solution methods.

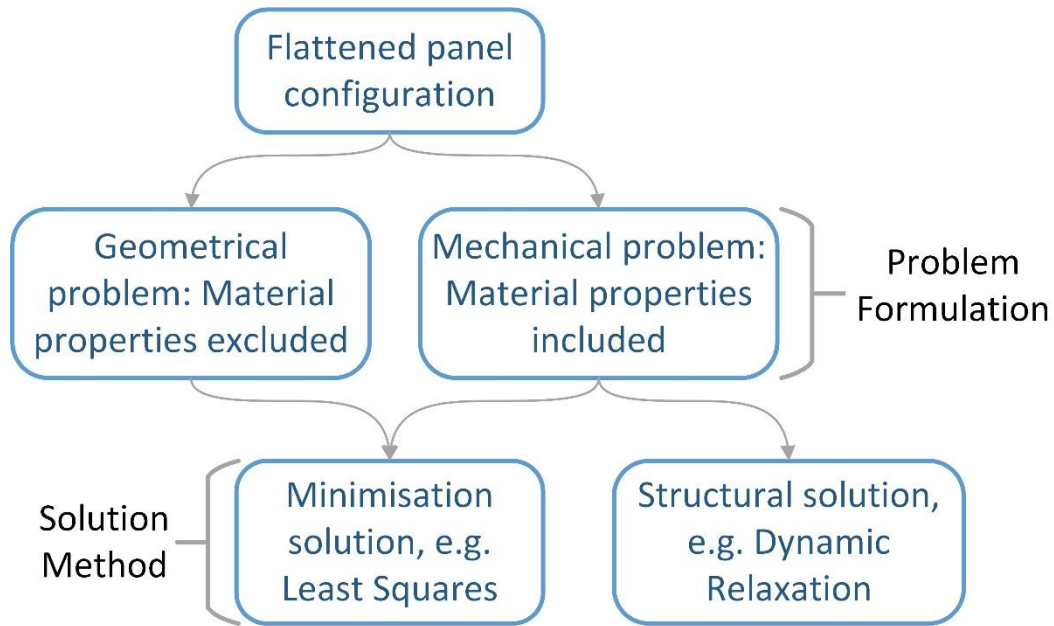


Figure 2.3 - Stress reduction problem formulations, solution methods and the relationship between them

2.1.6 Compensating for pre-stress

Following the flattening of the panel, and reduction of the stresses induced by this flattening, the planar panel geometry must be further altered to account for the intended pre-stress in the assembled membrane shape.

The 3D membrane geometry generated by form-finding represents a configuration of the surface that is in equilibrium under its own pre-stress. Since the fabric from which the panels will be cut is unstressed in its planar form, the pre-stress must be accounted for in the generation of the cutting pattern. In particular, the planar panel must have smaller width and length, and consequently area, than the form-found panel [18]. This process is known as compensation, and can be achieved by simple scaling of the panel, or by the application of the same structural solution methods [5] described in the previous section, with a prescribed pre-stress. At this point in the patterning process, the material properties must be considered.

It is possible to integrate the processes of stress reduction and compensation, and conduct them as one process [6]. The comparative benefit of conducting the two processes as one, or distinctly, is an issue of contention. In [28] it is stated that it is preferable to conduct the processes separately, whereas in [5,6] the processes are conducted simultaneously. Owing to the necessity for material parameters during compensation, integrated stress reduction and compensation is achievable only when using the mechanical problem formulation, though the method of the solution does not affect the possibility of integration. Figure 2.4 highlights the difference between integrated and distinct methods.

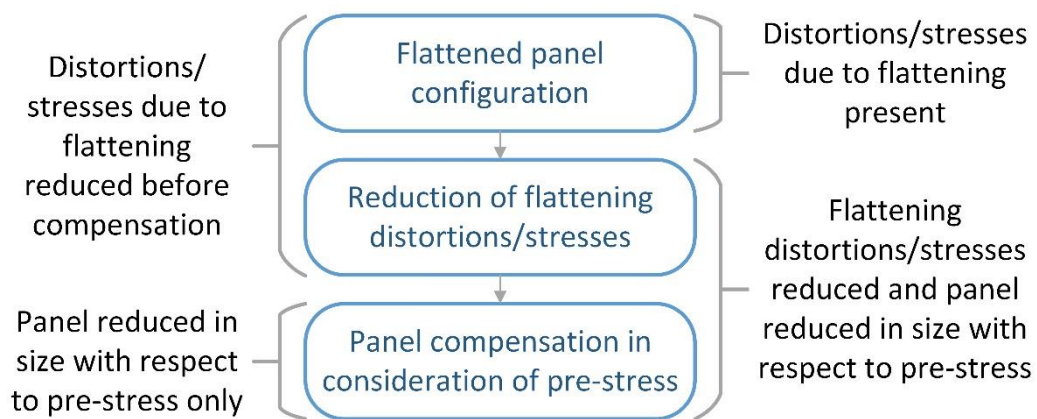


Figure 2.4 – Distinct vs integrated methods for stress reduction and compensation

2.1.7 Assembly of cutting patterns

Flattening, stress reduction, and compensation wholly define the cutting pattern, providing sufficient data for the manufacture of the membrane from planar fabric. To evaluate the suitability of the cutting pattern, patterning processes can include modelling of the assembly of the cutting pattern [4]. The aim in such a process is not to model the physical construction process, but rather to see how the combination of panels, which are generated independently by the flattening, stress reduction, and compensation processes, behave together. Additional conditions can be applied to model the effect of the seams. Where the fabric overlaps, the

stiffness of the surface is increased, and has, in terms of mechanical behaviour, the effect of acting like a stiff cable in the surface.

Owing to the mathematical considerations presented in section 2.1.1, the stress reduction process cannot completely nullify the stresses due to non-developability. Thus, it is expected that the stresses in the surface following pattern assembly will resemble the combination of the intended pre-stress, and the residual stresses resulting from the stress reduction procedure. It is not, however, sufficient to say that the stress deviation will simply be the reverse of the residual stresses – how the panels behave as an assembly cannot be defined without further analyses.

2.1.8 Integrated approaches, optimisation and genetic algorithms

Given the consideration outlined above, that the assembled structure cannot adopt exactly the stress distribution dictated during form-finding, and there will be residual stresses, some methods employ multiple adjustments of the planar pattern [3,6,26,29,30]. These methods repeatedly conduct flattening, stress reduction and compensation, using the resultant assembly from the previous iteration to inform the current iteration of these processes.

Adjustments are made based on the residual stresses in the assembled form. The method presented in [29] employed manual adjustment of the pattern, adding or removing material in areas of higher or lower stress respectively. In [26] the stress difference between the assembly of the cutting pattern for the previous iteration and the design stress was used to adjust the cutting pattern for the current iteration. In [3,6] the patterns were similarly adjusted by comparison with the assembled shape of the previous pattern in the iteration, through the formulation of the mechanical process is different. In [30] genetic algorithms were used to optimise the cutting patterns.

2.1.9 Patterning – research objectives identified

As mentioned above, stress reduction is necessary to reduce the stresses in the cutting pattern, which are generated during flattening. Stress reduction methods, whether employed in the geometrical or mechanical problem formulations, are iterative. The stress reduction problem in [3] was reported to be sensitive to the initial configuration when solving the iterations using the Newton-Raphson method. Difficulties with convergence of the Newton-Raphson iteration are well known [3], and have been stated previously [31]. The Newton-Raphson method, and its sensitivity to the initial configuration, is representative of the requirement for suitable initial conditions when using iterative methods. This is a more general problem, and particularly pertinent for flattening and stress reduction in the context of cutting pattern generation.

It was mentioned in [6], where Newton-Raphson iterations are repeatedly used as part of a larger iterative process, that the computational efficiency is improved by using an initial geometry that is close to the solution. Convergence issues become more acute as the mesh is made finer [31], effectively limiting the mesh size for specific initial configurations. As accuracy is related to the fineness of the mesh, initial configurations that are far from the eventual solution lead to low accuracy. Methods of mapping the 3D panel to the plane which reduce distortions, and are fast, non-iterative, and relatively predictable in their outcome, are desirable.

To this author's knowledge, no investigation or comparison of different flattening methods, in the context of tensile fabric structures, has been conducted. Some existing flattening methods have been described, and these include, but are not limited to: direct projection of the panel to the plane [6]; projection of surface points to the tangent plane of the surface at these points (projection along the surface normal vector) [28]; and mapping of the panel to a singly curved surface (the surface is based on the 3D panel geometry) which is unrolled to give the planar geometry [5]. It is possible to extend cloth unfolding to meshes with more than one row of elements across the width, for topologically rectilinear meshes of discrete elements.

Additionally, map projection theories have been explored as a method of reducing distortions [27]. Outside of tensile fabric structures research, methods for arraying equidistant meshes on surfaces have been investigated [32–34], and these methods can be applied to improve flattening, as shown in chapter 4.

It is on this basis research objective **RO 2 (a)** was suggested in chapter 1. This research seeks to develop straightforward geometric flattening methods, investigate their application, and examine the effect of such flattening methods on the resulting cutting patterns. New flattening methods are proposed in chapter 4, and a comparison of these different flattening methods, applied to the same geometry, is presented in chapter 5.

Because the shear stiffness is low (see sections 1.4.1 & 2.2.1), it has been suggested that it may be, and frequently is, ignored [20]. However, this is an issue of contention in tensile structure design. The inclusion or exclusion of the shear stiffness, during stress reduction and compensation, and when simulating the assembly of the panels, will have an effect on the configuration and suitability of the cutting pattern. For this reason, the effect of including or excluding the shear stiffness, throughout patterning, merits further study. It is on this basis that research objective **RO 2 (b)** was suggested in chapter 1.

2.2 Numerical modelling

The mechanical behaviour of architectural fabrics is complex, and the numerical modelling of fabrics in general has received considerable attention. Material behaviour and numerical modelling are discussed in this section.

2.2.1 Behaviour of architectural fabrics

As stated in chapter 1, architectural fabrics comprise a bidirectional weave of fibres, treated with a polymer topcoat to provide protection against moisture (Figure 1.3). Typical compositions are polyester fibres with a PVC topcoat, and glass fibres coated with PTFE. Such woven fabrics

are heterogeneous and exhibit nonlinear anisotropic material behaviour. The woven fibres make the principal contribution to tensile stiffness [18], and the coating provides resistance against shearing loads [17]. The warp direction of the fabric runs along the length of the fabric, while the weft (or, as named in North America, the fill) direction of the fabric runs across the width. Whilst coated fabrics exhibit shear stiffness, in relation to the tensile stiffness it is much lower than that exhibited by typical, stiff materials. As a rule of thumb, the shear stiffness of fabrics can be estimated at $1/20$ of the tensile stiffness [15,35], compared with $\approx 3/8$ of the tensile stiffness for traditional materials [36]. The fibres make a negligible contribution to the shear stiffness of the fabric, and similarly the coating makes a negligible contribution to the tensile stiffness. As explained in chapter 1, the stress in architectural fabrics is measured in units of kN/m – the stress per width, rather than stress over a cross sectional area [35].

Due to their heterogeneous nature, architectural fabrics exhibit complex material behaviour. Woven fabrics experience *crimp interchange* at low strain – tension in one direction of the fabric causes the fibres to straighten, in turn shortening the fibres in the other direction [37]. This amounts to a complex relationship between transverse strains and longitudinal strains. In homogeneous, isotropic, linear materials, a single Poisson's ratio relates longitudinal and transverse strains. For fabrics, a single value of Poisson's ratio cannot be defined [20], and the ratio of loading in the warp and weft directions leads to non-static values of Poisson's ratio [37]. Two Poisson's ratios are often used, one relating longitudinal warp strain to transverse weft strain, and vice-versa.

Crimp interchange similarly leads to material nonlinearity in terms of the stress-strain behaviour [37]. Not only is the behaviour nonlinear and anisotropic, but stress-strain relationships vary for different ratios of stress. The relationships between elastic moduli, shear modulus and Poisson's

ratio are not restricted to those of isotropic materials [17], as exemplified by the comparatively low shear stiffness.

Architectural fabrics exhibit hysteretic or path-dependent behaviour [37], and so a distinction between the behaviour of virgin fabrics and those subjected to load cycling, or environmental loading, must be made. The stress-strain behaviour of virgin fabric is noticeably different from that observed after several cycles of loading. For this reason, samples of fabric are subjected to load-cycling when determining material properties.

It has been suggested that in patterning, initial stress-strain relationships should be used in determining compensation parameters [37]. Initial behaviour is distinct from the behaviour of virgin fabric, and refers to the behaviour of the fabric after it has been subjected to load-cycling under stresses of approximately 150% of the pre-stress. This is intended to model the fact that to tension the membrane to the desired pre-stress, it is sometimes necessary to over-tension the fabric during installation, before the stress distributes across the surface [7] - in effect pre-cycling the fabric. Alternatively, contractors may employ pre-cycling of the fabric before installation. However, industrial practice is not standardised, and the extent of pre-cycling is not known.

The material properties determined for compensation do not equate to the material properties that develop in the structure over the long term. These long-term properties arise because environmental loads have the effect of mechanically conditioning the fabric [37].

Given that long term fabric properties are not known, the initial stress-strain relationships are used for evaluating cutting patterns by simulation of the assembly, and when performing stress reduction analyses after flattening. This is important when considering crimp-interchange. Since crimp-interchange occurs in uncycled fabrics at low strains, it is not necessary, or correct, to

include modelling of crimp-interchange in the model used for compensation, or for evaluating cutting patterns by simulation of the assembly.

Material testing makes use of load-cycling by subjecting fabric samples to repeated loading and unloading. The stress-strain curve used for design, which results from these tests, is based on an idealisation of the recorded stress-strain behaviour from the last cycle. In numerical modelling this is often simplified further by linearising the behaviour for each portion of the stress-strain curve.

The shear behaviour of fabrics is similarly nonlinear and hysteretic [37], though often modelled as linear [17], with elastic isotropic modelling being considered adequate [15]. Though the shear stiffness of the fabric mostly derives from the coating, at certain large values of shear angle, the fibres rotate sufficiently for the warp fibres to bear against the weft fibres [18]. This *shear locking* manifests itself as an increase in the shear stiffness of fabrics [19]. Tensile fabric structures should be designed in such a way as to avoid this issue.

In unstressed, planar fabric, such as that used for the cutting pattern, the fibres are generally orthogonal, though angular deviations of up to 5° have been observed [37]. However, for the fabric to adopt a doubly curved geometry, the fibres must rotate about their crossing points – the weave must shear [15–18]. Thus, in assembling the 2D planar cutting pattern into the 3D form, shear deformation must necessarily be introduced (Figure 2.5). The extent to which the weave must shear is dependent on curvature, so the resulting directions of the fibres vary across the surface. The mechanical behaviour of the fabric is thus locally defined, introducing uncertainty into the mechanical modelling of the structure.

Image removed
due to copyright

Figure 2.5 - Illustration of shear deformation resulting from the tensioning of a planar net into doubly curved geometry – adapted from Wagner [18]

This shear-dependent mechanical behaviour of the fabric, and the low shear stiffness of the fabric, indicate the need for a suitable mechanical description of the surface. That the fabric must shear to adopt a doubly curved geometry highlights the fact that a suitable mechanical description is particularly necessary for modelling patterning. In terms of what might be considered a suitable mechanical description, the description must account for the shear-dependent directions of the fibres when translating strains into stresses.

Which model is most appropriate for fabric modelling, in the context of tensile structures, remains an issue of contention [20]. Fabric modelling has seen considerable investigation in the fields of both tensile structures and non-structural textiles and computer graphics, and concepts devised therein are relevant to fabric modelling for tensile structures. Across disciplines, fabric models can be divided into two broad categories, continuum and discrete models. These are now discussed and contrasted.

2.2.2 Continuum models and Finite Elements

2.2.2.1 Continuum models

Continuum models are the more popular choice for fabric modelling in the context of tensile fabric structures. As with traditional continuum mechanics, the fabric is homogenised and analysed using appropriate finite element methods.

Although tensile fabric structures are geometrically nonlinear, the stress-strain relationship for the material is typically assumed to be linear. Thus, linear elastic constitutive relationships for the material are employed, coupled with nonlinear displacement-strain relationships. In formulating the displacement-strain relationship for *geometrically linear* structures, higher order terms can be ignored [38], as the magnitude of such terms is negligible when displacements are small. In the case of tensile structures however, large displacements are required if the structure is to resist loading [39,40], and for the translation of the cutting pattern to the assembled configuration [3]. Thus higher order terms in the strain formulation cannot be neglected.

Tabarrok and Qin [39,40] included higher order terms in their strain measure literally, extending the linear measure by including quadratic terms in the displacement-strain relation. Kim and Lee [26] formulated the strain as the summation of linear and nonlinear strain components, each calculated from their respective displacements and displacement-strain matrices. More recent work [6,29,30,41] makes use of Green's strain [42,43] to account for geometric nonlinearity. Green's strain is the change in square length of each material vector, with respect to the reference configuration [42]. Comparing Green's strain as presented in [43] to the strain measure of Tabarrok and Qin [39,40], it can be seen that they are similar – similar higher order terms appear in both definitions, with different notation.

The constitutive relations between strain and stress incur further nonlinearities. Here it is important to consider whether the displacement-strain relations are formulated as large displacements resulting in small strains, or large displacements resulting in large strains. Tabarrok and Qin [39,40] argued that for small strains, *linear elastic plane stress constitutive relations* were appropriate. The model presented in [40], did not account for anisotropy,

material nonlinearity or hysteresis, nor the irregular relationships between tensile moduli, shear modulus and Poisson's ratios.

Tabarrok and Qin's [39,40] constitutive model is, in implementation, similar to that of simple hyperelasticity, for example, the Saint-Venant Kirchoff model, which is applied to membrane structures in [6,30,44,45]. The Saint-Venant Kirchoff model is distinct from linear elasticity in that the Green's strain replaces the engineering strain, and the Second Piola-Kirchoff stress replaces the engineering stress [42]. The second Piola-Kirchoff stress is a symmetric stress tensor, with its components aligned with the vectors of the reference configuration. Saint-Venant Kirchoff models complement the use of Green's strain to account for geometric nonlinearity. It has been reported that such an implementation leads to a simple linear relationship between Green's strain and Second Piola-Kirchoff stresses [44,45]. Additionally, it has been suggested that such a material model is suitable for small strains only [43], but can readily account for anisotropy [42].

Alternative material models have been formulated based on a *unit cell approach* [46,47]. Such methods considered the underlying microstructure of the fabric, and used these to derive constitutive relations that were then employed in finite element schemes [29,46]. Pargana's model [29] was, similar to Saint-Venant Kirchoff models, limited to small strains.

A further alternative is that suggested by Wakefield [48]. Here, the combination of natural element stiffnesses, and a convected coordinate system were used to account for geometric nonlinearity.

2.2.2.2 *Implementation by Finite Elements*

The aforementioned material models have been applied to a variety of finite elements, such as: 3-node triangular elements; with constant strain [30,48], or constant stress [39,40]; linear isoparametric triangular elements [44,45]; 4-node isoparametric quadrilateral elements [6], or

higher order elements, for example: 6-node quadratic finite elements, with linear strain descriptions and quadratic descriptions of the element side geometry. Whilst higher order elements have been used, historically it has been suggested that sufficiently dense meshes of simple elements are superior to coarser meshes of complicated elements [4,39,40].

Solution of the numerical schemes have been achieved with the Newton-Raphson method [6,26,30,40,44,45], and Dynamic Relaxation [48].

2.2.2.3 Drawbacks of continuum modelling

Most of the work on nonlinear continuum formulations, implemented using FEM for tensile fabric structures, has focused on accounting for the geometric nonlinearity of such structures. Continuum mechanics offers a readily applicable model through appropriate nonlinear strain measures, but these are not specific to fabrics, and rely on several concepts: (i) the fabric, which comprises discrete yarns with a continuous but irregular coating, is homogenised and considered to be continuous; (ii) the geometric nonlinearity arises as a result of large out-of-plane displacements, resulting in a change in the structure's geometry, and consequently stiffness, such that the assembly of the global stiffness matrix is no longer accurate.

As mentioned, the fabric of the cutting pattern must undergo shear deformation during assembly of the panels, for them to adopt the appropriate doubly curved shape. Since the tensile stiffness of fabrics is derived from the fibres, when the fabric shears, the principal directions of stiffness of the fabric change. This is not reflected in continuum modelling, because the material stiffness vectors do not change according to the deformation. Thus, the main drawback of continuum models is that they do not easily accommodate changes in the material properties of the fabric. For patterning, this is particularly important owing to the necessity for shearing. Similarly, the treatment of geometric nonlinearity can be achieved with a formulation of the

element strain and stresses in natural coordinates, as proposed in [48], negating the need for complex strain measures such as Green's strain.

2.2.3 Discrete models

Discrete element models are distinct from continuum finite elements, in that they represent materials by a grid of nodes, with interconnecting elements. In this way, they are designed to reflect the fact that fabric tends to behave as a structural mechanism, as postulated by Breen et al. [49], not as a homogeneous isotropic plate. The mass of the system is lumped to the nodes, unlike finite element methods, where the mass is continuous across the subdivided surface, and equilibrium is enforced locally at the nodes, rather than globally [50]. Discrete element models comprise many forms of varying complexity. Figure 2.6 shows the relation between the physical fabric configuration, and the discrete models used to model it. Various names are attributed to discrete models such as *composite crimp*, *particle-spring systems*, *spring-mass systems*, *coupled particle systems*, etc. In the context of fabric modelling, discrete element models have received attention in the fields of garment textile modelling [51,52], visualisation and animation [49,50,53–55], the mapping of textiles to 3D surfaces [56,57], and engineering fabrics [58].

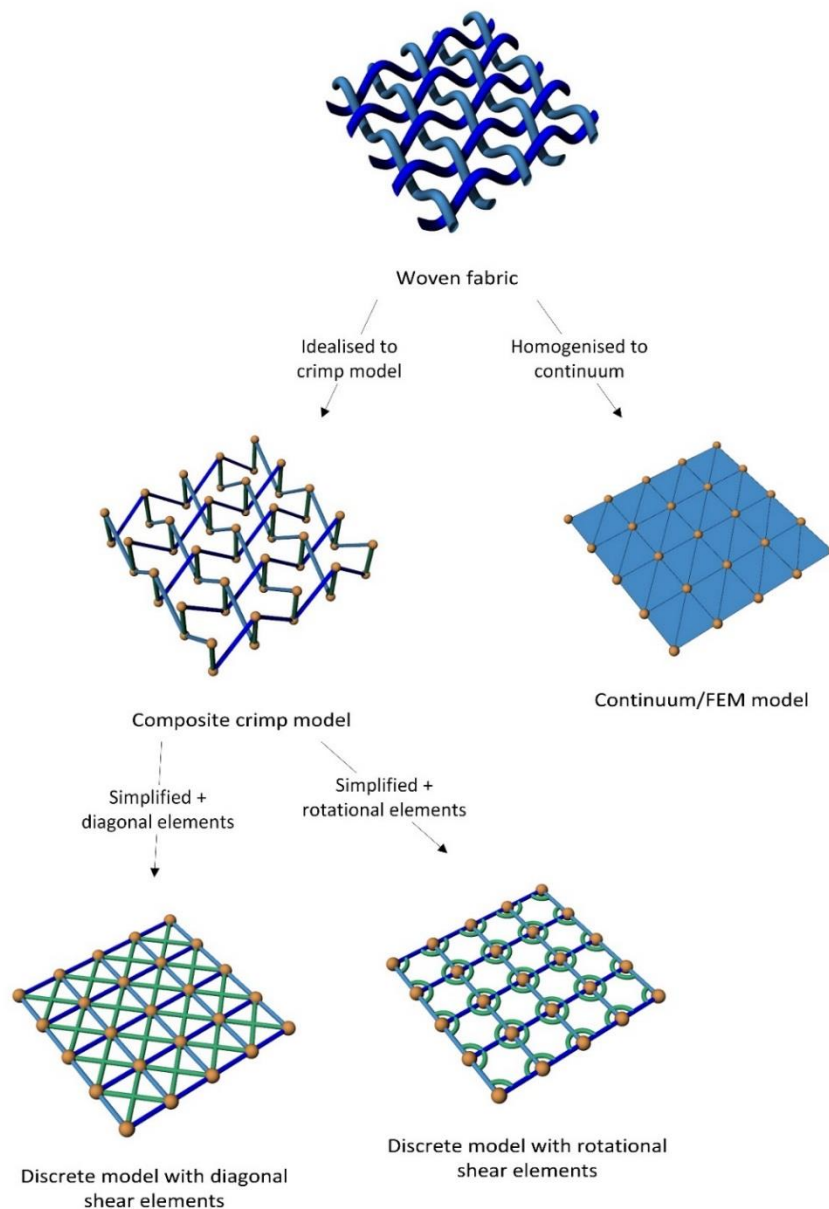


Figure 2.6 - Numerical models and their relation to base fabric

The discrete models that have been developed are, however, wide-ranging in their objectives, implementation and suitability for architectural fabric modelling. Models developed for use in visualisation [49,53–55] for example, naturally have focused on establishing the appearance of the deformed fabric correctly, rather than evaluating fabric stresses, and did not use real material properties to derive force-displacement relations. The model proposed in [50] incorporated material properties, indicating the potential for discrete elements to model real

physical behaviour, but the focus remained on visualisation. Work has been conducted to formulate discrete models from continuum mechanics, using real material parameters [51,52], such that stresses may be evaluated [51].

2.2.3.1 Deformation modes in discrete models

Multiple deformation modes are captured in discrete models, such as tensile, shear, yarn crimp/Poisson's ratio, bending/flexure, and twisting. In visualisation and garment fabric modelling, forces due to self-weight characterise the physical behaviour, due to the absence of external loading. In such cases, out-of-plane deformations arise due to, for example, buckling of the fabric under shear. In tensile structures, forces due to the self-weight of the fabric are negligible compared to the pre-stress and applied loads – self-weight has been reported to result in a change in the surface stress field of around 1% [24]. For this reason, the bending and twisting resistance of fabrics is negligible in the context of tensile fabric structures, and out-of-plane deformation due to buckling is of no interest – it is sufficient (and necessary) to simply incorporate the fabric's inability to resist compression loads.

For modelling tensile forces, discrete models that employ traditional material properties, such as Young's Modulus, derive the forces acting on the nodes from the stress-strain response of the surrounding fabric [51,52]. In [50] an additional fractional scaling factor was used to reduce the resistance of the fabric under negative straining. The method presented in [58] employed a variety of stiffnesses for each of the components of the model, having fitted these to experimental data. Other models that are not concerned with stresses, as noted above, either define tensile element stiffnesses for the specific visualisation [54], or derive the tensile resistance from energy functions [49,53].

Physical fabrics resist shear through friction between warp and weft fibres, and if coated, through stresses in the coating. In the context of tensile fabric structures, the friction between

fibres is negligible, and the shear response is dominated by the coating, as mentioned previously. The resistance of the fabric to shear deformation has been modelled in a number of ways. The simplest method is the addition of springs along the diagonal between nodes [54,56,57]. As noted in [55], introducing diagonal springs has the effect of causing transverse contraction of the fabric under uniaxial tensile load; in principle acting similar to Poisson's ratio. Since the shear resistance of architectural fabrics derives principally from the coating material, and the Poisson's ratio derives from the crimp effects of the fibres, it is advisable for these mechanisms to be decoupled in fabric modelling, and thus the use of diagonal springs is problematic. However, such an implementation of shear resistance in the context of the mapping textiles to 3D surfaces is of interest. In this context, deformation of the fabric during mapping is controlled by the ratio of stiffnesses between tensile and shear springs [57], highlighting the shear-dependent behaviour of the mapping. Stresses were, however, not calculated in [57].

Alternatively, the shear stiffness of the fabric may be modelled as a resistance to angular deformation between the warp and weft fibres at a node. This can be realised by introducing a rotational spring element between fibres at a node, calculating the in-plane moment of this spring, and deriving the equivalent restoring forces at nodes away from the spring [51,58]. Forces applied away from the location of angular deformation have also been derived from shear of the continuum [52] or from the energy functions for trellising [49,53]; in the case of energy functions, material properties were not considered. A further alternative is to reverse the shear forces required to produce angular deformation at a node, and apply these as a resultant force along the direction of the diagonal bisecting warp and weft fibres, as proposed in [50].

Several models are particularly relevant for the development of a discrete model for patterning.

These are summarised here:

- Ballhause et al. [58] employed fibre tensile elements, fibre shear elements, fibre crimp elements, coating tensile elements and coating shear elements.
- Dai et al. [51] employed extension springs, rotational springs for resisting shear, bending springs and twisting springs.
- Etmuss et al. [52] employed tension stress elements and shear stress elements, and a further calculation to model bending of the material.
- Eischen & Bigliani [50] employed square 'cells' comprising four tensile springs. Shear was modelled using an additional function derived for the square cell, and out-of-plane bending was modelled considering lines of three nodes.

Discrete element models are sensitive to the topology of their elements. In particular, triangulated meshes of discrete elements have been mentioned to be unsuitable [52] (originally [59]), not offering accurate simulation. It is stated in [60] that the issues in [59] stem from incorrect prescription of the Poisson's ratio. However, this discussion takes place in the context of modelling of isotropic solids with spring-meshes that are topologically identical to FEM meshes. Such an approach to modelling does not account for the fact that fabrics are anisotropic and heterogeneous. Fabrics comprise woven fibres that are arranged with a grid-like topology, and discrete models that reflect this topology are suitable [52].

2.2.4 Numerical modelling for patterning - research objectives identified

As mentioned, there remains controversy over which fabric model is most suitable for tensile fabric structures. The suitability of various models for patterning is a particular sub-problem of this larger discussion. Most models have been developed for application to all stages of the design process. Patterning, and in particular the assembly of the cutting patterns into the final

shape to evaluate the patterning procedure, encompasses specific material behaviour not found during, for example, load analysis. The material behaviour in patterning is characterised by:

1. **A dependence on the shear deformation of the fabric.** The fabric must shear to adopt its 3D form, and with this, changes in the principal stiffness directions of the fabric are present. This behaviour, and its effect in the computational process, must be accounted for in the mechanical model.
2. **An absence of hysteresis and crimp-interchange.** As mentioned in section 2.2.1, compensation parameters should be determined based on the behaviour of fabric subjected to load-cycling. Similarly, the evaluation of the cutting pattern, through simulation of the pattern assembly, should use material properties based on cycled fabric. For this reason, hysteretic behaviour and crimp-interchange effects need not be modelled.

Of the above characterisations, the necessity for the fabric to shear, and the effect of this on the fabric behaviour is most important. Since the shearing of the fabric is dependent on curvature, higher curvatures lead to greater differences in the behaviour of the fabric compared with planar fabrics. For structures of more complex geometry, accounting for changes in the fibre direction, and the consequent changes in the material response, becomes particularly important. It is on this basis that research objective **RO 1** was suggested in chapter 1.

2.3 Summary

This chapter has presented a review of tensile fabric structures and the appropriate literature relating to their design and analysis. This review of the literature drew attention to two areas which merit further research: (i) patterning, and (ii) numerical modelling of fabric behaviour. It is against this background that the research objectives from chapter 1 were proposed.

Numerical models for, and processes within, patterning, the focuses of this thesis, have been discussed in detail. The main points from this chapter are now summarised:

Patterning

- Appropriate form-found shapes for tensile membranes should be doubly curved. Such double curvature, along with pre-stress, allows the membrane to sustain imposed loads through non-excessive deformation of the surface.
- Doubly curved shapes are, however, not developable. Non-developability, and manufacturing constraints on the size of fabric panels necessitate a specialist design process be conducted. Patterning is thus used to determine the panels, which cut from planar fabric, will form the final membrane shape.
- Patterning comprises four sub-processes: (i) subdivision of the membrane; (ii) flattening of the panels; (iii) reduction of the planar panel stresses; and (iv) compensation of the panels to account for pre-stress. A further process is usually included to evaluate the performance of the final cutting pattern: (v) simulation of the assembly of the cutting patterns.

Numerical modelling

- Architectural fabrics exhibit complex material behaviour, such as nonlinearity, anisotropy and hysteresis, though these complexities are often reduced to linear constitutive relationships, and tensile fabric structures are geometrically nonlinear.
- Numerical modelling for fabrics has been explored outside of the field of tensile fabric structures. Here discrete models are more prevalent. Such discrete models offer promising methods for modelling tensile fabric structures, in particular for accommodating weave shear.

2.4 Identified gaps in knowledge

In addition to the points outlined in section 2.3, several gaps in knowledge were identified:

Patterning

- Much attention has been given to stress reduction, but few investigations have looked at improving computational efficiency through advanced flattening methods.
- For the cutting pattern to adopt a doubly curved shape, shear deformation is necessary. Shear deformation is a critical component of the problem of cutting pattern definition.

Numerical Modelling

- Little attention has been given to the effect of the weave shear on the fabric mechanical response. Numerical models for tensile fabric structures have either focussed on accounting for geometric nonlinearity in the structure, or modelling complex material behaviour on a small scale, e.g. fabric specimens under testing, rather than full scale tensile structures.
- Material behaviour during patterning is dominated by shear-dependency, and crimp interchange effects are less pronounced. A numerical model for patterning which reflects these characteristics is therefore desirable.

2.5 Research objectives and consequent direction of this thesis

In light of the identified gaps in knowledge, several research objectives were identified, as summarised in section 1.6. How the objectives relate to the identified gaps in knowledge, arising from the literature review, is elaborated below:

- The behaviour of the fabric during patterning is heavily dependent on shear deformation, yet little work has been conducted to address this. Discrete models offer a straightforward solution for modelling this behaviour, but have not been applied to tensile fabric structures. Thus, developing a discrete model that fully incorporates

material parameters and accounts for weave shear, and applying this to the problem of membrane patterning, would be desirable. This is the focus of **RO1**.

- Flattening methods have not been widely investigated, but where simple methods reduce distortions, they can be used to improve computational processes and the eventual cutting patterns. Developing novel flattening methods would be desirable. This is the focus of **RO2 (a)**.
- The effect of including or excluding the shear stiffness of the fabric, throughout patterning, has not been examined. Since the shear stiffness may be ignored, this is an important point of investigation. This is the focus of **RO 2 (b)**.

2.6 Research methodology

To address the research objectives, the following the following research methodology was employed:

1. Identification of the gaps in knowledge
 - 1.1. A full literature review was conducted, and gaps in the existing knowledge base were identified. This step was presented in this chapter.
2. Development of a numerical model and patterning method to address gaps in knowledge
 - 2.1. A discrete element model was developed to model the fabric membrane during patterning. The discrete model, and solution by the dynamic relaxation method, was implemented by programming in VB.Net. This is detailed in chapter 3.
 - 2.2. A patterning method was proposed, including advanced flattening methods, and implemented by programming in VB.Net. This is detailed in chapter 4.
3. Comparison with previous work, to evaluate the developed numerical model and patterning method.

3.1. With the discrete model and patterning method implemented in a software package, analyses using the geometry from existing work were conducted.

3.2. These analyses facilitated evaluation of the suitability of the proposed model, and definition of conditions for the successful use of the proposed discrete model.

2.7 Contributions to knowledge

The principal contributions to knowledge were made by addressing the identified gaps in knowledge, through the methodology outlined above. The contributions to knowledge of this thesis are:

- The development of a numerical model capable of accommodating weave shear, which is suitable for the modelling of tensile fabric structures.
- The evaluation of the numerical model and identification of conditions for its successful use.
- The development of advanced flattening methods, and evaluation of their suitability.
- The investigation of the effect of including the shear stiffness of the fabric in patterning analyses.

The discrete model and patterning method developed in pursuit of these contributions to knowledge are detailed in the following chapters.

3 Development of discrete element model

This chapter describes the fabric mechanical model and solution method, and how these are implemented in the numerical model. Given the considerations outlined previously, research objective **RO 1** – the development of a discrete model for patterning – was suggested. In fulfilment of this research objective, the discrete model presented in this chapter was developed.

In developing a mechanical model for architectural fabrics and patterning, there are several relevant points to be considered:

1. Architectural fabrics behave more like a structural mechanism than a continuum (as originally postulated by Breen et al. [49]).
2. Shearing of the weave is a critical component of the fabric deformation when assembling cutting patterns from planar fabric. Formulation of the mechanical model must reflect the effect this has on the stiffness and consequent response of the fabric to deformation and load.
3. Material behaviour at the patterning stage assumes some pre-cycling of the fabric. Thus crimp interchange effects need not be modelled.

Discrete models can encapsulate the above characteristics, and on this basis a discrete model is proposed by the author in this chapter. Several discrete models were discussed in the previous chapter (section 2.3.3), and particular emphasis was given to those presented by Ballhause et al. [58], Dai et al. [51], Etmuss et al. [52], and Eischen & Bigliani [50]. These existing models are of varying suitability for modelling architectural fabrics in the context of the patterning of tensile fabric structures. Thus a new model is proposed.

Critical characteristics for the model

In light of architectural fabric behaviour at the patterning stage, some critical characteristics are suggested:

1. The principal deformation modes in architectural fabrics are tension, resisted by the fibres, and shear of the weave, occurring in the local plane of the fabric, resisted by the coating. The bending resistance of fabrics is negligible and should be excluded from the model. Similarly the twisting resistance of fabrics is negligible and should be ignored.
2. For straightforward implementation and comparison with finite elements, typical material properties such as (i) elastic moduli in the warp and weft directions, and (ii) shear modulus, should be used. Some models, e.g. Ballhause et al. [58] use properties specific to the model, precluding straightforward implementation of typical material properties.
3. The geometries of the fabric panels, during all stages of patterning, are not rectilinear. Irregular spacing of nodes and elements is required to describe this geometry, and the model should accommodate this requirement.
4. It is impractical to model every fibre of the fabric with a corresponding element in the computational model. Whilst the directions of fibres are shear dependent across the whole surface, the difference in the fibre directions across small widths is negligible. For this reason, the fibres are assumed to be parallel for the width of fabric represented by one tensile element.

3.1 Proposed discrete element model

It is against the characteristics stated above that a moment-less discrete model is proposed, in which tensile elements in the two directions of warp and weft are employed to describe the fabric (Figure 3.1). Individual elements represent a width of fabric defined by the spacing of the

mesh, and consequently represent the approximate direction of fibres across this width. Stiffnesses are attributed to these elements depending on whether they represent warp or weft directions. These elements are assumed orthogonal in the planar cutting pattern, and as will be seen in later sections, can be assumed to follow geodesic paths over the 3D form-found surface. The shear response of the fabric is modelled by evaluating the rotation between warp and weft elements at the nodes, and considering the forces required to produce this shear deformation. A detailed description of the model is presented in the following sections.

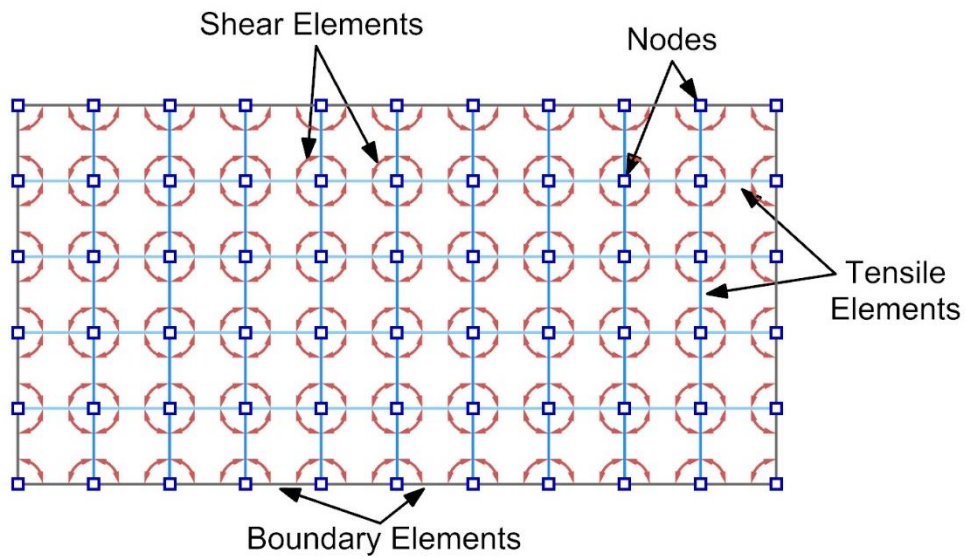


Figure 3.1 – Proposed discrete element mesh, comprising tensile elements, shear elements, and nodes

A feature of the discrete model is that to describe non-rectilinear geometries, elements that do not follow the direction of warp or weft are required. These elements contribute to the geometric description of the surface and its edges, but do not contribute to the calculation of forces or evaluation of stresses during the mechanical simulation.

3.1.1 Treatment of tensile deformation

Modelling the resistance of the fabric to tensile deformation is handled by line elements in the two principal directions of the fabric, the warp and weft directions. The following sections describe the calculations for these elements.

3.1.1.1 Strain calculation

Strain in an element is calculated from the scalar reference length of the element L_0 , and the scalar current length of the element L (Figure 3.2), where lengths are calculated from the position vectors of the nodes in the appropriate configuration. Such a strain calculation can be thought of as the prescription of a 1-Dimensional co-rotational basis, with its axis defined along the vector between node A and node B. In this way, the strain calculation for tensile elements accommodates large rigid body translations and rotations of the element, thus overcoming issues associated with geometric nonlinearity.

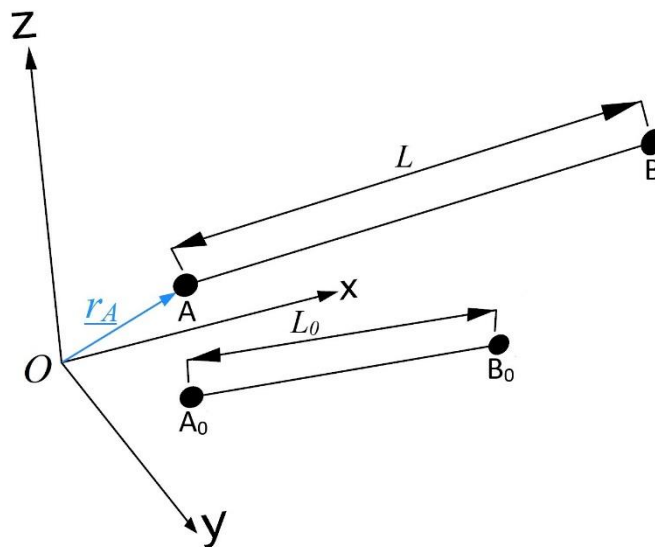


Figure 3.2 - Deformation of a single tensile element in 3D space

The strain ε is given by:

$$\varepsilon = \frac{L}{L_0} - 1 \quad (3.1)$$

Where:

$$\begin{aligned} L &= \left| \underline{r}_B - \underline{r}_A \right| \\ L_0 &= \left| \underline{r}_{B_0} - \underline{r}_{A_0} \right| \end{aligned} \quad (3.2)$$

Where \underline{r}_A and \underline{r}_B (Figure 3.2) are the position vectors, in the current configuration, of nodes A and B respectively, and \underline{r}_{A_0} and \underline{r}_{B_0} are the position vectors, in the original configuration, of nodes A and B respectively.

3.1.1.2 Stress calculation

A linear constitutive relationship is used for calculating the tensile stress. Elements represent either the warp or weft direction of the fabric.

Thus for an element the stress (σ) is calculated from:

$$\sigma = E_{(w/f)} \varepsilon + \sigma_{P(w/f)} \quad (3.3)$$

Where $E_{(w/f)}$ is the tensile modulus of the fabric in either the warp (w) or weft (f) direction, ε is the element longitudinal strain, and $\sigma_{P(w/f)}$ is the prescribed pre-stress in either the warp (w) or weft (f) direction. For warp elements, the tensile modulus and pre-stress in the warp direction are used, for weft elements, the tensile modulus and pre-stress in the weft direction are used.

The combination of warp and weft elements describe the state of stress in the fabric in both the warp and weft directions.

3.1.1.3 Element width calculation

Each tensile element within the discrete model represents a patch of the fabric adjacent to it. For calculation of the forces, the width of the fabric that the element represents is required. This is instead of the cross sectional area, since material properties and stresses for architectural fabrics are given in units of force/width rather than force/area.

The width is calculated by equating the relevant surface area of the fabric surrounding the element, to a rectangular strip of fabric with area and length equal to that of the element (Figure 3.3). In this way the width calculation for the element can accommodate initial configurations of the elements which are irregular and not orthogonal. This is particularly useful for the flattening stage of patterning, where a mesh on the 3D surface must be constructed (section 4.1.2.1), and calculating the widths of the elements is not trivial.

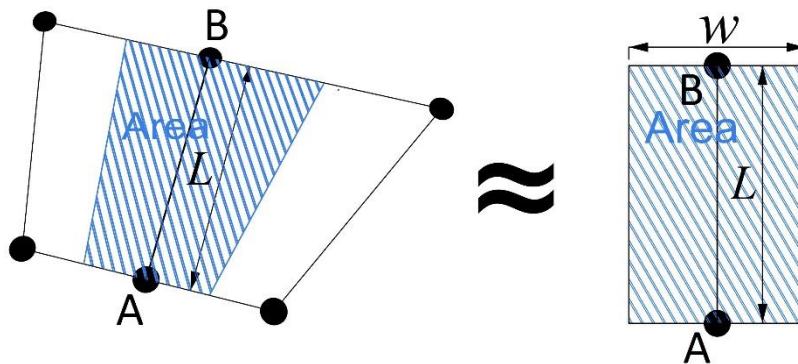


Figure 3.3 - Area of fabric represented by a given element

Elements are bounded by either one or two areas – elements that lie on the boundary have one adjacent area, internal elements have two adjacent areas. For example, the element A-B shown in Figure 3.3 has two areas, A1 and A2 adjacent to it (Figure 3.4):

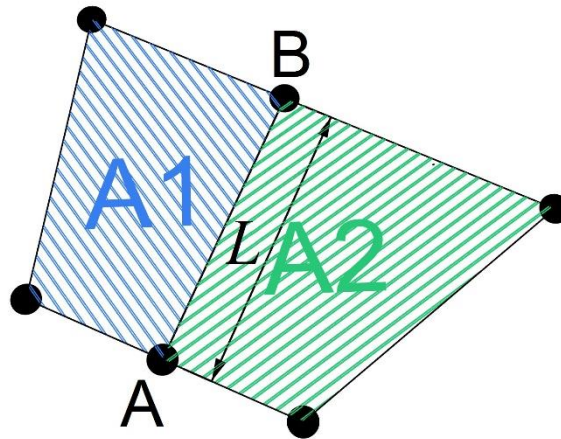


Figure 3.4 – Areas bound by other elements, adjacent to the element for which the width is being calculated

The total surface area that the element A-B represents is the sum of the halves of each adjacent bounding area. The width is therefore calculated from:

$$w = \left(\frac{A_1}{2} + \frac{A_2}{2} \right) \frac{1}{L} = \frac{A_1 + A_2}{2L} \quad (3.4)$$

Where w is the width of the element, A_1 is the first adjacent area, A_2 is the second adjacent area, and L is the length of the element.

When meshing non planar geometries, such as when creating a mesh for flattening on the form-found surface, where an adjacent area is formed by a quadrilateral, this quadrilateral will not necessarily lie in a plane. To circumvent this issue, the centre of the quadrilateral is found from the intersection of the lines from opposing midpoints, and split into 4 triangles (Figure 3.5). The areas of these triangles are calculated and summed to give the area of the quadrilateral.

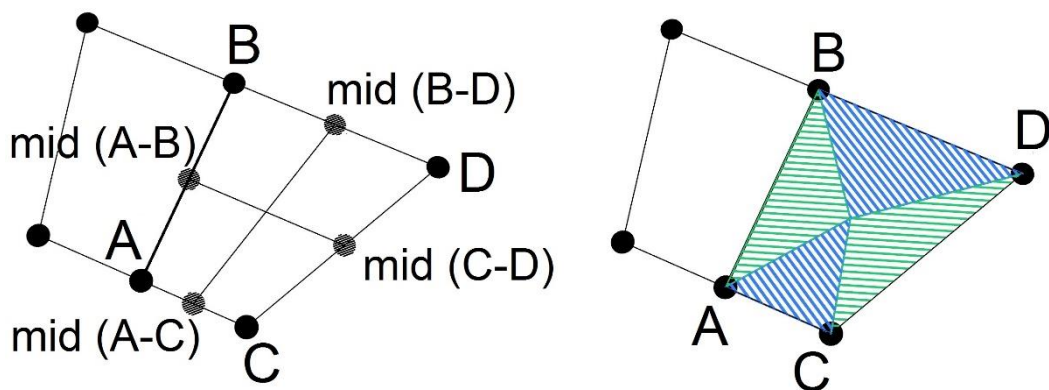


Figure 3.5 - Calculation of area by splitting a quadrilateral into four triangles

3.1.1.4 Non-rectangular edge geometries

Further complications arise when meshing geometries with non-rectangular boundaries. Since the tensile elements represent either the warp or weft directions of the fabric, boundary elements that do not lie in either direction are excluded from the calculation. Thus when calculating the area which an element represents, taking half of the area from either side of the element results in part of the fabric being unattributed to any element e.g. the green triangular patch in Figure 3.6. Referring to Figure 3.6, calculating the width for element A-B requires that the whole adjacent area A-B-C, not half, should be apportioned to the element (Figure 3.7).

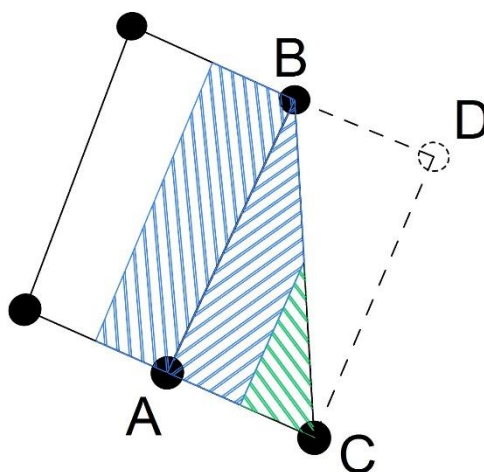


Figure 3.6 - Omission of part of the fabric from the material response, if only half of the area is used to define the width for elements adjacent to non-parallel boundaries

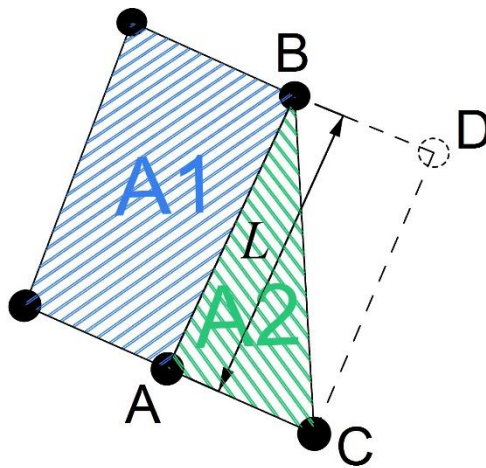


Figure 3.7 – Relevant areas when calculating width for element A-B

Thus, referring to the areas in Figure 3.7, the calculation of the width for element A-B is adjusted to:

$$w = \frac{A_1}{2L} + \frac{A_2}{L} \quad (3.5)$$

Where w is the width of the element, A_1 is the first adjacent area, A_2 is the second adjacent area, L is the length of the element.

3.1.1.5 Force from stress and width

The force is simply calculated by multiplying the stress by the width. This includes both the stress due to straining, and the pre-stress. The tensile force F in an element is thus calculated from equation 3.6:

$$F = \sigma w \quad (3.6)$$

Where σ is the stress in the element, and w is the width of the element, calculated using the methods outlined in 3.1.1.3 & 3.1.1.4.

3.1.1.6 Forces applied to nodes

The force calculated from equation 3.6 is a scalar, so to drive the dynamic relaxation algorithm, it must be resolved into global components. This is achieved by multiplying the scalar force in the element, by the element direction unit vector, which is defined as:

$$\underline{d} = \frac{\underline{r}_B - \underline{r}_A}{|\underline{r}_B - \underline{r}_A|} \quad (3.7)$$

Where \underline{r}_A and \underline{r}_B are the position vectors in the current configuration of nodes A and B (Figure 3.2). This vector is reversed, depending on whether the force is being apportioned to node A or B.

3.1.2 Treatment of shear deformation

3.1.2.1 Remarks on methods of modelling shear in discrete models

Numerous methods for modelling the shear response of the fabric were identified in the literature review. The method, adopted in the proposed model, of modelling the shear response of the fabric is similar to that presented in [50], but differs in several ways.

Consider the following pure shear deformation of an initially orthogonal quadrilateral piece of fabric (Figure 3.8):

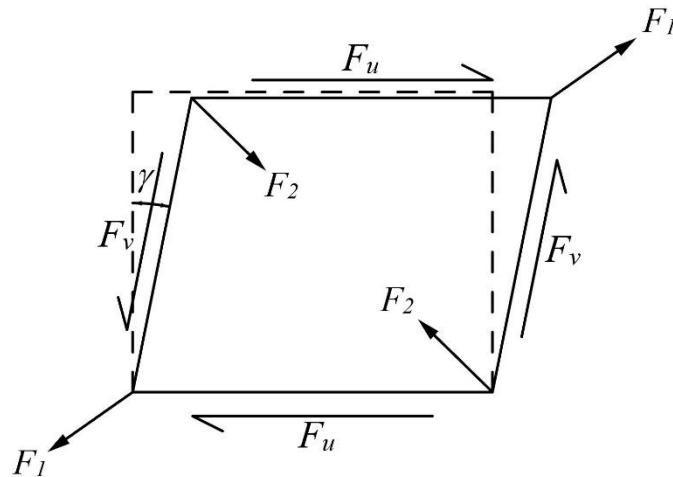


Figure 3.8 - Shear forces producing shear strain on quadrilateral piece of fabric

The shear forces F_u and F_v can be resolved into single forces applied at the corners. The model in [50] took the shear strain γ , calculated the shear stress, and formulated the resolved forces F_1 and F_2 as forces acting along the diagonals of the fabric patch. Implicit in this calculation was the requirement that shear strains of the same magnitude be present at each of the four corners. It is important to note that changes in the edge lengths, due to straining in the tensile elements, mean that the shear strain will not necessarily be constant across a given quadrilateral. Furthermore, the diagonal of the unstrained quadrilateral was used to derive the forces [50], limiting the formulation to small displacements and thus geometrically linear behaviour.

The model in [50] was also limited to square patches – square patches give $F_1 = F_2$. In the discrete model this corresponds to an equal spacing of nodes. Furthermore, the shearing forces were calculated for a square patch on the assumption that the patch remains within its own plane [50]. Since out of plane deformation is necessary for the 2D cutting pattern to adopt a 3D doubly curved shape, there is no guarantee that a given square patch will remain in plane.

A formulation not restricted to equally spaced planar quadrilaterals, but retaining the simple relation between shear strain and forces apportioned to nodes, is proposed and implemented by the author. The model presented here formulates the shear response by considering the change in angle between two tensile elements, and apportions forces to their common node. Additionally, the vectors of the deformed configuration are used to establish the direction of the forces, accommodating larger displacements and rigid body transformations.

The model proposed by the author is subject to the following limitations; (i) the effect of out-of-plane deformation is ignored, and (ii) the constitutive relationship is modelled as linear. Limitation (i) is considered acceptable because the out-of-plane bending and twisting resistance of architectural fabrics is negligible. Additionally, the shearing formulation considers angle changes between two elements (which by definition are within their own plane), meaning that no spurious shear strain is introduced by out-of-plane deformations. Limitation (ii) is considered acceptable because the model is developed for patterning analyses, and for the comparatively low stresses occurring during patterning, the fabric behaviour may be idealised as linear.

The shear model proposed by the author is now presented in detail.

3.1.2.2 *Shear strain between elements*

The shear strain is measured as the change in the angle between warp and weft elements at a node, from an initial rest angle ϕ_0 (Figure 3.9):

$$\gamma = \phi_0 - \phi \quad (3.8)$$

Where γ is the shear strain, measured in radians, and ϕ is the angle between the warp and weft elements in the current configuration.

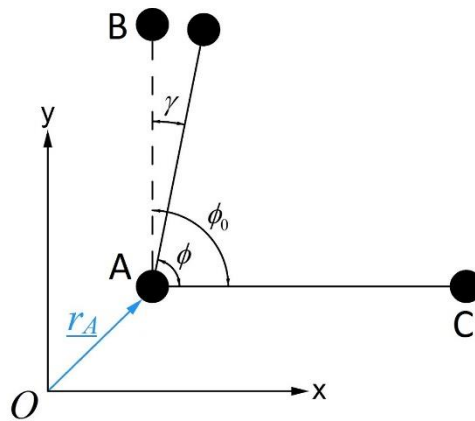


Figure 3.9 - Shear strain represented as angle change between warp and weft elements

The angle ϕ is calculated from the dot product of the relevant position vectors $\underline{r}_A, \underline{r}_B$ & \underline{r}_C of the nodes A, B & C respectively:

$$\phi = \cos^{-1} \left(\frac{(\underline{r}_C - \underline{r}_A) \cdot (\underline{r}_B - \underline{r}_A)}{|\underline{r}_C - \underline{r}_A| |\underline{r}_B - \underline{r}_A|} \right) \quad (3.9)$$

In this way, the shear strain is calculated in the plane defined locally by the vectors of the two elements. Equation 3.8 indicates that a reduction in the angle between two elements gives a positive shear strain.

3.1.2.3 Shear stress

Shear stress τ is calculated from the shear strain defined in equation 3.8, and the shear modulus G (measured in kN/m), through a linear constitutive relationship:

$$\tau = G\gamma \quad (3.10)$$

3.1.2.4 Shear forces and fabric response

To drive the solution method, the stresses must be related to forces at the nodes. The shear forces required to produce the deformation shown in Figure 3.9, are shown on the deformed configuration, in Figure 3.10.

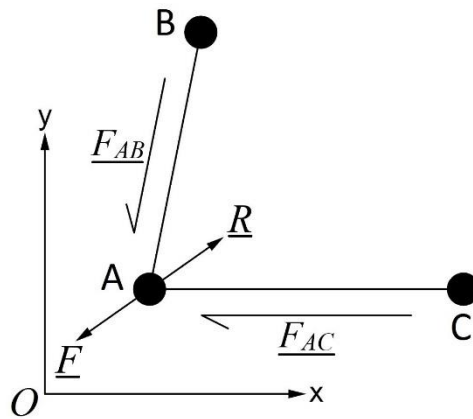


Figure 3.10 - Shear forces, resolved shear force, and resistance force for shear deformation in Figure 3.9

The two shear forces, \underline{F}_{AB} and \underline{F}_{AC} , acting along sides $\underline{v}_{BA} = \underline{r}_A - \underline{r}_B$ and $\underline{v}_{CA} = \underline{r}_A - \underline{r}_C$, can be resolved into one force acting at node A. The magnitude of each shear force may be calculated from the shear stress, and the appropriate length, which is the magnitude of the vector \underline{v}_{BA} or \underline{v}_{CA} , depending on which shear force is being calculated:

$$|\underline{F}_{AC}| = \tau |\underline{v}_{CA}| \quad (3.11)$$

$$|\underline{F}_{AB}| = \tau |\underline{v}_{BA}| \quad (3.12)$$

Where $|\underline{F}_{AC}|$ and $|\underline{F}_{AB}|$ are the magnitudes of forces \underline{F}_{AC} and \underline{F}_{AB} respectively.

To calculate the vector expressions of forces \underline{F}_{AC} and \underline{F}_{AB} , their magnitudes are multiplied by their directions. The directions are given by the relevant unit vectors:

$$\underline{F}_{AC} = (\tau |\underline{v}_{CA}|) \underline{v}_{CA} \quad (3.13)$$

$$\underline{F}_{AB} = (\tau |\underline{v}_{BA}|) \underline{v}_{BA} \quad (3.14)$$

Where the bracketed parts of equations 3.13 and 3.14 are the magnitudes of the shear forces, and \underline{v}_{CA} and \underline{v}_{BA} are the unit vector directions of the respective forces.

Each force is thus the shear stress, multiplied by the magnitude of the appropriate vector, multiplied by the appropriate unitised vector. However, the relationship between a vector, its magnitude and its corresponding unit vector is the following (for an arbitrary vector \underline{u}):

$$\underline{u} = |\underline{u}| \underline{u} \quad (3.15)$$

Thus forces \underline{F}_{AB} and \underline{F}_{AC} may be simplified:

$$\underline{F}_{AC} = \left(\tau |\underline{v}_{CA}| \right) \underline{v}_{CA} = (\tau) \left(|\underline{v}_{CA}| \underline{v}_{CA} \right) = \tau \left(\underline{v}_{CA} \right) \quad (3.16)$$

$$\underline{F}_{AB} = \left(\tau |\underline{v}_{BA}| \right) \underline{v}_{BA} = (\tau) \left(|\underline{v}_{BA}| \underline{v}_{BA} \right) = \tau \left(\underline{v}_{BA} \right) \quad (3.17)$$

Force \underline{F} in Figure 3.10 is the vector sum of the two vector shear forces:

$$\underline{F} = \underline{F}_{AC} + \underline{F}_{AB} = \tau \left(\underline{v}_{CA} + \underline{v}_{BA} \right) \quad (3.18)$$

Force \underline{F} is the force required to produce a shear strain of γ at node A. Thus, given a shear strain γ , the force generated by the fabric to resist this deformation is the vector opposite of \underline{F} , and is given as \underline{R} :

$$\underline{R} = -\underline{F} = \tau \left(\underline{v}_{AC} + \underline{v}_{AB} \right) \quad (3.19)$$

The shear force is defined in the plane defined locally by the two element vectors, but is expressed in terms of global coordinates. It can thus be apportioned to the nodes directly.

3.1.3 Examination of the proposed shear model - shear forces for a simple square

The method outlined above is now demonstrated. A simple square of fabric, subjected to a small shearing strain, is modelled using two methods. The forces acting at the corners are first calculated by treating the patch as a continuum and resolving the edge forces. Second, the patch of fabric is replaced by an equivalent representation comprising the discrete elements proposed above, and the forces at the corners are calculated using the equations in section 3.1.2.

3.1.3.1 Calculation of corner forces by treating the patch as a continuum

In this sub-section, calculation of the restoring forces at the corners, by treating the patch of fabric as a continuum, is shown.

The square of fabric, dimensions $L \times L$, in Figure 3.11 undergoes a small shearing strain γ consistent with pure shear. The shear forces required to produce such a deformation are F_u and F_v .

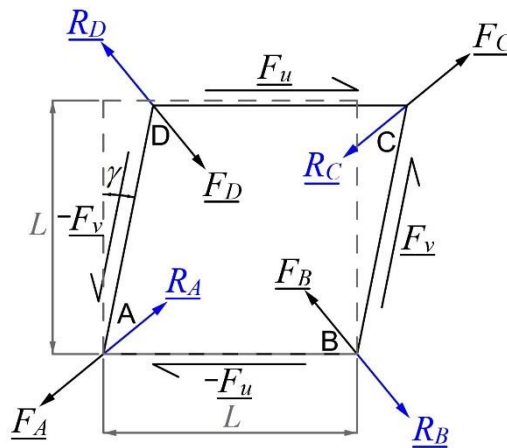


Figure 3.11 - Square of fabric, dimensions $L \times L$, with shear action forces, and corner reactions

By symmetry F_u & F_v have equal magnitude but different direction, and the magnitudes of these shear forces acting along the edges of the square are given by:

$$|\underline{F}_u| = |\underline{F}_v| = G\gamma L \quad (3.20)$$

For small displacements, the difference between the reference configuration and the deformed configuration is negligible. Thus the unit direction vectors of the edge shearing forces are:

$$\underline{F}_u = (1, 0) \quad (3.21)$$

$$\underline{F}_v = (0, 1) \quad (3.22)$$

The forces $\underline{F}_A, \underline{F}_B, \underline{F}_C$ & \underline{F}_D , at nodes A, B, C, & D respectively, can be simply computed by the vector sum of the appropriate forces:

$$\underline{F}_A = \left| -\underline{F}_u \right| \left(-\underline{F}_u \right) + \left| -\underline{F}_v \right| \left(-\underline{F}_v \right) = G\gamma L \left((-1, 0) + (0, -1) \right) = G\gamma L (-1, -1) \quad (3.23)$$

$$\underline{F}_B = \left| -\underline{F}_u \right| \left(-\underline{F}_u \right) + \left| \underline{F}_v \right| \left(\underline{F}_v \right) = G\gamma L \left((-1, 0) + (0, 1) \right) = G\gamma L (-1, 1) \quad (3.24)$$

$$\underline{F}_C = \left| \underline{F}_u \right| \left(\underline{F}_u \right) + \left| \underline{F}_v \right| \left(\underline{F}_v \right) = G\gamma L \left((1, 0) + (0, 1) \right) = G\gamma L (1, 1) \quad (3.25)$$

$$\underline{F}_D = \left| \underline{F}_u \right| \left(\underline{F}_u \right) + \left| -\underline{F}_v \right| \left(-\underline{F}_v \right) = G\gamma L \left((1, 0) + (0, -1) \right) = G\gamma L (1, -1) \quad (3.26)$$

The resistance of the fabric to these shearing forces, and therefore the forces $\underline{R}_A, \underline{R}_B, \underline{R}_C$ & \underline{R}_D that should be generated at the corners to restore equilibrium, are the vector opposite of those calculated above:

$$\underline{R}_A = G\gamma L (1, 1) \quad (3.27)$$

$$\underline{R}_B = G\gamma L(1, -1) \quad (3.28)$$

$$\underline{R}_C = G\gamma L(-1, -1) \quad (3.29)$$

$$\underline{R}_D = G\gamma L(-1, 1) \quad (3.30)$$

3.1.3.2 Calculation of the corner forces using the proposed discrete model

Now the same patch of fabric is replaced with an equivalent representation of the proposed discrete elements and nodes. The restoring forces acting at the corners (now represented by the nodes) are calculated using the equations from section 3.1.2, as in the proposed discrete model.

By calculating the forces acting on the nodes using the proposed discrete model, it is shown that the method converges to the same result as that found by treating the patch as a continuum (section 3.1.3.1).

Figure 3.12 shows the square of fabric replaced with 4 nodes and 4 elements.

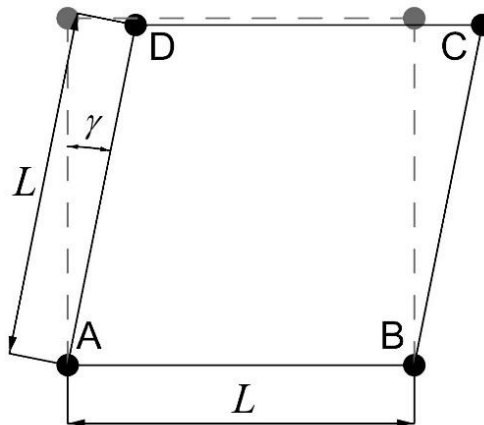


Figure 3.12 - Equivalent representation with proposed discrete elements

The position vectors of the nodes in the deformed configuration are calculated, taking A as the origin, as:

$$\underline{r}_A = (0, 0) \quad (3.31)$$

$$\underline{r}_B = (L, 0) \quad (3.32)$$

$$\underline{r}_C = (L(1 + \sin \gamma), L \cos \gamma) \quad (3.33)$$

$$\underline{r}_D = (L \sin \gamma, L \cos \gamma) \quad (3.34)$$

To find the forces at node A, a free body diagram is drawn (Figure 3.13).

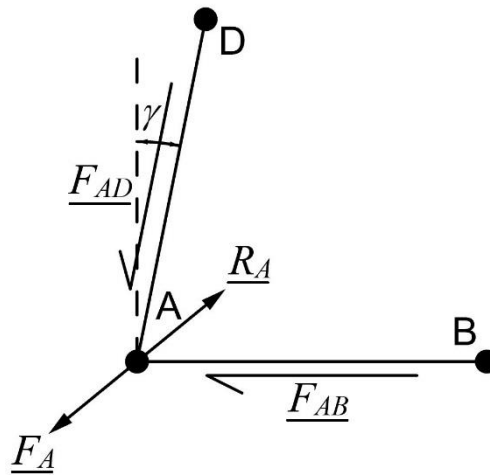


Figure 3.13 - Free body diagram of node A

Equation 3.19 is used to calculate the force \underline{R}_A acting on the node.

$$\underline{R}_A = \tau (\underline{v}_{AB} + \underline{v}_{AD}) \quad (3.35)$$

$$\underline{v}_{AB} = \underline{r}_B - \underline{r}_A = (L, 0) - (0, 0) = (L, 0) \quad (3.36)$$

$$\underline{v}_{AD} = \underline{r}_D - \underline{r}_A = (L \sin \gamma, L \cos \gamma) - (0, 0) = (L \sin \gamma, L \cos \gamma) \quad (3.37)$$

Since $\tau = G\gamma$, \underline{R}_A from Eq. 3.35 becomes:

$$\underline{R}_A = G\gamma [(L, 0) + (L \sin \gamma, L \cos \gamma)] \quad (3.38)$$

$$\underline{R}_A = G\gamma(L(1 + \sin \gamma), L \cos \gamma) \quad (3.39)$$

Since γ is small, the small angle assumption may be used:

$$\begin{aligned} \sin \gamma &\approx \gamma \\ \cos \gamma &\approx 1 \end{aligned} \quad (3.40)$$

This gives \underline{R}_A as:

$$\underline{R}_A = G\gamma(L(1 + \gamma), L) \quad (3.41)$$

Factorising gives:

$$\underline{R}_A = (G\gamma L + G\gamma^2 L, G\gamma L) \quad (3.42)$$

Similarly, since γ is small, higher order terms, and specifically the γ^2 term, are negligible, reducing \underline{R}_A to:

$$\underline{R}_A = (G\gamma L, G\gamma L) = G\gamma L(1, 1) \quad (3.43)$$

\underline{R}_B is calculated in the same way (Figure 3.14):

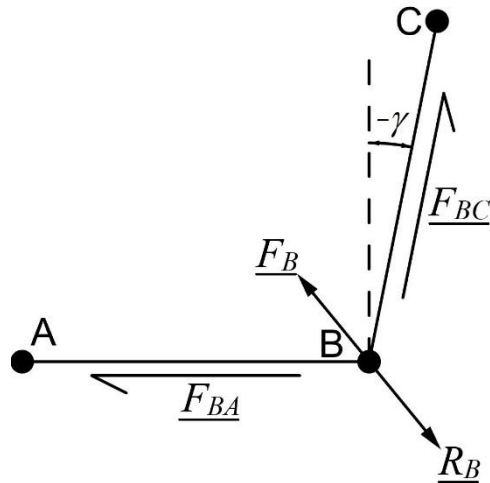


Figure 3.14 - Free body diagram of node B

$$\underline{R}_B = \tau (\underline{v}_{BC} + \underline{v}_{BA}) \quad (3.44)$$

$$\underline{R}_B = \tau [(L + L \sin \gamma - L, L \cos \gamma - 0) + (0 - L, 0 - 0)] \quad (3.45)$$

In this case $\tau = G(-\gamma)$, giving, after simplification:

$$\underline{R}_B = -G\gamma L [(\sin \gamma - 1, \cos \gamma)] \quad (3.46)$$

Employing the small angle approximation and ignoring higher order terms reduces this to:

$$\underline{R}_B = G\gamma L (1, -1) \quad (3.47)$$

\underline{R}_C is similarly calculated (Figure 3.15):

$$\underline{R}_C = \tau (\underline{v}_{CD} + \underline{v}_{CB}) \quad (3.48)$$

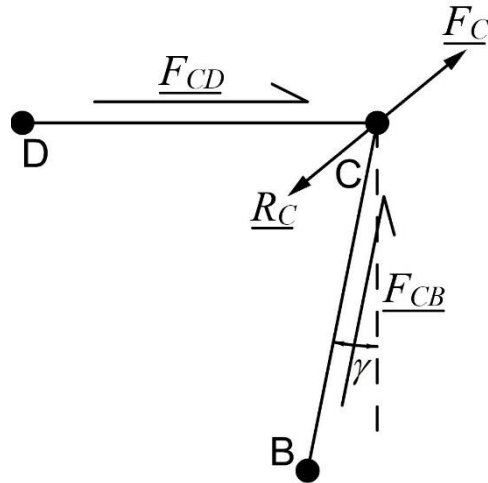


Figure 3.15 - Free body diagram of node C

This is equal to:

$$\underline{R}_C = G\gamma \begin{bmatrix} (L \sin \gamma - L(1 + \sin \gamma), L \cos \gamma - L \cos \gamma) \\ +(L - L(1 + \sin \gamma), 0 - L \cos \gamma) \end{bmatrix} \quad (3.49)$$

Simplifying and ignoring higher order terms reduces this to:

$$\underline{R}_C = G\gamma L(-1, -1) \quad (3.50)$$

Finally R_D is calculated in the same way (Figure 3.16):

$$\underline{R}_D = \tau(\underline{v}_{DA} + \underline{v}_{DC}) \quad (3.51)$$

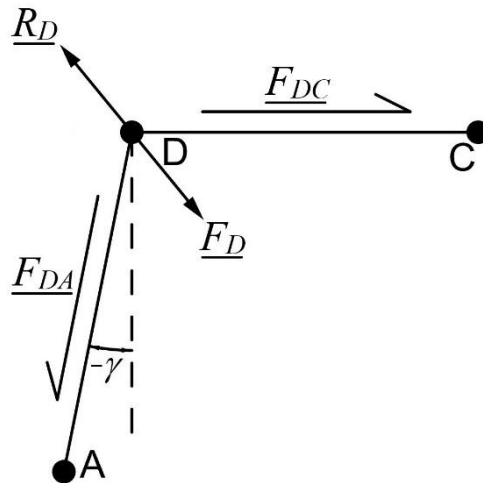


Figure 3.16 - Free body diagram of node D

Which is equal to:

$$\underline{R}_D = \tau \left[(0 - L \sin \gamma, 0 - L \cos \gamma) + (L(1 + \sin \gamma) - L \sin \gamma, L \cos \gamma - L \cos \gamma) \right] \quad (3.52)$$

Again in this case $\tau = G(-\gamma)$, giving, after simplification:

$$\underline{R}_D = -G\gamma(L - L \sin \gamma, -L \cos \gamma) \quad (3.53)$$

Employing the small angle approximation and ignoring higher order terms reduces this to:

$$\underline{R}_D = G\gamma L(-1, 1) \quad (3.54)$$

3.1.3.3 Comparison of approaches

The values calculated by treating the fabric patch as a continuum (section 3.1.3.1) are reproduced in equations 3.55 to 3.58:

$$\underline{R}_A(\text{continuum}) = G\gamma L(1,1) \quad (3.55)$$

$$\underline{R}_B(\text{continuum}) = G\gamma L(1,-1) \quad (3.56)$$

$$\underline{R}_C(\text{continuum}) = G\gamma L(-1,-1) \quad (3.57)$$

$$\underline{R}_D(\text{continuum}) = G\gamma L(-1,1) \quad (3.58)$$

The values calculated from the equivalent representation by the proposed discrete elements (section 3.1.3.2) are reproduced in equations 3.59 to 3.62:

$$\underline{R}_A(\text{discrete}) = G\gamma L(1,1) \quad (3.59)$$

$$\underline{R}_B(\text{discrete}) = G\gamma L(1,-1) \quad (3.60)$$

$$\underline{R}_C(\text{discrete}) = G\gamma L(-1,-1) \quad (3.61)$$

$$\underline{R}_D(\text{discrete}) = G\gamma L(-1,1) \quad (3.62)$$

Comparing the results, it can be seen that the two methods give the same forces at the corners.

This simple comparison indicates that the shear modelling implemented in the proposed discrete model converges to the same solution as that found by evaluating the shear of a continuum for the case of small strain.

3.2 Analysis by Dynamic Relaxation

This section discusses the solution of the discrete element model by the Dynamic Relaxation (DR) method [24,61]. DR is an iterative method that employs a pseudo-dynamic model of the structure over time. It is contingent on the structure being discretised in such a way that the mass and stiffness of the structure is concentrated at the nodes. The discrete element model uses exactly this discretisation, and so DR is chosen as the solution method employed by this author.

In the pseudo-dynamic model used by DR, the structure oscillates, and comes to rest in its equilibrium position under the influence of damping. This damping can be achieved in one of two ways; *viscous* or *kinetic*. In the case of viscous damping, a fictitious damping coefficient is supplied to the model. Kinetic damping employs the observation that the equilibrium position of a structure corresponds to the position of minimum potential energy, and consequently, the position of maximum kinetic energy. Kinetic damping is used in this work.

3.2.1 Dynamic relaxation with kinetic damping

3.2.1.1 Governing equation of motion and iterative procedure

Dynamic relaxation is achieved by the repetitive use of several equations, constructed from the centred finite difference form of the equation of motion. The governing equation, for a discretised system, is adapted from [24] as:

$$N_{ji} = m_{ji}a_{ji} + Cv_{ji} \quad (3.63)$$

Where m_{ji} is the lumped mass, C is the damping coefficient, v_{ji} & a_{ji} are the first and second derivatives of the displacement with respect to time, i.e. the velocities and accelerations of individual nodes, and N_{ji} is the residual force. The first subscript j refers to the node, and the

second subscript i refers to the direction. The residual force N_{ji} is calculated from the difference of the external and internal forces, applied to the node by the loads and the attached elements, respectively:

$$N_{ji} = P_{ji} - \left[\sum K_{EL} \delta \right]_{ji} \quad (3.64)$$

Where P_{ji} is the external force from applied loads, with the same subscript convention as above, and $\left[\sum K_{EL} \delta \right]_{ji}$ is the sum of internal forces from the elements. K_{EL} refers to the stiffness of an element connecting to the node, and δ is the nodal displacement.

Kinetic damping renders the damping coefficient unnecessary, reducing equation 3.63 to:

$$N_{ji} = m_{ji} a_{ji} \quad (3.65)$$

Equation 3.65 represents the motion of the structure (discretised into nodes) due to out of balance forces.

The governing equation for a single node, expressed using vector quantities is thus:

$$\underline{N} = m \underline{a} \quad (3.66)$$

Where \underline{N} is the residual force vector for the node, m is the mass of the node, and \underline{a} is the acceleration vector for the node.

Equation 3.66 is re-expressed in centred finite difference form, where the acceleration is represented by the change in velocity at discrete points in time, over the time interval:

$$\underline{N} = m \frac{v^{k+\frac{1}{2}} - v^{k-\frac{1}{2}}}{\Delta t} \quad (3.67)$$

Where \underline{v} is the velocity vector for the node, the superscript k corresponds to the iteration number, and Δt is the time interval.

Rearranging equation 3.67 yields a form which can be used to ‘push’ the analysis forward – starting from an initial configuration, the time is increased incrementally, yielding the velocity at the next time step:

$$\underline{v}^{k+\frac{1}{2}} = \underline{v}^{k-\frac{1}{2}} + \frac{N\Delta t}{m} \quad (3.68)$$

Velocities can then be used to calculate displacements:

$$\underline{\delta}^{k+1} = \underline{\delta}^k + \underline{v}^{k+\frac{1}{2}}\Delta t \quad (3.69)$$

Where $\underline{\delta}$ is the displacement vector for the node.

To increase the efficiency of the numerical implementation, the following convergence criterion has been established [24]:

$$\Delta t = \sqrt{2 \frac{m}{K}} \quad (3.70)$$

Where, m is the mass for a given node, and K is the nodal stiffness for a given node, calculated from the sum of the stiffnesses of the elements adjoining the node. Setting $\Delta t = 1$ and substituting for Δt in equation 3.68, simplifies equations 3.68 and 3.69:

$$\underline{v}^{k+\frac{1}{2}} = \underline{v}^{k-\frac{1}{2}} + \frac{2N}{K} \quad (3.71)$$

$$\underline{\delta}^{k+1} = \underline{\delta}^k + \underline{v}^{k+\frac{1}{2}} \quad (3.72)$$

Again, in equations 3.70 & 3.71, K is the stiffness for the node, calculated from the sum of the stiffnesses of the elements adjoining the node.

Equation 3.72 gives the displacement from the original position of the node at time $k+1$. The new position of the node is thus calculated from:

$$\underline{X}^{k+1} = \underline{X}^0 + \underline{\delta}^{k+1} \quad (3.73)$$

Where \underline{X} is the position vector at the specified iteration, indicated by the superscript. \underline{X}^0 is the position vector of the node at $k = 0$, which is recorded once and used to calculate new positions for future iterations.

Equations 3.71 to 3.73 can be used repeatedly in a loop to model the structure over time. However, in the absence of damping, this loop simply results in the oscillation of the structure. To achieve equilibrium, kinetic damping must be implemented.

3.2.1.2 *Kinetic damping by identification of kinetic energy peaks*

The theory of kinetic damping is derived from the observation that oscillating structures pass through their equilibrium position with maximum kinetic energy (KE). The algorithm uses this observation by iterating until a KE peak has been detected, and then stopping the iterative scheme at this *approximated equilibrium position* [24]. It is not possible, for complex systems with multiple nodes, to achieve the full equilibrium of the structure after only one KE peak. Thus the algorithm restarts the iterations from the approximated equilibrium position, with zero velocity.

It is possible to detect when the structure has passed a peak, by recording the value of the kinetic energy at each interval of the time step. It is however only necessary to record the total kinetic energy of the structure for the current iteration and two previous iterations. It is not possible to calculate the exact time at which the KE peak occurs, because the iterative scheme records values only at discrete time intervals. However it is inferred that a kinetic energy peak has been

passed, by comparing the value of kinetic energy at $k + \frac{1}{2}$ with that at $k - \frac{1}{2}$. If

$$KE^{k+\frac{1}{2}} < KE^{k-\frac{1}{2}}, \text{ a peak has been passed.}$$

To estimate the point in time corresponding to the KE peak, the kinetic energy trace is approximated by a quadratic function, fitted through the three recorded values of the kinetic energy at $k + \frac{1}{2}$, $k - \frac{1}{2}$, and $k - \frac{3}{2}$. An example kinetic energy trace is shown in Figure 3.17.

For the derivation of the establishment of the KE peak, k is replaced by t .

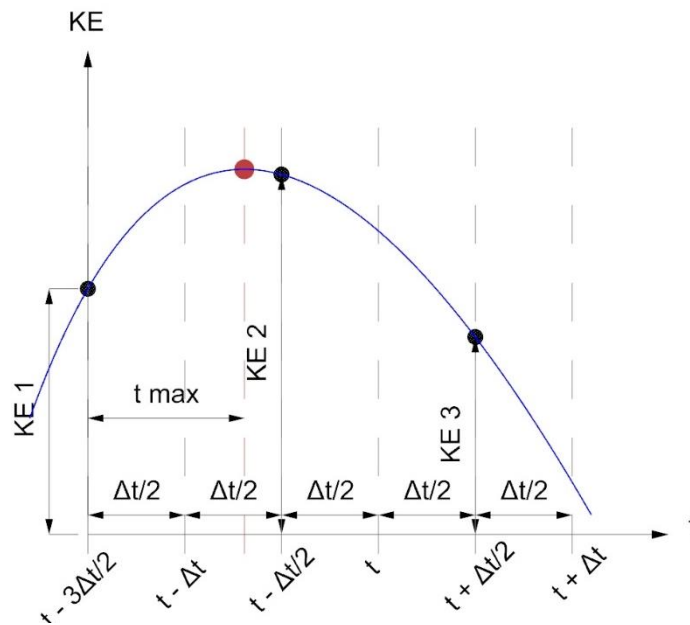


Figure 3.17 - Trace of kinetic energy around peak

The specific point in time corresponding to the KE peak is estimated by finding the maximum of the quadratic function fitted through the three recorded values of KE.

The quadratic function passing through the three values of kinetic energy is given by:

$$KE = at^2 + bt + c \quad (3.74)$$

Where a , b & c are typical coefficients for a quadratic function.

The maximum value of a quadratic function, and thus of the KE is found at time t_{\max} :

$$t_{\max} = -b/2a \quad (3.75)$$

t_{\max} is measured from $t - \frac{3}{2}$.

The following equations for known values of KE, at intervals separated by time steps of Δt , can be expressed in terms of the quadratic function coefficients:

$$KE(0) = c = KE_1 \quad (3.76)$$

$$KE(\Delta t) = a\Delta t^2 + b\Delta t + c = KE_2 \quad (3.77)$$

$$KE(2\Delta t) = a(2\Delta t)^2 + b(2\Delta t) + c = KE_3 \quad (3.78)$$

Substituting Eq. 3.76 into Eqs. 3.77 & 3.78 yields a pair of simultaneous equations with two unknowns, a & b , which can be solved to give the following expressions:

$$a = \frac{1}{2\Delta t^2} (KE_3 - 2KE_2 + KE_1) \quad (3.79)$$

$$b = \frac{1}{2\Delta t} (4KE_2 - 3KE_1 - KE_3) \quad (3.80)$$

Taking $\Delta t = 1$ (in respect of the convergence criterion established in equation 3.70), gives the following expression for t_{\max} :

$$t_{\max} = \frac{KE_3 - 4KE_2 + 3KE_1}{2(KE_3 - 2KE_2 + KE_1)} \quad (3.81)$$

As can be seen in Figure 3.17, the kinetic energy peak occurs before the current iteration. For this reason, calculating the displacement for iteration $t + \Delta t$ using equation 3.72 would lead to the algorithm *overshooting* the equilibrium position.

The DR algorithm therefore iterates until a KE peak is detected, and then *corrects* the displacement calculated by equation 3.72 according to the location of the KE peak along the KE trace curve.

In the method detailed in [24] for correcting displacements due to the passing of a KE peak, the displacements were corrected by calculation of an adjustment factor β .

However, the equations can be simplified to the following (for one node with vector quantities):

$$\underline{\delta}_{corrected}^{k+1} = \underline{\delta}^k - \left(\frac{3}{2} - t_{max} \right) \underline{v}^{k-\frac{1}{2}} \quad (3.82)$$

Where $\underline{\delta}_{corrected}^{k+1}$ is the corrected displacement for iteration $k + 1$.

The calculation of the corrected new position for each node is thus:

$$\underline{X}_{corrected}^{k+1} = \underline{X}^0 + \underline{\delta}_{corrected}^{k+1} \quad (3.83)$$

Where $\underline{X}_{corrected}^{k+1}$ is the corrected new position for iteration $k + 1$.

The residual force vector for each node is then checked to see if it is sufficiently close to zero. Since the algorithm is unlikely to result in exactly zero residual force at all nodes, the force is compared with a prescribed maximum force, usually of the order of $< 10^{-6}$ kN.

If the residual force is lower than the specified maximum force for each node, equilibrium has been found, and the final structure position and stresses are known.

If the structure is not in equilibrium, the iterations are restarted from the adjusted position, with the node velocities and kinetic energies set to zero. Iterations continue until further KE peaks are detected, and eventual equilibrium found.

3.3 Computational implementation

The discrete element model, and numerical simulation using dynamic relaxation, has been implemented by the author in a plug-in for the existing program Rhino3D. Rhino3D is a 3D modelling program [62], complimented by the existing plug-in RhinoMembrane [63] that facilitates the form-finding of tensile surface structures. The plug-in for implementation of the discrete model was coded in VB.Net.

The implementation of the discrete element model by the author was achieved using object oriented programming, employing in particular, several classes programmed by the author:

- *Element3D* – an element class used to model the tensile deformation of the fabric. The element strain, stress, and force are calculated from equations 3.1 – 3.7, and apportioned to the end nodes of the element.
- *ShearTriangle* – an element used to model shearing. *ShearTriangles* are used to record changes in angle between warp and weft elements, calculate the shear stress and force, and apportion the force to the appropriate node.
- *Node3D* – a node class that displaces under the effect of out-of-balance forces in the simulation scheme.
- *AnalysisMesh3D* – a container class that comprises *Element3Ds*, *ShearTriangles*, and *Node3Ds* for running the physical simulation scheme. Dynamic relaxation is run on the *AnalysisMesh3D*, and the structure kinetic energy is calculated by summing the kinetic energy of every *Node3D* contained by the *AnalysisMesh3D* class.

- *DynamicRelaxationSolver* – a class for running the dynamic relaxation algorithm on an *AnalysisMesh3D*.

Figure 3.18 shows an *AnalysisMesh3D* with its constituent *Element3Ds* (tensile elements and boundary elements), *ShearTriangles* and *Node3Ds* (nodes) in the Rhino3D viewport.

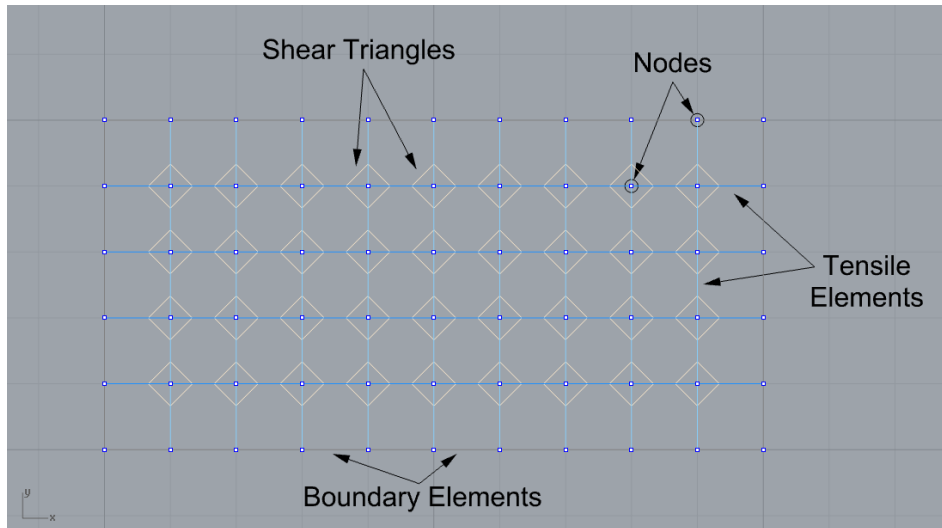


Figure 3.18 - Screenshot of the discrete element model implemented using VB.Net

Boundary elements may be excluded from certain analyses, if for example, both nodes of an element are fixed, or its direction deviates from the warp or weft direction (as mentioned earlier when calculating widths).

Nodes may be restrained in the three global coordinate directions, (x, y, z) . Since the model is moment-less, no rotational restraints are implemented.

Applying forces or displacements to a given discrete element mesh results in a configuration of the mesh that is not in equilibrium. To solve for the equilibrium position of the mesh, dynamic relaxation was implemented in VB.Net. How the dynamic relaxation algorithm operates on the discrete element mesh is illustrated through the pseudocode in Figures 3.19 to 3.21.

Figure 3.19 shows the set up process for running dynamic relaxation. The algorithm records the rest configuration of the mesh, calculates the widths for each element from this rest configuration, and assigns appropriate material parameters.

```
// Set up the analysis  
  
// Record the position of each node in the rest configuration  
For each Node3D in AnalysisMesh3D  
    Record X0 position  
Next  
  
// Calculate the width for each element  
For each Element3D in AnalysisMesh3D  
    Calculate width  
Next  
  
// Assign the shear stiffness to each shear triangle  
For each ShearTriangle in AnalysisMesh3D  
    Assign Shear Stiffness  
Next  
  
// Assign tensile element stiffness (warp or weft dependent)  
// Assign tensile element pre-stress (warp or weft dependent)  
For each Element3D in AnalysisMesh3D  
    Assign Element Stiffness  
    Assign Element Pre-stress  
Next
```

Figure 3.19 - Pseudocode describing the set up process for running dynamic relaxation

Following the setup of the mesh, iterations in the dynamic relaxation scheme are run (Figures 3.20 & 3.21).

```

// Run dynamic relaxation
For i = 0 to n //Perform n iterations of DR
  // Set new position for each node (no change when i = 0)
  For each Node3D in AnalysisMesh3D
    Set new position
    Push back velocities, displacements, KEs
  Loop

  // Calculate strains, stresses and forces for each element
  For each Element3D in AnalysisMesh3D
    Calculate strain
    Calculate stress and force
    Apportion force to Node3Ds
  Loop

  // Calculate strain, stress and force for each shear triangle
  For each ShearTriangle in AnalysisMesh3D
    Calculate current angle
    Calculate shear strain
    Calculate shear stress
    Calculate force
    Apportion force to Node3Ds
  Loop

  // Sum tensile and shear forces at each node
  // Calculate residual force, velocity and displacement
  For each Node3D in AnalysisMesh3D
    Calculate residual force
    If update geometric stiffness Then
      Calculate geometric stiffness
    End If
    Calculate velocities
    Calculate displacement
    Calculate kinetic energy
  Loop

  // If a KE peak was detected in the previous iteration
  // Check for equilibrium of each node
  If last iteration was KE peak Then
    For each Node3D in AnalysisMesh3D
      Check residual force < max nodal force
    Loop

    If F < max force for all nodes in AnalysisMesh3D Then
      Equilibrium found
      Exit Loop
    End If
  End If
End If

```

Figure 3.20 – Dynamic Relaxation pseudocode


```

// Sum Node KE
Structure KE = Sum of Node3D KE

// If current KE < previous KE, a peak has been passed,
// Correct node displacements, set velocity=0 and KE=0
If Structure KE at k+1/2 < Structure KE at k-1/2 Then
    Calculate Tmax
    For each Node3D in AnalysisMesh3D
        Correct displacements using Tmax
        Set velocity = 0
        Set KE = 0
    Loop
End If
Loop

```

Figure 3.21 - Dynamic Relaxation pseudocode continued

Figures 3.20 & 3.21 show the DR algorithm, which comprises the following general steps:

1. Each node position is updated based on the displacements calculated in the previous iteration.
2. Tensile and shear forces are calculated and apportioned to the nodes.
3. Node residual forces, velocities, displacements and kinetic energies are calculated.
4. If a KE peak was detected in the previous iteration, the structure is checked to see if it is in equilibrium, if so, the algorithm exits.
5. If equilibrium was not found in step 4, the structure kinetic energy is computed.
6. If a KE peak is detected, the displacements calculated in step 3 are corrected according to equation 3.82, and the velocities are set to zero. If not, no correction is made.
7. The algorithm loops back to step 1, completing one iteration.

3.4 Summary

This chapter described the discrete element model proposed by the author, drawing on the conclusions from chapter 2. The proposed discrete model was developed to fulfil research objective **RO 1** – the development of a discrete model for patterning.

The conclusions from chapter 2 established the requirements for a discrete element model for modelling tensile fabric structures during patterning. The model was developed to meet these requirements.

The proposed model was presented, and calculations for modelling the tensile deformation were described. The calculation of widths for tensile elements was described, along with the challenges incurred by geometries of non-rectangular boundary. Adjusted width calculations to overcome these challenges were presented.

Shear deformation in the discrete model was presented, illustrating how the author's proposed model overcomes the limitations of the method presented by Eischen & Bigliani [50]. It was shown that the proposed method for modelling shear gives the same result as that of continuum elasticity for small strains.

The solution by dynamic relaxation was justified and described. Key equations for the algorithm were presented.

The application of the dynamic relaxation method to the proposed discrete element model, programmed using VB.Net, was described. Pseudocode for the VB.Net algorithm was presented, to show how the elements programmed for modelling the tensile and shear response of the fabric, Element3D and ShearTriangle respectively, were incorporated in the dynamic relaxation scheme.

The proposed patterning method, incorporating the discrete element model, is presented in the next chapter.

4 Proposed patterning method

To demonstrate the proposed discrete model, it is implemented in a proposed patterning method. This chapter presents the proposed computational patterning method. The patterning method presented here follows the general structure of patterning outlined in chapter 2, section 2.1.2, but improves upon certain processes, and adds new sub-processes, resulting in an alternative patterning method.

In chapter 2, section 2.1.2, patterning as a general computational process was presented as a 4-5 step process (where step 5 *Panel Assembly* is not always included):

1. **Subdivision** of the membrane by defining seams on the form-found surface
2. **Flattening** of the resulting panels from 3D to 2D
3. **Stress reduction** to reduce the stresses induced by flattening
4. **Compensation** to scale the 2D panel to account for pre-stressing
5. **Panel assembly** to visualise the final 3D form and calculate stresses

Steps 1-4 concern the *method of determining the cutting pattern*. Step 5 concerns the simulation of the *assembly of the cutting pattern* to determine its suitability, in terms of accurate representation of the 3D, form-found geometry. The proposed patterning method in this chapter is thus presented under these headings. The method comprises the following stages:

Stage 1: Method of determining the cutting pattern

1. **Subdivision** of the membrane by defining seams on the form-found surface
2. **Flattening** of the resulting panels from 3D to 2D
3. **Integrated stress reduction and compensation** to reduce the stresses induced by flattening and scale the 2D panel to account for pre-stressing

Stage 2: Method of cutting pattern assembly and evaluation

4. **Re-meshing** of the cutting pattern panels with an orthogonal mesh, to better represent the fabric
5. **Assembly of the panels** as a pre-process for equilibrium finding
6. **Equilibrium finding** to visualise the final 3D form and calculate stresses

The proposed patterning method differs from existing methods in the following ways:

1. In step 2, flattening, simple methods of flattening that minimise stresses, with little additional computational effort, are included. The inclusion of simple flattening methods means that in step 3, integrated stress reduction and compensation, there is less computational 'work' to be done. Step 2 is included in the method to address **RO 2(b)** – the development of improved flattening methods.
2. In step 4, an additional process in the pattern assembly and equilibrium finding is included. The panels in the cutting pattern are re-meshed with an orthogonal mesh, to represent the directions of the fibres in the fabric. When the mesh is assembled, these fibres deform under shear, giving a more representative description of the final assembled shape and equilibrium geometry.
3. The use of the discrete model (presented in chapter 3) accounts for the shear-dependent behaviour of the fabric throughout. This is included in light of **RO 1** – the implementation and examination of a discrete model for patterning.

Form-finding

To explain the proposed patterning method, and in future chapters demonstrate its applications, form-found membrane shapes are necessary. Thus, form-finding precedes patterning and is achieved using the RhinoMembrane plug-in for Rhino3D.

4.1 Method of determining the cutting pattern

The first stage in the proposed patterning method is the determination of the cutting pattern. This is the pattern that would be cut from an unstrained, woven fabric, which, when assembled and stressed gives the final 3D membrane shape. This shape is intended to reproduce the form-found surface. As mentioned previously, the three sub-processes conducted to determine the cutting pattern, in the proposed cutting pattern method, are (i) Subdivision of the membrane, (ii) Flattening of the resulting 3D panels, and (iii) Integrated stress reduction and compensation of the flattened panels. The processes for conducting these steps, in the proposed patterning method, are now presented in turn.

4.1.1 Subdivision of the form-found membrane shape

The first step in determining the cutting pattern is to divide the form-found surface into individual panels. This should be conducted in such a way that ensures the resulting panels have a width lower than the maximum (typically 2-3 m [5], though widths as large as 5 m have been reported [7]). As noted in chapter 1, section 1.2, the form-found surface represents an idealised surface geometry for the given boundary condition and pre-stress state. In the case of computational form-finding, this surface geometry is in the form of a mesh. In this work, form-finding is conducted using RhinoMembrane [63], resulting in a mesh of quadrilaterals. To divide the surface into panels such that their seams follow geodesics, a surface description that facilitates the construction of geodesic curves is required. In the proposed patterning method, a spline surface, specifically a Non-Uniform Rational B-Spline (NURBS) surface, is interpolated over the mesh, to facilitate the use of Rhino's in-built *shortpath* function. Rhino's in-built functions were used for constructing the surface from the interpolation of the mesh nodes. The *shortpath* function finds the shortest curve between two points, over a given NURBS surface. Used correctly it can thus define geodesic curves.

The procedure for defining panels bounded by geodesics is thus:

1. Define a NURBS surface by interpolating the mesh nodes from form-finding.
2. Define an array of start and end points at suitable locations on the boundaries of the mesh.
3. Construct geodesics over the surface, between start and end points on the boundaries, using the *shortpath* function. Manually check that the resulting panels have a width lower than the maximum.
4. Use these geodesic curves to divide the surface into further sub-surfaces, which define the 3D shape of the panels, suitable for flattening.

Figures 4.1 (a) through 4.1 (c) demonstrate the above process on a catenoid shape. Since a catenoid represents a surface of revolution, to interpolate a NURBS surface, a curve between the boundaries is defined and then revolved around the central axis. The curve is defined along the edges of the elements between the boundaries (the black line in Figure 4.1 (a)). The form-found mesh is shown in green in Figure 4.1 (a). Points along the upper and lower circular boundaries are defined such that they are equally spaced (the green points in Figure 4.1 (b)). These points define the geodesics (the red lines in Figure 4.1 (b)), which ultimately allow the surface to be split into sub-surfaces that define the 3D panels (Figure 4.1 (c)). In the case of this catenoid, the panels are identical due to rotational symmetry.

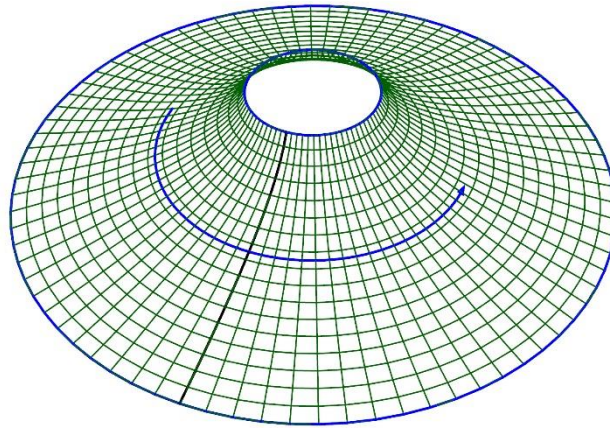


Figure 4.1 (a) - Interpolation of a catenoid shape by revolving a radial line of element edges around the centre axis. The original mesh is shown in green.

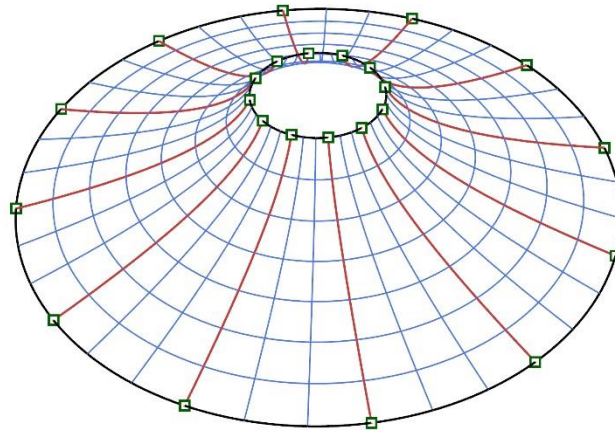


Figure 4.1 (b) - Interpolated surface with geodesic seams defined.

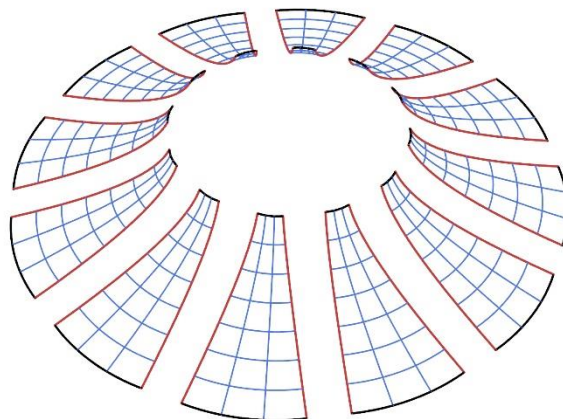


Figure 4.1 (c) - Surface split into individual panels, which can now be flattened.

Following subdivision of the membrane into panels, the panels are flattened into the plane.

4.1.2 Flattening

Subdivision of the form-found membrane shape defines the 3D geometry of the panels used in patterning. The planar geometry corresponding to these panels must then be determined. To achieve this, the panels are flattened into the plane. It is at this stage that the proposed patterning method differs from that of existing methods, by attempting to minimise the distortions arising from flattening using some simple procedural methods of unfolding. To flatten the panels, a suitable mesh must first be constructed on the panels, and this is achieved using geodesic lines, as follows.

4.1.2.1 Geodesic meshing of the 3D panels

Unlike the later stage of orthogonal re-meshing (see section 4.2.1), the directions of the fabric fibres on the 3D surface are not known. The construction of the mesh is not trivial. In the proposed patterning method, geodesics are used to define the elements on the 3D panel, on the following basis: the form-found shape represents a surface with an isotropic stress distribution, and this is the ideal shape for the membrane. A geodesic across this surface represents a direction along which tension force is uniform. Uniform tension in the fibres implies they should follow geodesics. Additionally, a mesh comprising geodesics across the 3D surface should inherently minimise element lengths, and thus give highest accuracy.

However, the author's investigation into the use of meshes constructed from geodesic curves in both directions found issues with numerical ill conditioning. In such meshes, longer elements occurs in some areas and not in others, resulting in inconsistent element widths (Figure 4.2). The disparity in widths results in an uneven distribution of stiffness across the surface. For this reason, in the proposed patterning method, geodesic curves are used for defining elements in the first direction, in particular, the direction of higher curvature, and then elements in the

second direction, that of lower curvature, are interpolated across the geodesic curves of the first direction.

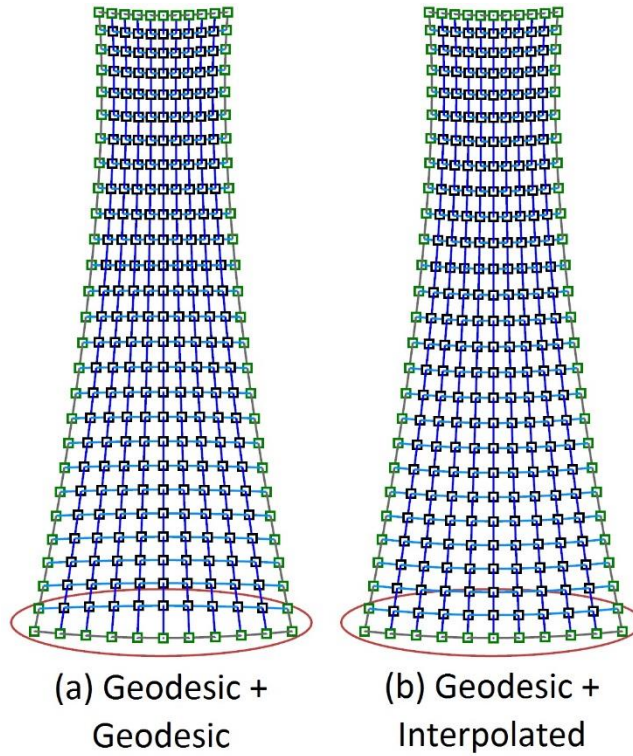


Figure 4.2 - Comparison of different mesh constructions. The red circle indicates the longer elements in mesh (a), not present in mesh (b)

The methods for generating both fully and partially geodesic meshes are defined as follows. To generate a mesh in which all elements follow portions of geodesics, the following method is used (Figure 4.3).

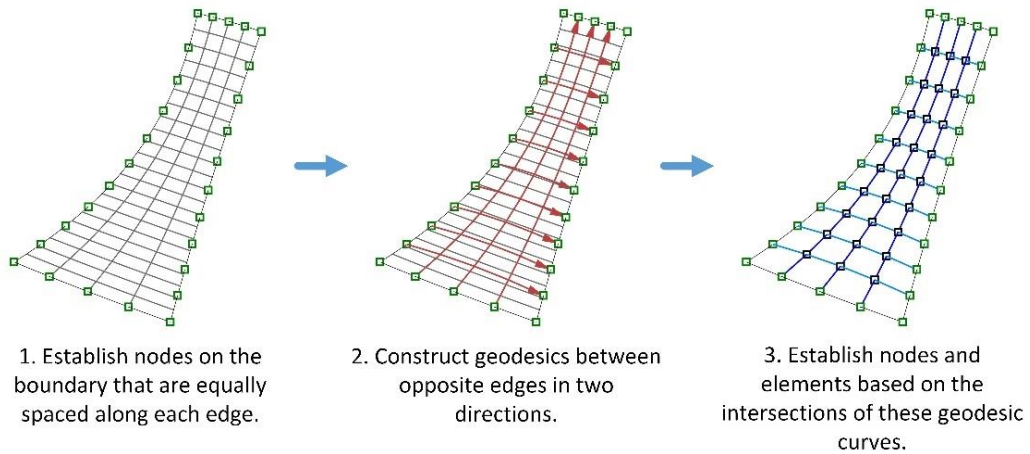


Figure 4.3 - Meshing a panel by constructing geodesics in two directions

To generate a mesh in which elements in one direction follow portions of geodesics, the following method is used (Figure 4.4):

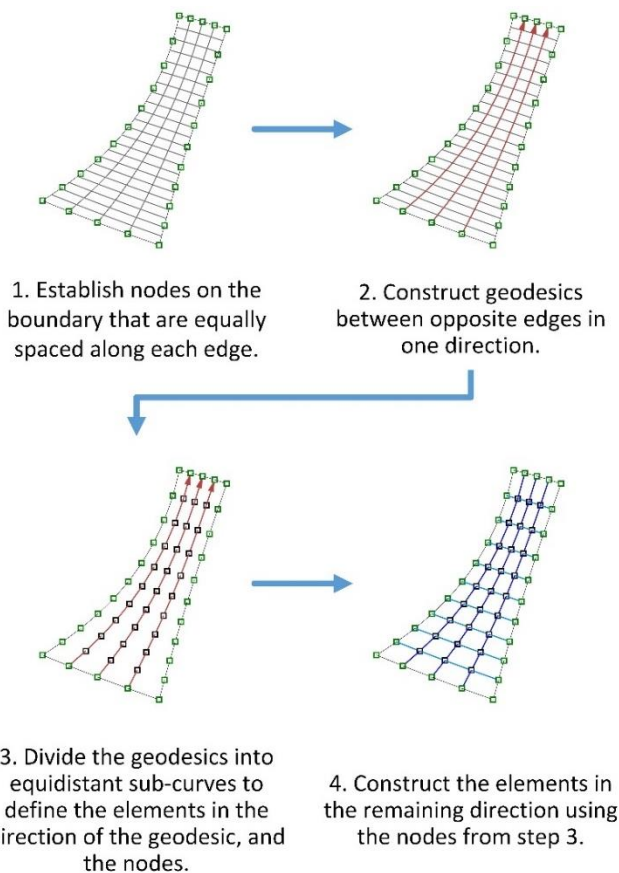


Figure 4.4- Meshing a panel using geodesics in one direction. These geodesics are then divided into equal segments that dictate the node positions. Elements in the second direction are then interpolated.

With the mesh defined on the 3D panel from either of the above methods, the next step in the proposed method is to flatten the panel into the plane.

4.1.2.2 Flattening methods

As mentioned, the proposed method attempts to improve on existing methods by seeking to reduce the distortions incurred by flattening, through the use of some simply defined flattening methods. The flattening methods were developed in response to **RO 2 (a)** – the development of improved flattening methods.

Three methods of flattening implemented in the proposed patterning method are presented in the following subsections. The first method, direct projection, is a trivial method in current use by other researchers [6], but is included for future comparison. The second and third methods were developed by the author as an improvement over the method of direct projection.

4.1.2.3 Flattening by direct projection

The first flattening method is the direct projection of the mesh to a defined ‘target’ plane (Figure 4.5). When projecting to the global x-y plane, this is equivalent to taking the global coordinate (x, y, z) of each node within the mesh, and setting the value to $(x, y, 0)$ for each node. This leads to a shortening of the element lengths – where the elements are aligned with the target plane, distortions are zero, and where the elements are perpendicular to the plane, the distortion is infinite. Thus the highest distortions incurred by mapping the surface occur in the higher curvature regions, where the deviation in the alignment between 3D elements and the plane is highest.

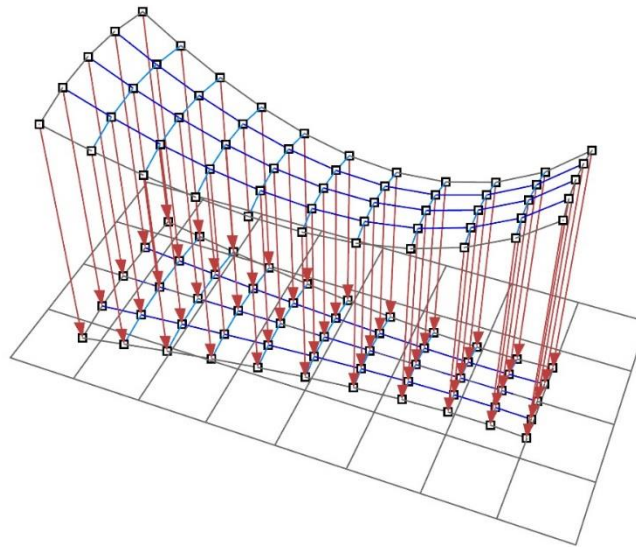


Figure 4.5 - Flattening of a panel by direct projection, showing projection of nodes to the plane

Flattening by direct projection is computationally ‘cheapest’, and simple to implement. However, it can incur considerable distortion for surfaces with higher curvature, and is sensitive to the orientation of the mesh to the plane of projection. Such large distortions lead to numerical ill conditioning of the flattened mesh, when attempting to reduce stresses using dynamic relaxation.

4.1.2.4 Flattening by unrolling with a single spine of elements

An alternative method for flattening the mesh is to ‘unroll’ or ‘unfold’ the mesh. As mentioned, historically this method alone was used to generate the cutting pattern for individual panels in the membrane structure.

Two methods of unrolling the mesh have been developed by the author. The first unrolls the mesh as follows, and is known as *unrolling with one spine*. Figures 4.6 (a) through 4.6 (d) illustrate the method diagrammatically.

1. Define a 'spine' – a line of elements near to the midline of the mesh.
2. Unroll the spine to the plane.
3. Using the unrolled spine, unroll lines of elements perpendicular to the spine.
4. Unroll the boundary elements in the approximate direction of the lines unrolled in step 3.
5. Interpolate elements in the direction approximately parallel to the spine.
6. Interpolate the boundary elements in the approximate direction of the lines interpolated in step 5.

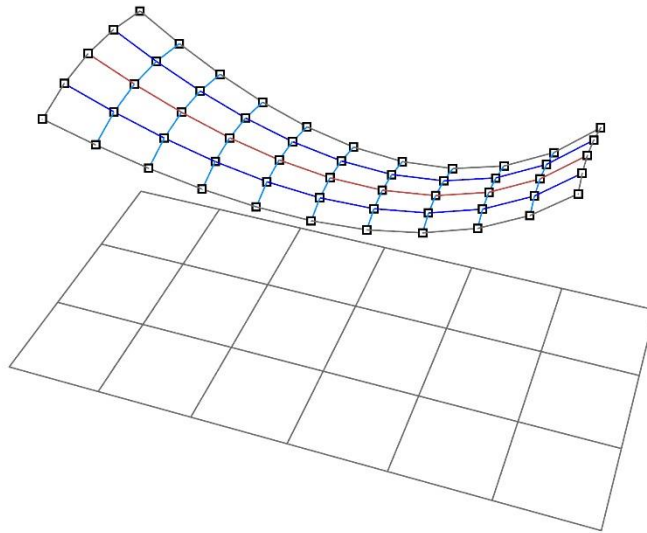


Figure 4.6 (a) - Definition of the 'spine' of elements on the panel to be flattened

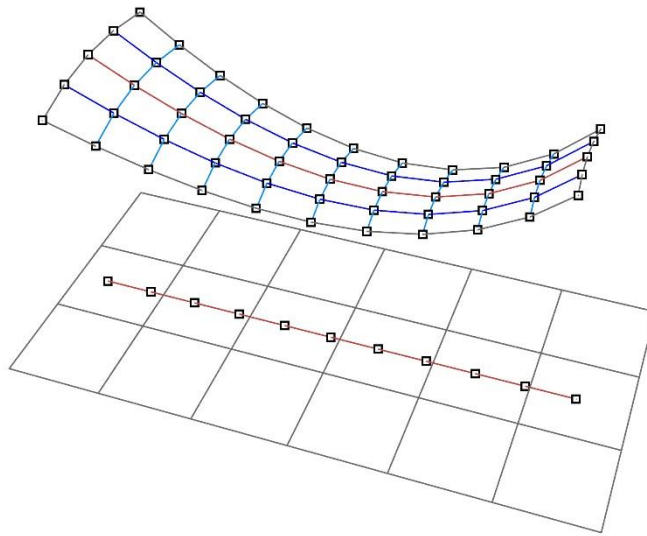


Figure 4.6 (b) - Unrolling of the spine of elements to the plane

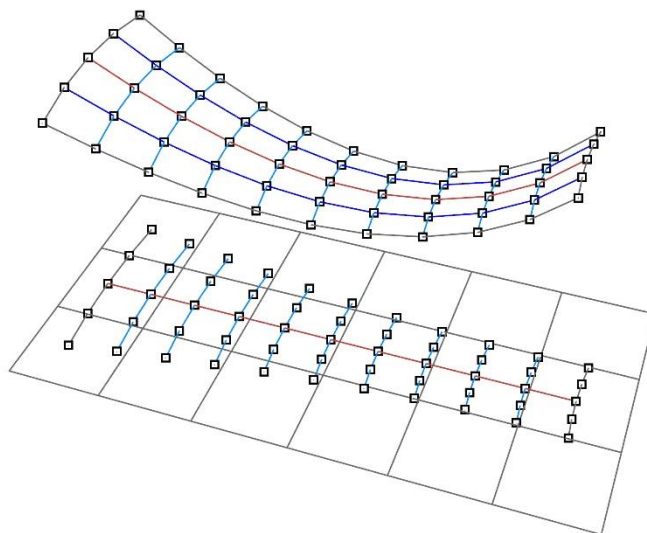


Figure 4.6 (c) - Unrolling of the elements (including boundary elements) approximately perpendicular to the spine

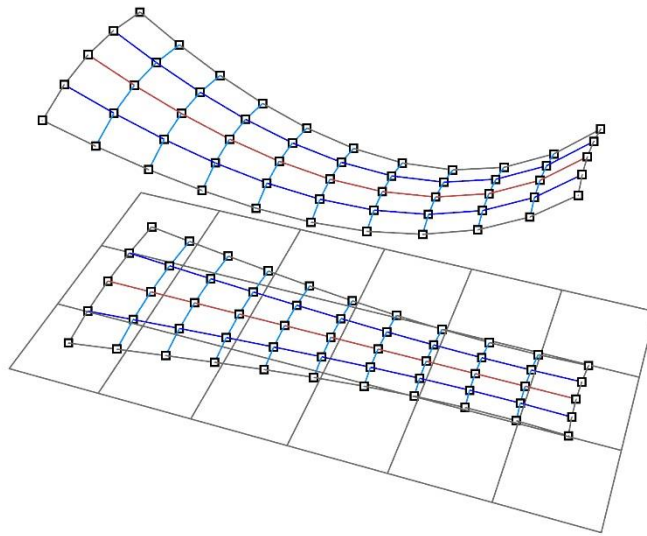


Figure 4.6 (d) - Interpolation of the elements (including boundary elements) approximately parallel to the spine, thus completing the unrolling of the mesh

Since the spine elements, and elements in the direction approximately perpendicular to the spine are unrolled, no tensile distortion is incurred in these elements. Tensile distortion is incurred only in the remaining elements. Shear distortions are incurred throughout. The method thus effectively prioritises the reduction of tensile distortions over shear distortions. This is considered acceptable since the shear stiffness of architectural fabrics is low in comparison with the tensile stiffness.

4.1.2.5 Flattening by unrolling with two spines of elements

The second proposed un-roller method makes use of the rectilinear topology of the generated mesh to unroll the pattern with zero tensile distortion. The method is similar to that proposed by Aono et al. [33,34], but simplified to two dimensions. The method proposed by Aono et al. [33,34] concerned the mapping of an equidistant grid over a 3D surface. This was achieved by calculating the location of points on the surface from two other points, and the distances between them, by intersecting two spheres of appropriate radii and the surface on which the grid was being arrayed [33,34]. For example, given two points A and B on a surface S, to find the point C that is distance L_1 from point A, and distance L_2 from point B, two spheres P_1 and P_2 are

constructed, with origin A, radius L_1 , and origin B, radius L_2 respectively. The intersections of P_1 , P_2 and S correspond to points on the surface S which are both distance L_1 from point A and L_2 from point B. This is shown in Figure 4.7.

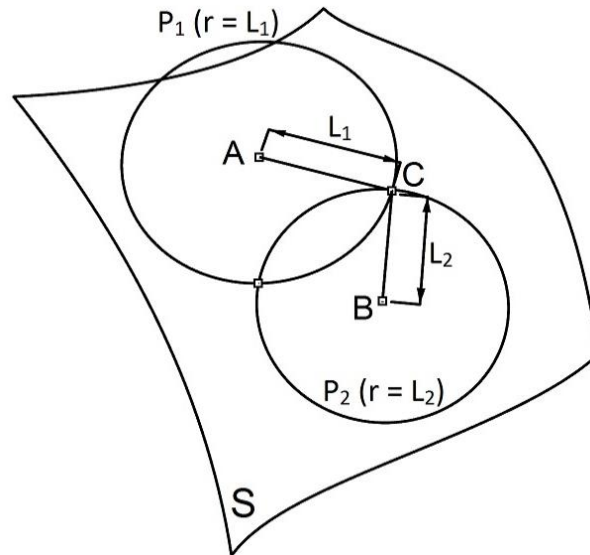


Figure 4.7 - Construction of a point C on a surface S that is distance L_1 from a point A and distance L_2 from a point B

Applying this logic to the plane, given two points U and V on a plane P, a point W that is distance L_1 from U and distance L_2 from V, can be found from the intersections of two circles C_1 and C_2 , in the plane P, with origin U, radius L_1 , and origin V, radius L_2 , respectively. The intersections of these two circles are positions of the point W such that the distances are as required. This method is suggested in [64], and is essentially the same as the ‘compass method’ originally attributed to Frei Otto in [65], but generalised to include grids that are irregularly spaced.

The intersection of planar circles as just described is implemented in the second flattening method, *unrolling with two spines*, as follows. The method is illustrated diagrammatically through Figures 4.8 (a) to 4.8 (d).

1. Two spines are defined along approximate midlines of the mesh (Figure 4.8 (a)).

2. These spines are unrolled to the plane as in the method “unrolling with one spine” (Figure 4.8 (b)).
3. The first row of nodes corresponding to the elements approximately in the direction of the first spine is unrolled to the plane by the intersection of appropriate planar circles, depending on the lengths of the elements (Figure 4.8 (c)).
4. Further rows of nodes corresponding to the elements approximately in the direction of the first spine are unrolled to the plane in a similar manner, until all nodes have been mapped to the plane (Figure 4.8 (d)).

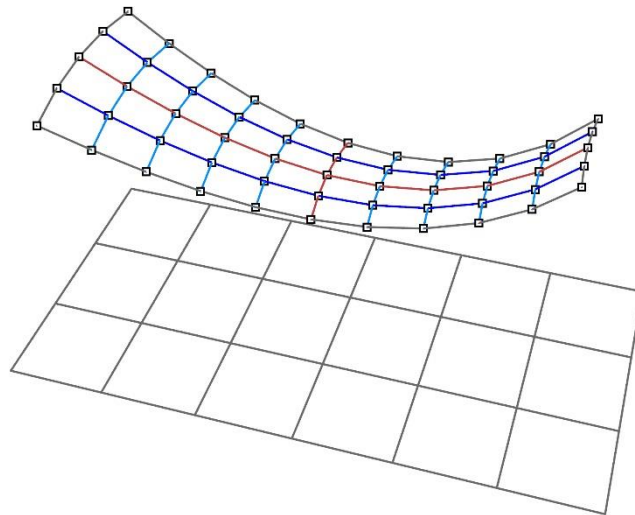


Figure 4.8 (a) - Definition of two spines on the mesh

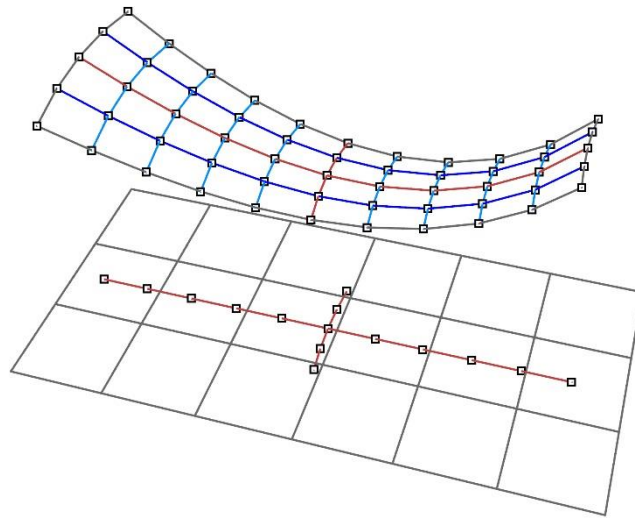


Figure 4.8 (b) - Mapping of the spines to the plane

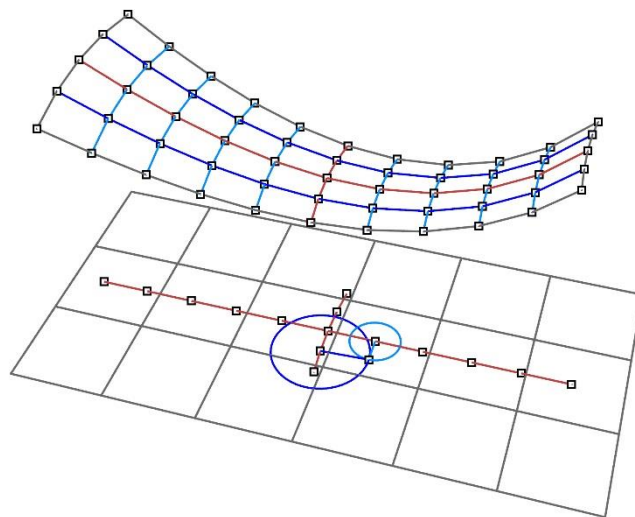


Figure 4.8 (c) - Mapping of the first line of nodes using the intersection of two circles in the plane

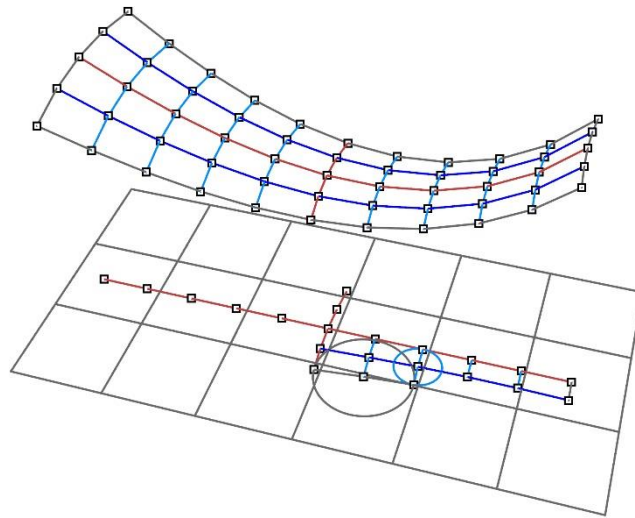


Figure 4.8 (d) – Mapping of the next line of nodes using the intersection of two circles in the plane

This method of flattening with two spines confers no tensile distortion in any of the elements, as the method of intersecting circles preserves element lengths exactly. This method of flattening achieves zero tensile distortion at the cost of shear distortion. This is similarly considered acceptable given the shear stiffness of architectural fabrics is low in comparison with the tensile stiffness.

Since none of the flattening methods give patterns with acceptably low distortions, the next step in the proposed patterning method is to perform stress reduction and compensation on the flattened panels.

4.1.3 Integrated stress reduction and compensation by dynamic relaxation

The flattening methods presented above produce planar patterns with varying degrees of distortion, comprising tensile and/or shear stress. To reduce these stresses further, and produce a pattern suitable for cutting from planar cloth, the proposed method employs dynamic relaxation to relax the panel into an equilibrium shape, to ‘release’ the stresses. The stresses induced through flattening, and the necessary reduction in panel size to account for pre-stress

are considered simultaneously in this analysis. Referring to the terms in chapter 2, sections 2.1.5 & 2.1.6, the proposed method is thus an *integrated stress reduction and compensation* method, employing a *structural solution method* and the *mechanical problem formulation*.

To measure the strains due to flattening, the 3D form-found geometry of the panel is taken as the reference geometry. Defining the strain as such means that the flattened elements produce zero residual force when their length (in 2D) is equal to their original length on the 3D form-found surface. The planar element geometry resulting in zero force thus represents no distortion due to flattening. When the analysis is run, the stresses release as the elements tend towards their zero force configurations. The effect of pre-stress is then simply added to the force formulation. To give zero force in the element, with the pre-stress included, the element must have a negative strain such that the strain balances with the pre-stress (equation 3.3 in chapter 3, section 3.1.1.2).

As mentioned in chapter 2, section 2.1.5, careful selection of the restraints is required to ensure convergence to a solution. The flattened panel, with the strain convention described above, represents a stressed geometry. The panel must be restrained in the equilibrium analysis to prevent rigid body rotation and translation, but the restraints must be sufficiently 'loose' to allow convergence to an equilibrium position. In the proposed method, the panel is realigned such that the centrelines of the mesh approximately coincide with that of the global (x, y) axis. A node on each boundary intersecting the x centreline, is fixed in the y direction. A node on each boundary intersecting the y centreline, is fixed in the x direction. Since only planar deformation is desired, all nodes are additionally restrained in the z direction. Figure 4.9 shows a typical panel with such restraints:

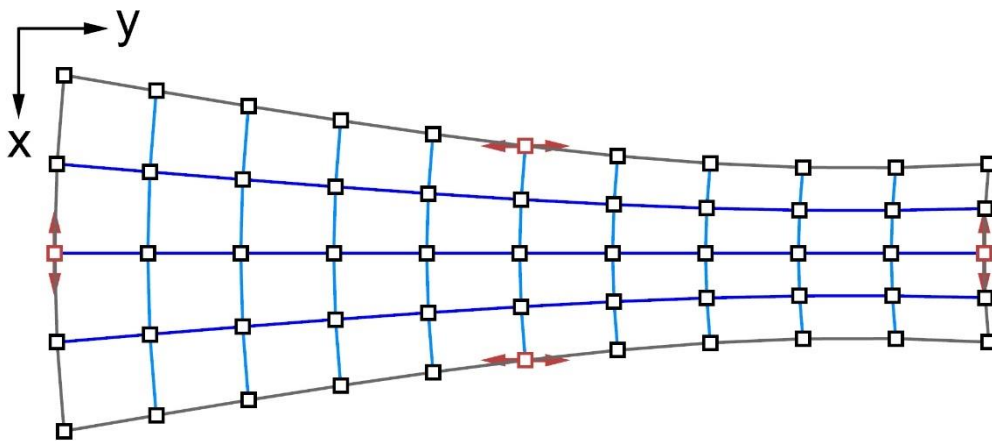


Figure 4.9 - Typical restraints for a flattened panel. Nodes in red are restrained in the directions indicated by the arrows. All nodes are additionally restrained perpendicular to the plane of the panel

With the panel restrained, dynamic relaxation is then performed as described in chapter 3, section 3.2. Under the effect of the flattening stresses, the nodes displace until they settle into equilibrium. The algorithm is run until the residual forces at the nodes are sufficiently small. Typically, a maximum nodal force of 10^{-6} kN is achievable. As mentioned in chapter 2, section 2.1.7, it is not possible to fully nullify the stresses due to flattening. Consequently, residual stresses will be present in the panel even at the equilibrium position. The magnitude of these stresses is between 0 and $\pm 100\%$ of the pre-stress, as discussed in chapter 5.

Once all panels have been meshed, flattened and undergone stress reduction and compensation, the cutting pattern for the structure is fully defined. To evaluate this cutting pattern, the next step in the proposed patterning method is to model the assembled pattern within the 3D boundary.

4.2 Proposed method of cutting pattern assembly and evaluation

With the cutting pattern determined by the methods shown throughout section 4.1, the next step is to evaluate the suitability of the cutting pattern. This is achieved by simulating the assembly of the cutting pattern, while omitting the residual stresses from flattening, stress

reduction and compensation. Here the focus is not on replicating the exact erection procedure, but on finding the equilibrium shape of the assembled geometry.

The equilibrium geometry of the assembled panels is the geometry that the fabric in the physical structure, after erection and tensioning has been completed, is intended to adopt. Since the flattening, and integrated stress reduction and compensation processes cannot produce completely stress-free geometries for the panels, there will be deviations from the intended pre-stress in the assembled cutting pattern. It is thus this equilibrium geometry that should be analysed for performance under external load, as this takes account of the varying pre-stress across the surface.

In the proposed pattern assembly method, an additional step of re-meshing the cutting pattern panels with an orthogonal mesh is introduced, to give a model that is more representative of the fabric. This section describes the method of orthogonal mesh generation, and some conditions for its successful use. Furthermore, this section presents the processes for assembling the cutting patterns, and finding their equilibrium position. These three sub-processes of (i) orthogonal re-meshing, (ii) assembly of the re-meshed panels, and (iii) equilibrium finding of the assembled patterns, define the proposed method of cutting pattern assembly. The final equilibrium position of the assembled pattern facilitates the evaluation of the cutting pattern, as the deviation of the stress from the intended pre-stress is calculated.

4.2.1 Orthogonal re-meshing of planar panels

The first step in assembling the determined cutting patterns is to re-mesh the panel with an orthogonal mesh. This step is included on the following basis:

As mentioned, the weave of the fabric must shear for it to adopt a doubly curved geometry. Fibre directions are unknown in the 3D geometry, so assumptions are made in the earlier processes (see section 4.1.2.1). This is not the case once the cutting pattern has been

determined by the methods outlined in section 4.1. In the determined cutting pattern, it is known that the fibre directions are broadly orthogonal (deviation of up to 5° [66] is possible), since this is the direction of the fibres in the fabric from which the pattern will be cut.

By constructing an orthogonal mesh using the discrete element model, proposed in chapter 3, the warp and weft directions of the fabric are represented exactly. The elements representing the fibres undergo shear deformation during the assembly of the panels, and so the directions of the fibres change appropriately. By including this step of orthogonal re-meshing, the fabric behaviour is more accurately represented.

4.2.1.1 Construction of the orthogonal mesh

Construction of an orthogonal mesh on the generated cutting pattern panel boundary is straightforward. Two arrays of orthogonal grid lines, representing the warp and weft directions, are intersected with the panel boundary, shown on an example pattern in Figure 4.10:

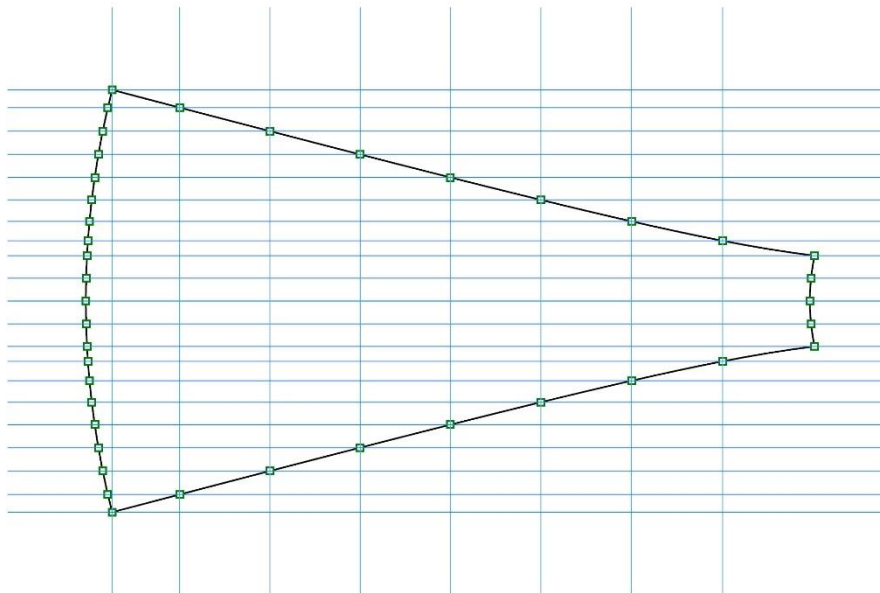


Figure 4.10 - Intersection of orthogonal lines with defined cutting panel boundary

However, the positioning of the orthogonal grid lines in relation to the panel boundary affects the quality and suitability of the mesh. Thus the grid lines cannot be defined arbitrarily.

4.2.1.2 Factors affecting the suitability of the orthogonal mesh

Two factors affect the condition of the mesh and its suitability for use in the modelling of the pattern assembly. These factors are (i) the location of the nodes along the boundary, and (ii) the triangulation of the mesh along the boundaries.

(i) Node location along the boundary

The location of the nodes along the boundary affects the accuracy of the re-meshing. The boundary of the generated cutting pattern is represented by a polyline. Intersecting the orthogonal grid lines with the boundary results in new nodes along the boundary, and thus the boundary is redefined by the elements between these nodes.

Figure 4.11 shows a close up of an example boundary curve (black lines) from a generated cutting pattern. The original nodes are shown in red. This curve is intersected with several orthogonal grid lines (blue lines in Figure 4.11) to give new nodes (green points in Figure 4.11). Redefining the boundary curve based on these points, it can be seen that the length of the boundary between nodes is not necessarily preserved. Referring to Figure 4.11 again, the part of the new boundary, with length x , is not equal to that of the original boundary, comprising lengths a and b .

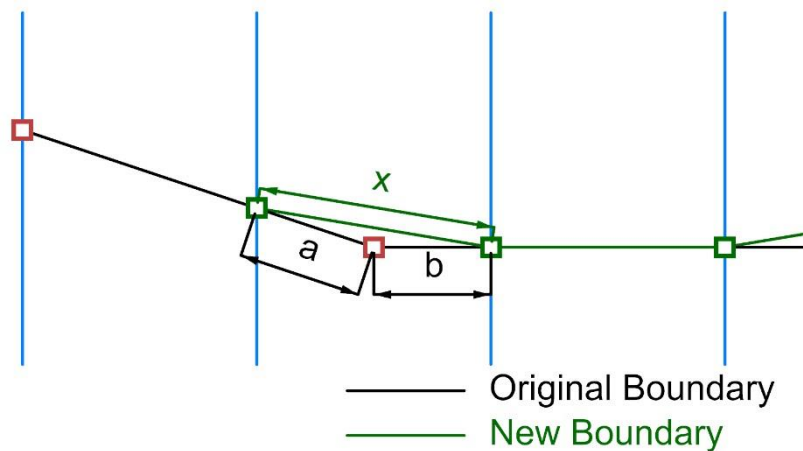


Figure 4.11 - Misrepresentation of boundary due to poor choice of orthogonal grid lines

Though the disparity in this example is exaggerated, when the new nodes are mapped to the 3D panel boundary (necessary for the joining of panels, see section 4.2.2.2), fictitious straining is induced. For cable boundaries, and the seam edges of panels that are free to move in the equilibration scheme, these strains naturally dissipate as the structure finds equilibrium. However, if both ends of an element are fixed, such as along rigid boundaries, this fictitious straining is not dissipated. Since these nodes then represent the base points for other elements, erroneous positioning of the nodes results, affecting the analysis.

This issue can be overcome by using a suitably fine mesh, but such a solution can result in excessive elements elsewhere in the mesh. A more appropriate solution is to use the boundary nodes, from the mesh used to determine the cutting pattern, as the base points for generating the orthogonal gridlines from which the mesh is then constructed. This ensures an accurate redefinition of the boundary, and the nodes may be mapped back to the 3D panel boundary with virtually no distortion. Using the original nodes to define the new mesh requires careful consideration, as for some cutting patterns, achieving a more consistent spacing of the mesh is of more importance.

(ii) Triangulation of the mesh along the boundaries.

For meshes on non-rectilinear geometry, such as that shown in Figure 4.10, the boundary will not align with either the warp or weft direction. Nodes along such boundaries should have a valency of 2 – i.e. one warp and one weft element should attach to each node. (*The valency of a node, in this context, refers to the number of elements connected to the node*). This results in triangulation of the mesh near the boundary, and is necessary to prevent numerical ill conditioning, and to ensure correct construction and apportioning of the fabric width to elements.

Throughout the remainder of this thesis, a 'triangulated mesh' refers to a mesh where the nodes along the boundaries have a valency of two, and as a result, where the elements along the boundary form triangles.

Where boundaries between panels are merged (section 4.2.2) to give internal seam lines, triangulation will similarly result. It is most important to ensure triangulation when the boundary is unrestrained or partially restrained. Figure 4.12 shows a portion of a mesh near the boundary, both for triangulated and non-triangulated configurations:

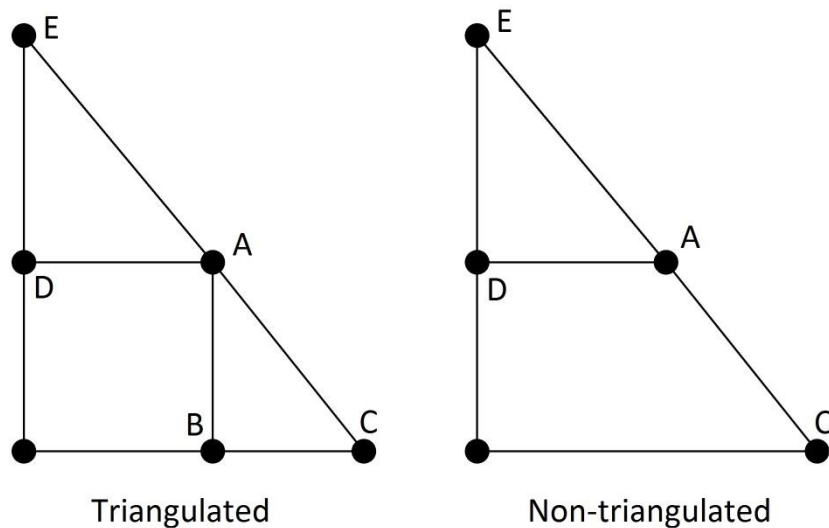


Figure 4.12 - Portions of triangulated and non-triangulated meshes

In the triangulated mesh, nodes A & E have a valency of two – two elements attach to both nodes. As such, the elements along and near the boundary form triangles, e.g. A-B-C, and A-D-E. In the non-triangulated mesh, node B and element A-B are missing, and thus node A has a valency of one, and triangles are not formed along the boundary. It is shown in chapter 5, that a node with a valency of one, such as node A in the non-triangulated mesh, will undergo gross deformations and result in failure of the numerical analysis.

The triangulation condition is a finding of this research, and relates to **RO 1 (c)** – the identification of conditions and guidance for successful use of discrete models in patterning. As mentioned above, this condition for the configuration of the mesh is expanded upon in chapter 5, section 5.4.3.

Following the re-meshing of the panels, the next step is to assemble these panels.

4.2.2 Assembly of orthogonally meshed panels

To model the assembly of the panels, nodes and elements along the edges of adjacent panels are merged to create a new mesh. For this to be possible, along the common edges of adjacent panels, the boundary nodes that will be merged should be close together.

Some deviation is acceptable, but to ensure the boundary nodes are sufficiently close, the pattern determination processes should produce a pattern such that; (i) the common edges shared between adjacent panels are near equal in length, (ii) the individual panel meshes have the same number of boundary nodes, and (iii) the boundary nodes of the two panels have approximately equal spacing, as shown in Figure 4.13:

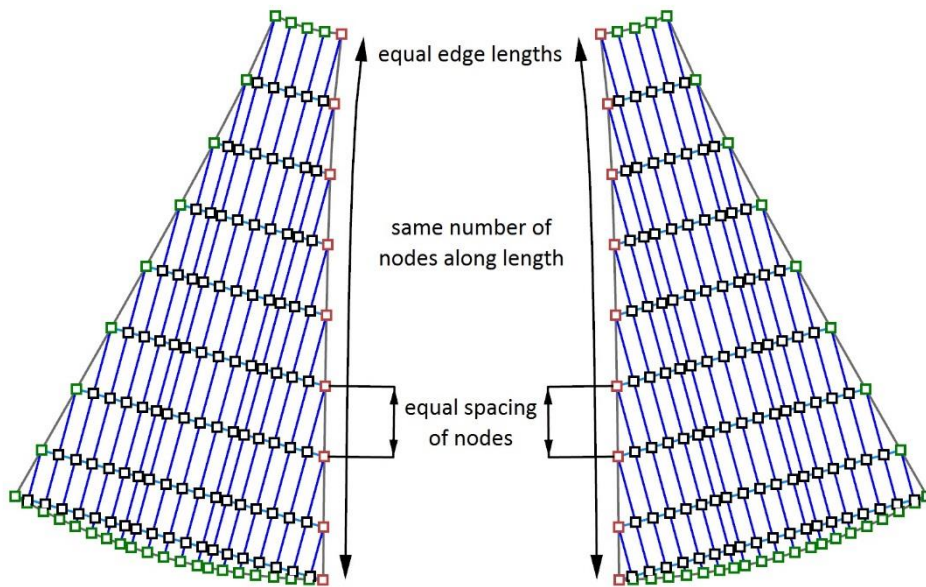


Figure 4.13 - Conditions for joining of panels

In the re-meshed cutting pattern, the 2D seam lines represent the common edges between adjacent panels. Even if the generated cutting pattern meets the criteria of length, number of nodes and spacing of nodes, as above, the 2D boundaries will still deviate significantly from each other in terms of geometry.

For this reason, the boundary nodes of the planar meshes, for each panel, are mapped to the boundaries of the original 3D panels. The original 3D panels are those defined by the subdivision of the form-found membrane (section 4.1.1), which were flattened, and subjected to stress reduction and compensation (sections 4.1.2 & 4.1.3) to give the cutting pattern.

Original panels that are adjacent have a common edge, the seam line, and so mapping the boundary nodes in this way ensures that the nodes along the boundaries of adjacent panels are sufficiently close to join the panels.

4.2.2.1 Mapping the panels

The procedure for mapping a panel is as follows, and is described diagrammatically in figures 4.14 (a) through 4.14 (c):

1. Re-orient 3D boundary to reduce distortion from mapping (4.14 (b)).
2. Map boundary nodes to re-oriented 3D panel boundary (4.14 (b)).
3. Move 3D boundary back to original position (4.14 (c)).

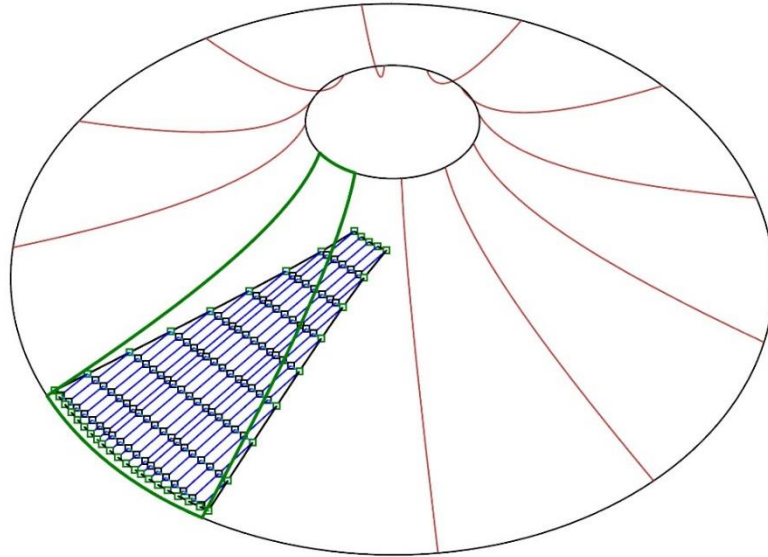


Figure 4.14 (a) - Planar pattern in relation to original 3D panel geometry

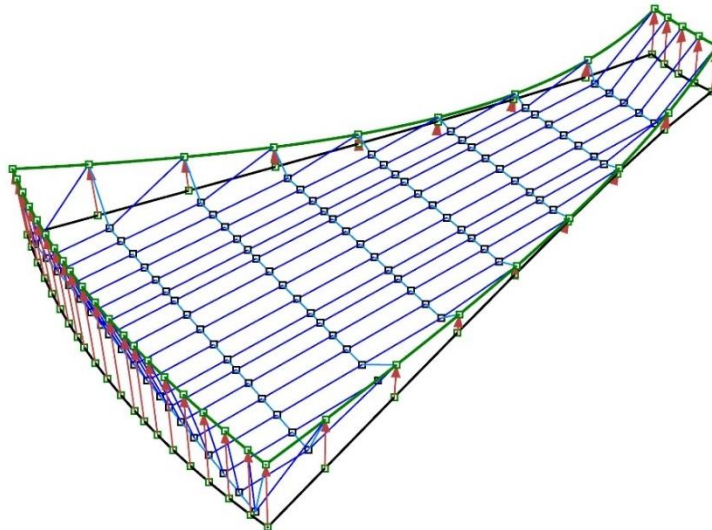


Figure 4.14 (b) - Re-orientation of 3D panel geometry, and subsequent mapping of boundary nodes (steps 1 & 2)

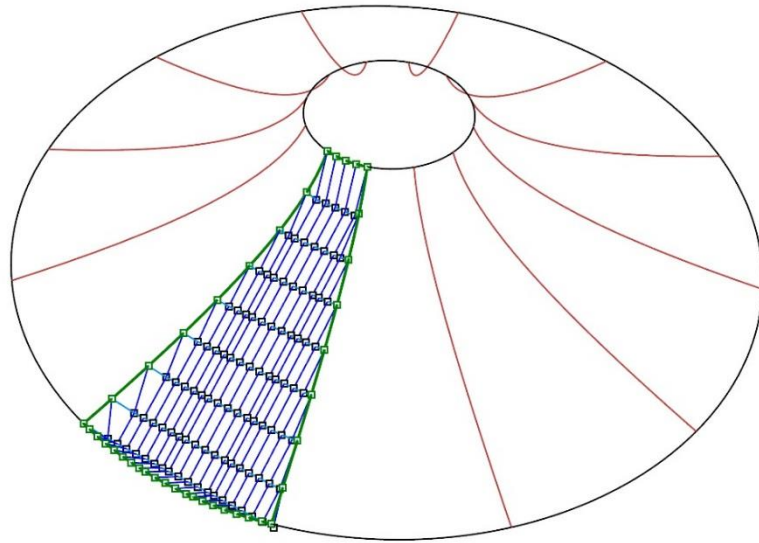


Figure 4.14 (c) - Rotation and translation of mapped panel to appropriate location in assembled structure (step 3)

This procedure is repeated until all panels are in their appropriate 3D position (Figure 4.15). In the case of a catenoid, due to rotational symmetry, it is acceptable to simply duplicate and rotate one mapped panel.

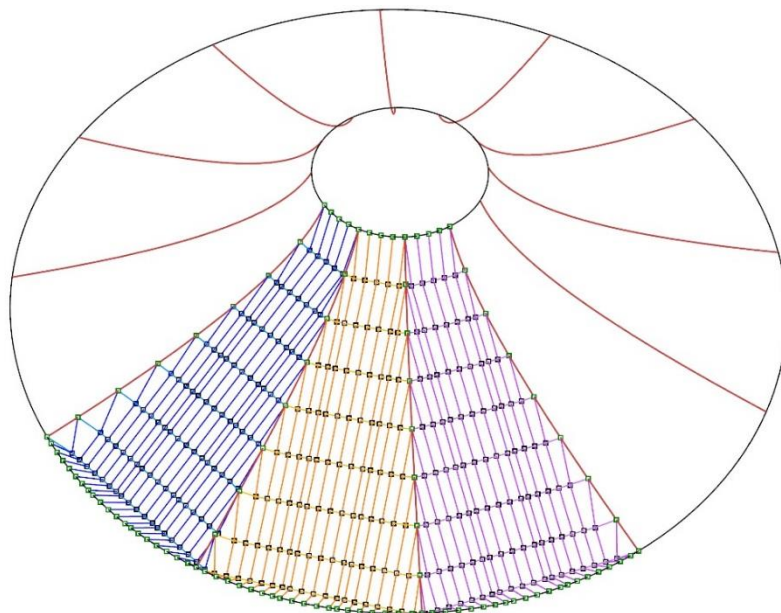


Figure 4.15 - Multiple panels arranged appropriately, to allow joining of adjacent panels (due to symmetry one quarter of this structure is sufficient for performing analyses)

The next step in the proposed method of cutting pattern assembly is to join the constituent panels into one mesh that can be analysed.

4.2.2.2 Joining the panels

With the panels arranged into an appropriate position for joining, the individual meshes are converted to a single mesh. This is achieved by merging approximately coincident nodes along the seam lines, hence the requirement to ensure approximate coincidence of the resulting 3D nodes when meshing the panels. Merging of the nodes is achieved by simply averaging the global coordinates of the two nodes.

Elements along the seam lines must similarly be merged. Since the seam lines of the mesh do not represent the warp or weft direction of the fabric, they are excluded in the equilibrium analysis (discussed in section 4.2.3). Elements along the seam lines therefore contribute only to the geometric description of the surface. For this reason it is sufficient to simply construct a new element between the positions of the new merged nodes. For example, consider the elements along the common seam edges highlighted (in red) in Figure 4.16:

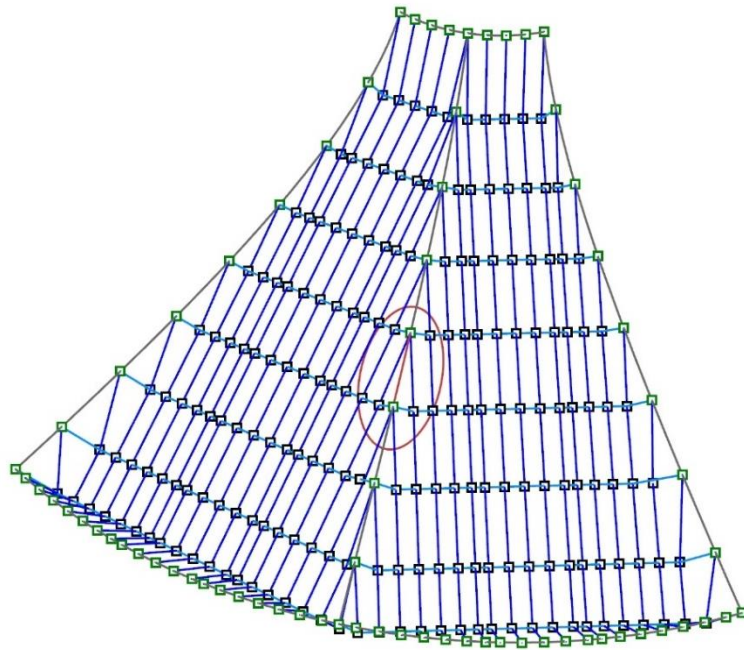


Figure 4.16 – Elements along a common edge

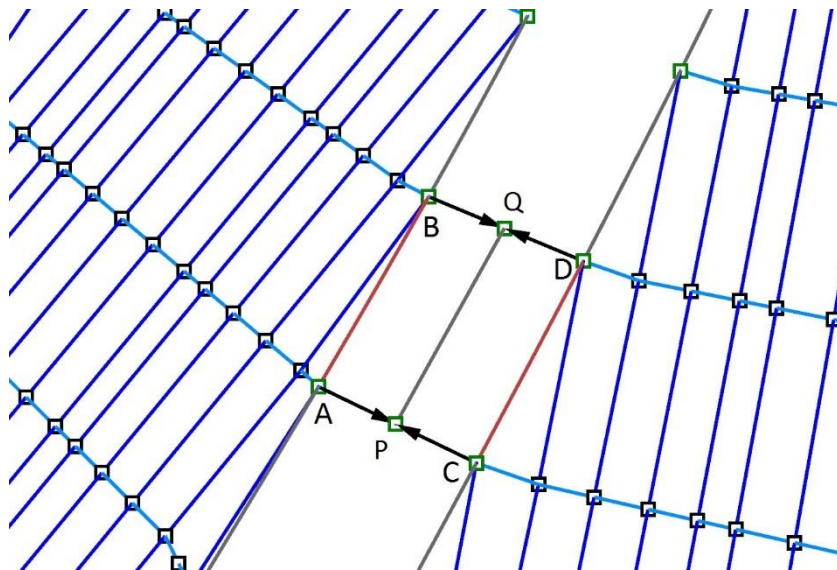


Figure 4.17 – Elements A-B and C-D become element P-Q

As illustrated in Figure 4.17, Nodes A and C merge to become node P, and nodes B & D merge to become node Q. Thus, elements A-B and C-D must be discarded, and a new element, P-Q created. Because this element comes from two boundary elements, and represents part of a

seam line (not a warp or weft element), it does not contribute to the mechanical behaviour of the model.

A new mesh is thus created comprising the original non-seam nodes and elements, and the new merged nodes and elements. Figure 4.18 shows the multiple meshes in Figure 4.15 merged into one mesh. The mesh at this stage is not in equilibrium, representing only the assembly of the panels as an intermediate step in the computational analysis.

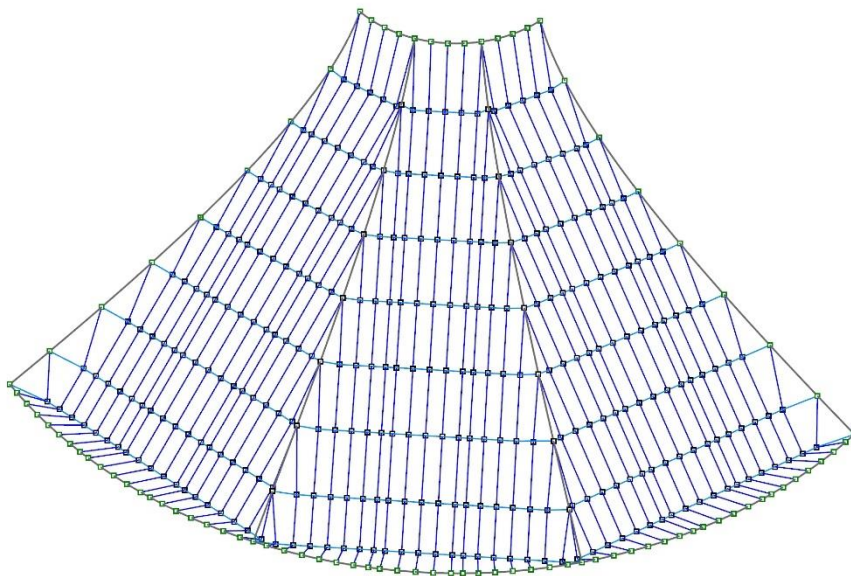


Figure 4.18 - Joined mesh representing portion of structure (due to symmetry one quarter of this structure is sufficient for performing analyses)

To evaluate the suitability of the cutting pattern, the final step in the proposed method of cutting pattern assembly is to find the equilibrium position of the assembled pattern, so that final stresses are known.

4.2.3 Equilibrium finding of the assembled mesh by dynamic relaxation

With a joined mesh representing the assembly of the cutting pattern, the proposed method again makes use of dynamic relaxation, to find the equilibrium position of the assembled cutting pattern within the 3D boundary.

To measure the stress in the fabric, which arises due to displacement of the panel into the boundary, the analysis is formulated such that the 2D orthogonal mesh geometry is the reference geometry. As mentioned, since the elements along the seam lines of the panels do not represent either the warp or weft directions of the mesh, they are excluded in the analysis, contributing only to the geometric description of the surface.

Restraints are applied appropriate to the boundary conditions. Effectively rigid boundaries such as beams or trusses, are represented by nodes restrained in all three global directions (*fixed nodes*). With the assembly appropriately restrained, dynamic relaxation is then performed as described in chapter 3, section 3.2. The algorithm is run until the residual forces at the nodes are sufficiently small. Typically, a maximum nodal force of 10^{-6} kN is achievable.

Because the method of cutting pattern generation does not produce completely stress free cutting patterns, the assembly and equilibration of the cutting pattern will not result in exactly the intended pre-stress state. Thus, after equilibrium has been found, the deviation of the stress-state from the intended pre-stress is known, giving a measure of the suitability of the cutting pattern.

4.3 Summary

This chapter presented the proposed patterning method, comprising two constituent stages: *the method of cutting pattern determination, and cutting pattern assembly and evaluation.*

The proposed *method of cutting pattern determination* was shown to comprise (i) subdivision of the form-found surface, (ii) subsequent flattening of the panels, and (iii) integrated stress reduction (reduction of stresses arising from flattening) and compensation (reduction in size to account for pre-stress). Constructing a discrete element mesh based on geodesics was explored and it was concluded that a mesh constructed from geodesics in one direction was most appropriate for flattening. Three flattening methods were described, two of which were developed by the author to reduce distortions in the planar panels, before integrated stress reduction and compensation. The presented flattening methods, based on unrolling of the panel, result in better initial configurations for stress reduction. This improvement over existing methods is supported through examples presented in chapter 5. Restraints and stress formulations for integrated stress reduction and compensation were discussed.

The *cutting pattern assembly and evaluation* stage was shown to comprise (i) orthogonal re-meshing of the planar panels, (ii) assembly of the re-meshed panels through mapping of the panels to their original 3D boundaries, and (iii) equilibrium finding of the assembled pattern by dynamic relaxation.

Re-meshing of the panel with an orthogonal mesh is rarely included in patterning analyses. Coupled with the discrete element model, the fabric behaviour is more accurately represented by the proposed method. The method for assembly of the re-meshed panels was presented, including consideration of the coincidence of the boundary nodes, and mapping of the 2D panel boundaries to the 3D boundaries to provide an initial configuration from which equilibrium of the assembly is determined. The method for joining the constituent panel meshes into one mesh was described. The proposed method for equilibrium finding of the joined mesh, to give the final stresses in the membrane, and evaluate the cutting pattern was presented.

In the following chapter, results are presented to show the effectiveness of the proposed patterning method.

5 Application of the method to examples and results

5.1 Introduction

This chapter presents results for each stage of the patterning process proposed in chapter 4, employing the discrete model described in chapter 3. Cutting patterns and final stress distributions for two examples are presented, facilitating comparisons with results from published work, which are used to demonstrate the suitability of the model. The results presented demonstrate how the proposed discrete model and patterning method address the research objectives stated in chapter 1:

RO 1: The development, application and examination of a discrete model

RO 2: The advancement of the computational process of patterning

The results are presented in the order in which the computational processes were conducted for each example. How the research objectives are fulfilled by the results is indicated throughout the chapter.

In the first section, section 5.2, the methods for determining the cutting pattern are demonstrated. The stresses incurred by the different proposed flattening methods, their subsequent effect on residual cutting pattern stresses, and the resultant cutting patterns, are investigated in depth for the first comparison with the work of Linhard et al. [6]. These results address research objective **RO 2 (a)** – concerned with the improvement of flattening. Cutting patterns generated by excluding and including shear during the stress reduction and compensation are presented, and address research objective **RO 2 (b)**. The cutting patterns generated for the second comparison, with the work of Moncrieff & Topping [4], are presented briefly, such that they may be compared with the final pattern assembly later in the chapter.

In the second section, section 5.3, the assembly of the cutting patterns is presented. This facilitates comparison with the published work. It is shown that the final membrane stresses are within the ranges reported in the literature. These results are presented in relation to research objectives **RO 1 (a)** and **RO 1 (b)**, concerned with implementation of the model and examination of its suitability for patterning.

In the third section, section 5.4, critical factors affecting the analysis of the pattern assembly are explored. One intention of this research is to identify conditions for successful use of discrete models **RO 1 (c)**. In addition to investigating (i) the effect of including shear in the analysis, two further factors were identified. These are (ii) the conditioning of shear elements, and (iii) the triangulation of the mesh near the boundary. The effects of these factors are discussed through the use of further analyses of the cutting pattern assembly.

5.2 Flattening, stress reduction and compensation results

In this first section, results relating to the proposed methods for determining the cutting pattern are demonstrated. The results in this section are presented to address research objectives **RO 2 (a)**, concerned with the investigation of flattening methods, and **RO 2 (b)** – the investigation of the effect of including shear on the cutting pattern.

5.2.1 Specification for geometry from Linhard et al. [6]

The first comparison is made with the work of Linhard et al. [6]. This example is used to:

- Highlight the differences in incurred flattening stresses, for each of the three proposed flattening methods.
- Show the effect of the flattening method on the subsequent stress reduction and compensation, and the resulting residual stresses and cutting pattern geometry.
- Show the effect of including shear, during stress reduction and compensation, on the residual stresses and geometry of the final cutting pattern.

The assembly of the most suitable cutting pattern is shown later, in sections 5.3.1 and 5.4.1.

5.2.1.1 Method used by Linhard et al. [6]

Linhart et al. [6] made use of a continuum model, and employed an iterative procedure to incrementally improve the cutting pattern. This was achieved through the use of a *mechanical problem formulation*, as detailed in Chapter 2, section 2.1.5, and so material properties were used for generation of the cutting patterns. Residual stresses in the cutting pattern after flattening were reduced by using the Newton-Raphson iteration to relax the stressed panels into a reduced stress state. Compensation of the patterns to account for pre-stress was not included in the original analysis by Linhard et al. [6]. Figure 5.1 shows the catenoid geometry from Linhard et al. [6].



Figure 5.1 – Form-found Catenoid geometry from Linhard et al. [6]

5.2.1.2 Patterning conducted by the author

A catenoid with geometry taken from [6] was form-found using RhinoMembrane [63], and cutting patterns were generated using the methods outlined in chapters 3 & 4. The relevant dimensions specified in [6] were an upper ring diameter of 1.2 m, a lower ring diameter of 5.6 m, and a ring separation of 1.0 m. The prescribed pre-stress was 2 kN/m, and the tensile stiffness modelled as isotropic, with a value of $E = 220$ kN/m. No shear stiffness was specified in [6], so the shear stiffness was estimated as 1/20 of the tensile stiffness, in accordance with the recommendation in [15,35]. Applying this heuristic to the tensile stiffness of 220 kN/m gave a

shear stiffness of $G = 11 \text{ kN/m}$. Consequently, the relevant material properties for stress reduction and compensation were:

- Tensile stiffness: $E = 220 \text{ kN/m}$
- Shear stiffness: $G = 11 \text{ kN/m}$
- Prescribed pre-stress: $\sigma_p = 2 \text{ kN/m}$

Owing to symmetry, one quarter of the shape was form-found and analysed for patterning, with this $\frac{1}{4}$ surface divided into 3 panels, 12 panels having been used in the original analysis by Linhard et al. [6]. Since the surface is rotationally symmetric, only one panel must be flattened, and subjected to stress reduction and compensation to generate the cutting pattern. Thus one panel was extracted from the form-found shape, and the processes of flattening, stress reduction and compensation applied, as detailed in sections 5.2.2 to 5.2.4.

5.2.2 Stresses incurred through flattening for geometry from Linhard et al. [6]

The first step in the patterning process is to flatten the panel into the plane, to generate an initial cutting pattern. The stresses incurred during flattening depend on the method of flattening used. To investigate the effect of the flattening method on residual stresses in the initial cutting pattern, three flattening methods were used to generate the cutting pattern:

1. Direct projection (chapter 4, section 4.1.2.3)
2. Unrolling the panel with one spine (chapter 4, section 4.1.2.4)
3. Unrolling the panel with two spines (chapter 4, section 4.1.2.5)

As mentioned in chapter 4, the first case, direct projection, is the simplest method and offers a benchmark with which to compare methods 2 & 3. Methods 2 & 3 were proposed by the author in chapter 4, with the intention of improving on direct projection. To evaluate the effectiveness of these flattening methods, the initial cutting pattern for the panel extracted from the form-

found shape was generated using each method. The stresses incurred by each flattening method are shown in the following section.

5.2.2.1 Axial stresses incurred

Figures 5.2 – 5.4 show the axial stresses incurred through the use of each method. It is relevant to consider the incurred stresses in comparison with the original panel curvatures. Figure 5.5 shows the Gaussian curvature as it varies across the panel, for comparison with the residual stress distributions.

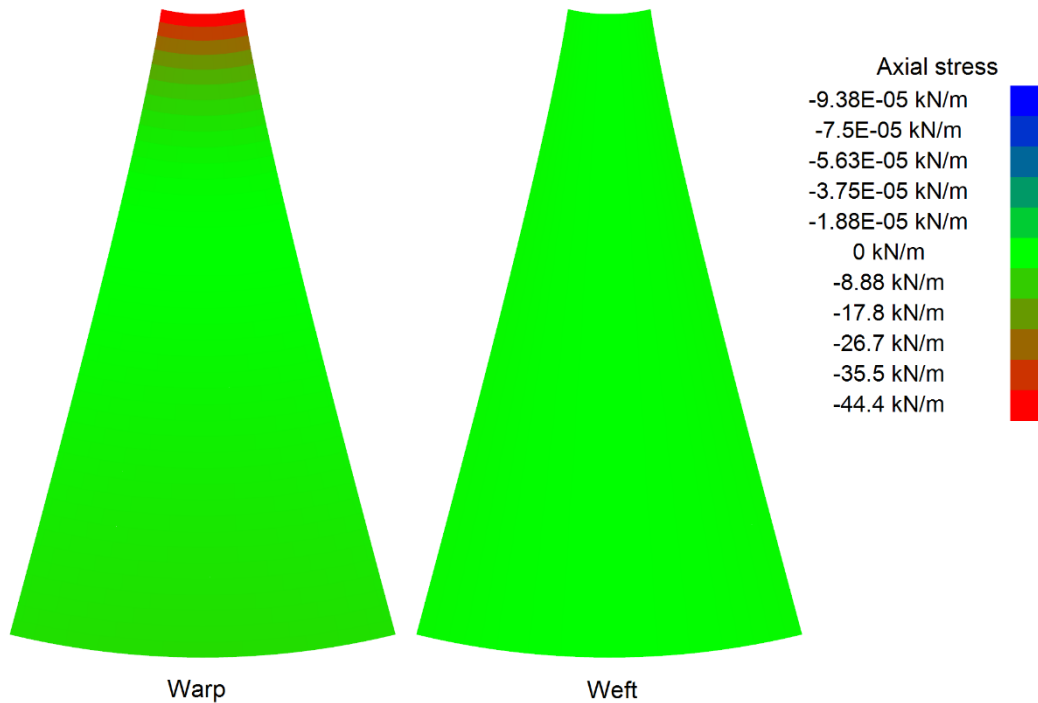


Figure 5.2 – Axial stresses incurred by direct projection

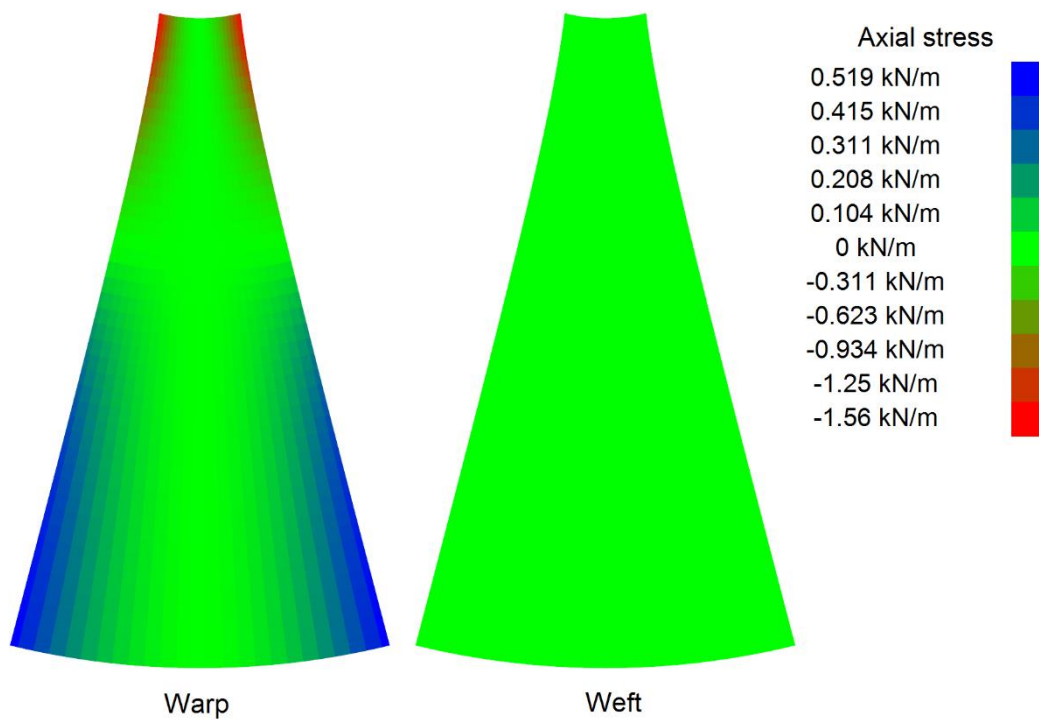


Figure 5.3 – Axial stresses incurred through unrolling with one spine

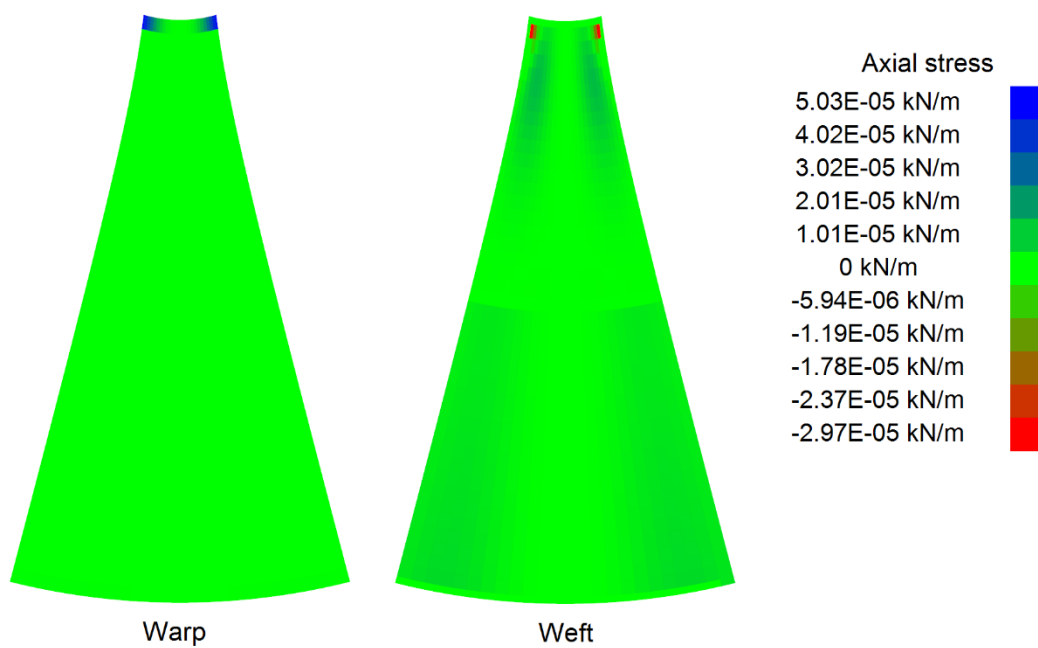


Figure 5.4 – Axial stresses incurred through unrolling with two spines

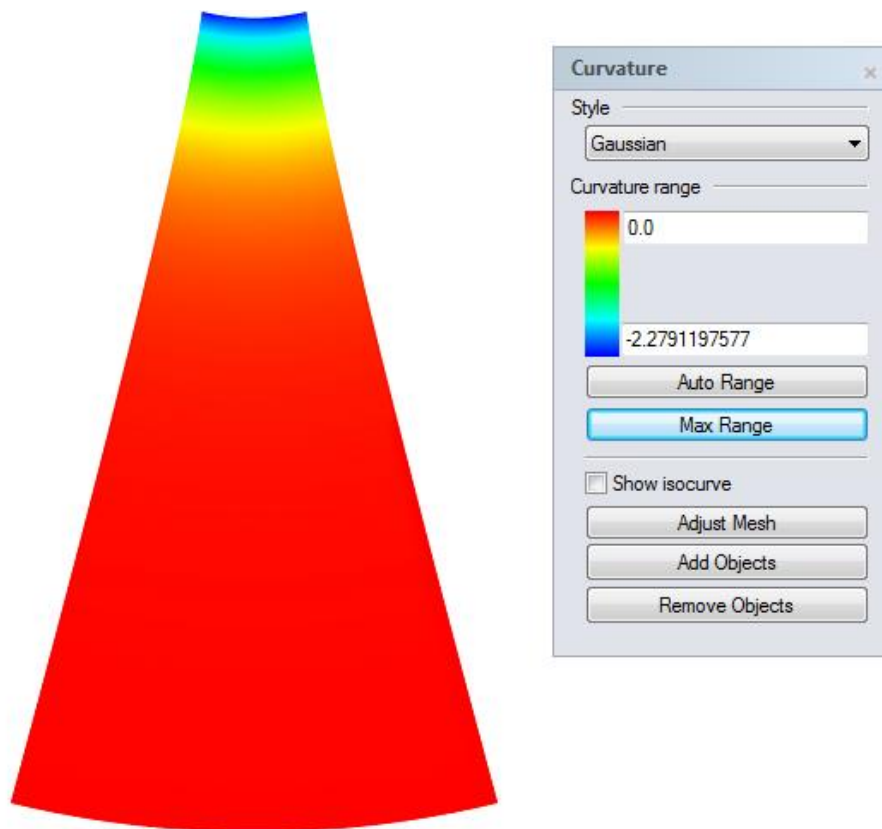


Figure 5.5 - Gaussian curvature across the panel for the geometry from Linhard et al. [6]

It is important at this point to state that for the stress reduction and compensation analysis, the fabric is modelled as capable of sustaining compression. This is necessary to successfully generate the cutting pattern. In the assembly of the cutting patterns (section 5.3), the fabric is modelled as incapable of sustaining compression, giving zero stress and force for negative strain, and more realistically representing the fabric.

Flattening the panel with direct projection (Figure 5.2), incurs high negative stresses in the warp direction towards the upper boundary, corresponding to the area of highest Gaussian curvature (see Figure 5.5). There is little stress incurred away from this region of high curvature or in the weft direction. This is expected, since the curvature is higher in the warp direction, and the deviation between the panel and the plane is greatest towards the upper boundary.

Flattening the panel by unrolling with one spine (Figure 5.3), incurs minor positive and negative stresses in the warp direction. These stresses are spread across the panel, rather than concentrating towards the upper boundary, though that is where the greatest distortion occurs. Very little stress is incurred in the weft direction, because the warp direction was used for defining the spine, meaning that the weft elements were mapped first, with zero distortion. Since the spine was located along the centre of the panel, the stresses accumulate towards the edges of the panel.

Flattening the panel by unrolling with two spines (Figure 5.4), incurs negligible axial stresses across the panel, though noticeably different stresses occur in very local regions near the neck. This is expected, since the mapping is intended to achieve zero axial distortion, though this is not completely possible due to limitations of the accuracy of the algorithm.

It should also be noted here that the Gaussian curvature across the panel shown in Figure 5.5 indicates some areas of very flat fabric. This is in part due to the inaccuracy of the legend, and also due to the accumulation of various errors throughout the process of defining the panel. Inaccuracies during form-finding, and when converting the mesh to a spline surface contribute to this.

5.2.2.2 Shear stresses incurred

In addition to the axial stresses incurred by each flattening method, shear stresses are similarly incurred. Figures 5.6 – 5.8 show the shear stresses incurred by each flattening method.

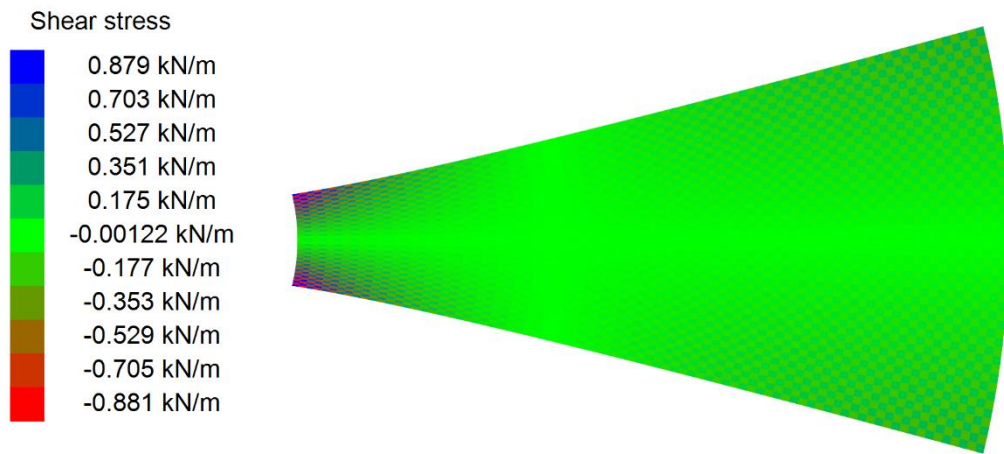


Figure 5.6 – Shear stresses incurred through flattening by direct projection

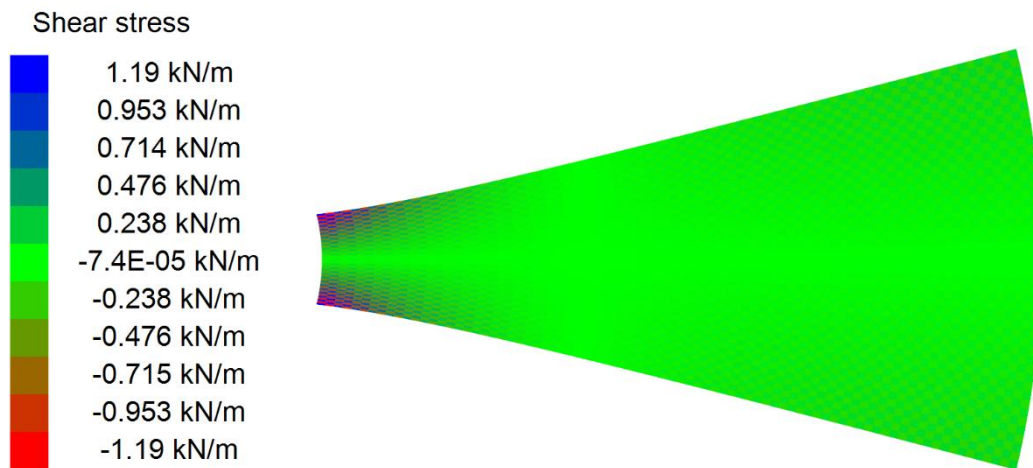


Figure 5.7 - Shear stresses incurred through unrolling with one spine

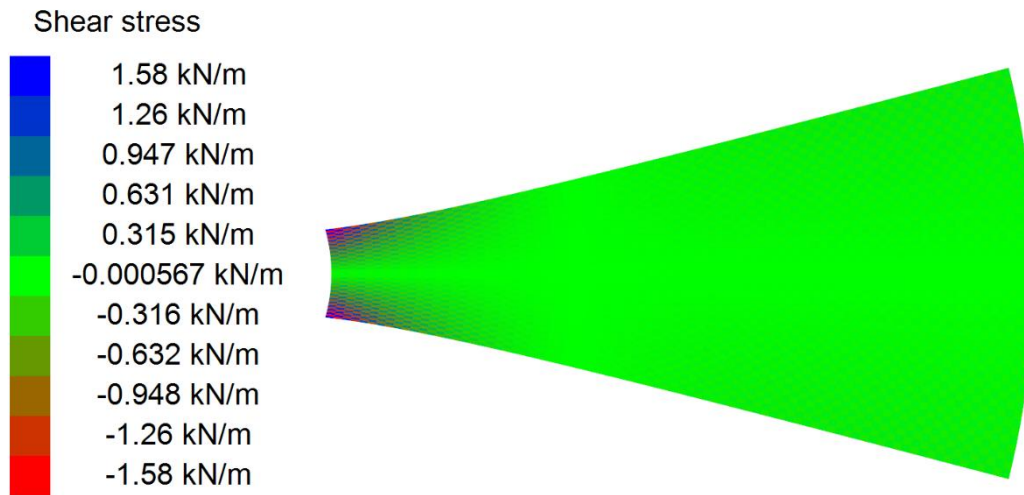


Figure 5.8 – Shear stresses incurred through unrolling with two spines

The distribution of shear stresses is similar for all three flattening methods. However, flattening with direct projection (Figure 5.6) gives the least shear stress, followed by unrolling with one spine (Figure 5.7). Finally, unrolling with two spines (Figure 5.8) gives the greatest shear stress.

5.2.2.3 Comparison of flattening methods

Comparing the incurred axial and shear stresses together for all flattening methods yields some interesting insights. Table 5.1 summarises the incurred stresses for each flattening method.

Table 5.1 – Maximum and minimum incurred stresses for all flattening methods

Method	Maximum axial stress (kN/m)	Minimum axial stress (kN/m)	Maximum shear stress (kN/m)	Minimum shear stress (kN/m)
Direct projection	-9.38E-05	-44.4	0.879	-0.881
Unrolling (one spine)	0.519	-1.56	1.19	-1.19
Unrolling (two spines)	5.03E-05	-2.97E-05	1.58	-1.58

The highest and lowest axial and shear stresses are highlighted in bold in Table 5.1. Considering the methods together yields the following insights:

- Direct projection gives minimal shear stress at the expense of high axial stresses.
- Unrolling with two spines gives near-zero axial stress at the expense of high shear stresses.
- Unrolling with one spine offers a compromise between the two, reducing the maximum and minimum axial stresses to acceptable values, whilst incurring only a marginal increase in shear stress when compared with direct projection.

Since the initial cutting patterns generated through the flattening method are the initial condition for the subsequent stress reduction and compensation steps, the residual stresses shown in Figures 5.2 – 5.4 and 5.6 – 5.8 will affect the cutting pattern. The effect of these different stress distributions, incurred through different flattening methods, on the resulting cutting patterns is discussed in the following sections.

5.2.3 Residual stresses after stress reduction and compensation for geometry from Linhard et al. [6]

To generate patterns suitable for cutting from planar cloth, the stresses incurred by flattening must be removed, or reduced as much as possible. The proposed patterning method makes use of dynamic relaxation to achieve this, as detailed in chapter 4, section 4.2.3. The effectiveness of the proposed method is now demonstrated. With the initial cutting patterns defined by each flattening method, stress reduction and compensation were applied. To investigate the effect of including shear stiffness in the analysis, cutting patterns were generated both excluding and including the shear stiffness.

Throughout all stress reduction and compensation processes, nodes at the midpoint of each edge were restrained approximately perpendicular to this edge, to prevent rigid body rotations and translations of the panel. This is as proposed in chapter 4, section 4.1.3.

5.2.3.1 Residual stresses excluding the shear stiffness of the fabric

The first application of stress reduction and compensation by dynamic relaxation was made without including the shear stiffness in the analysis. Figures 5.9 – 5.11 show the residual axial stresses after stress reduction and compensation.

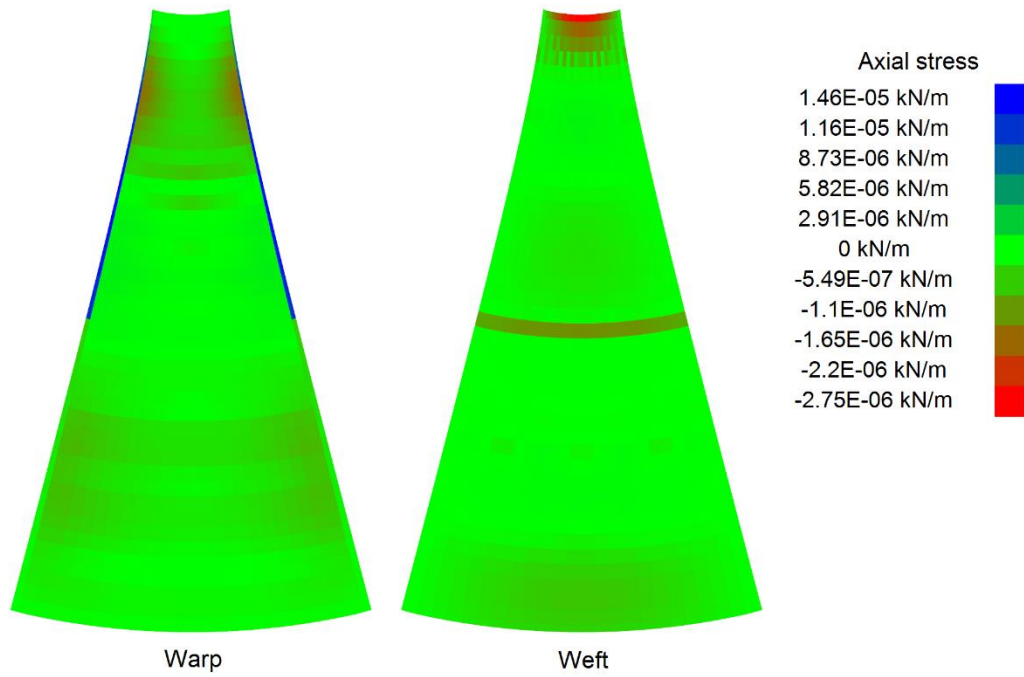


Figure 5.9 – Residual stresses after stress reduction and compensation without including the shear stiffness of the fabric, after direct projection flattening

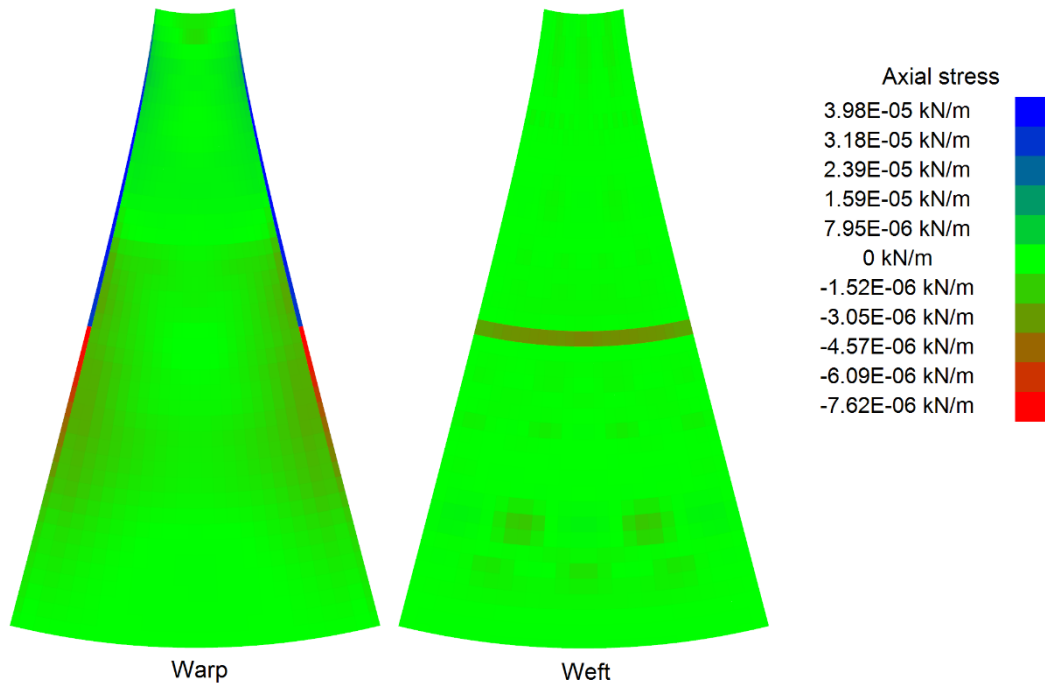


Figure 5.10 – Residual stresses after stress reduction and compensation without including the shear stiffness of the fabric, after flattening by unrolling with one spine

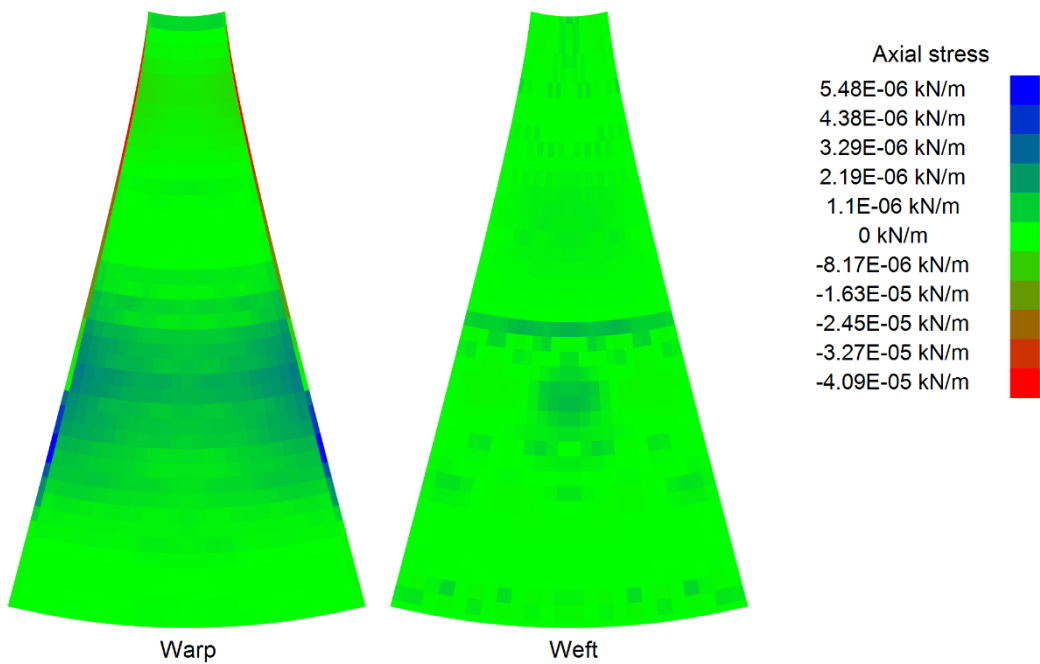


Figure 5.11 – Residual stresses after stress reduction and compensation without including the shear stiffness of the fabric, after flattening by unrolling with two spines

The residual stresses after stress reduction and compensation, for all flattening methods are negligible. It is theoretically possible to achieve zero residual stress when excluding shear during stress reduction and compensation, but in practice this is limited by the accuracy of the numerical method used; in this case the dynamic relaxation algorithm (see section 3.2.1.2). The stresses are, however, negligibly low, and are acceptably close to the theoretically possible zero distortion. Whilst the residual stresses are negligible, some similarities and differences in the pattern of stresses can be seen across Figures 5.9 – 5.11. In the weft direction, there is a clear band of differing stress across the middle of the panel. The location of this band aligns with the edge nodes that were partially restrained, indicating that the restraints used have some effect on the stress distribution. The stresses along the edges are different from those in the body of the panel for all three methods, but between methods the distribution of these edge stresses differs.

5.2.3.2 Residual stresses including the shear stiffness of the fabric

The second application of stress reduction and compensation was made including the shear stiffness of 11 kN/m in the analysis. Figures 5.12 to 5.14 show the residual axial stresses, and Figures 5.15 – 5.17 show the residual shear stresses after stress reduction and compensation.

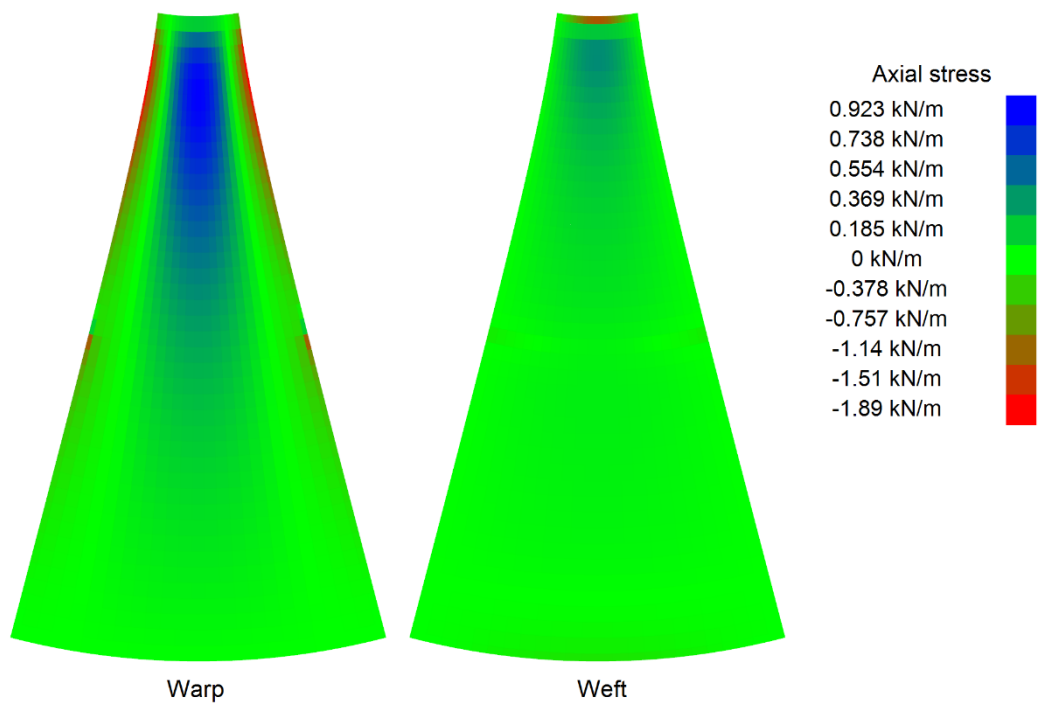


Figure 5.12 – Residual stresses after stress reduction and compensation, including the shear stiffness of the fabric, after direct projection flattening

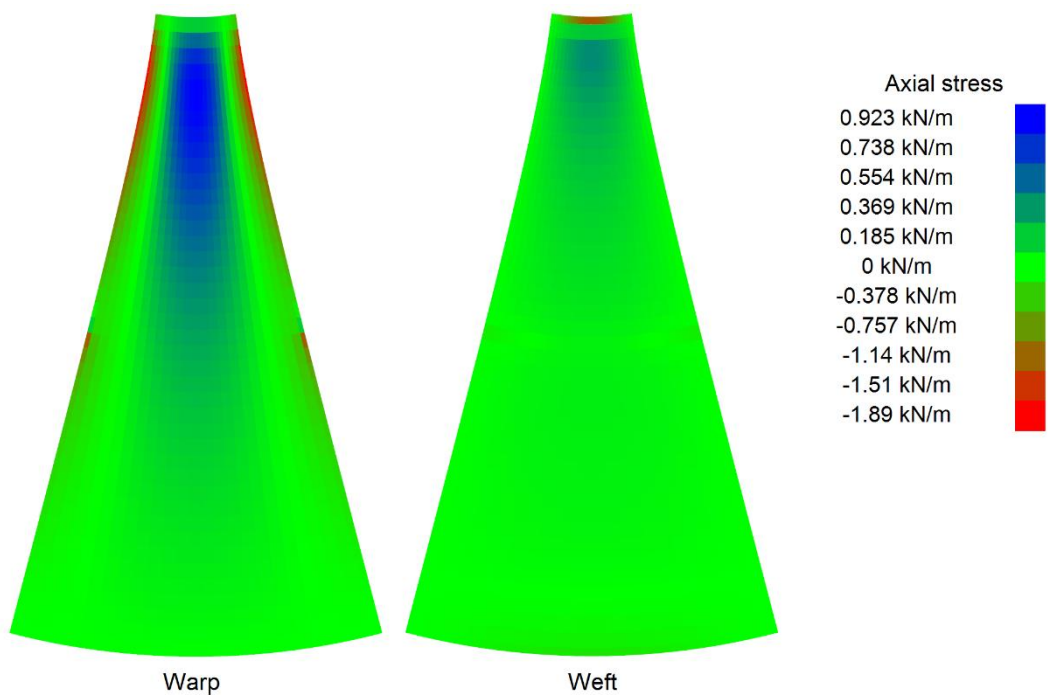


Figure 5.13 – Residual stresses after stress reduction and compensation, including the shear stiffness of the fabric, after flattening by unrolling with one spine

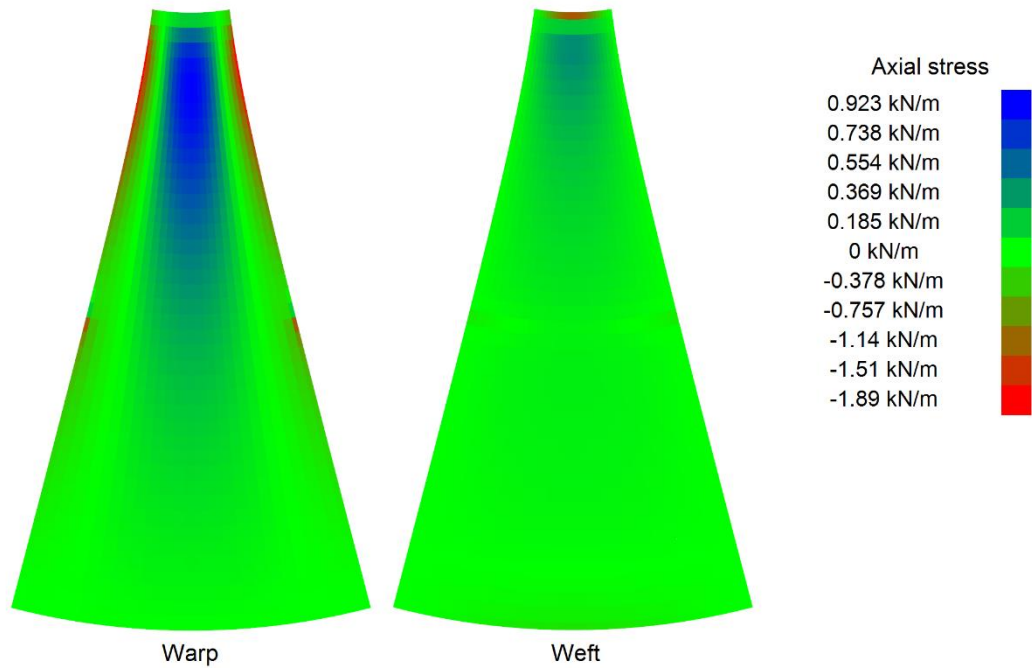


Figure 5.14 – Residual stresses after stress reduction and compensation, including the shear stiffness of the fabric, after flattening by unrolling with two spines

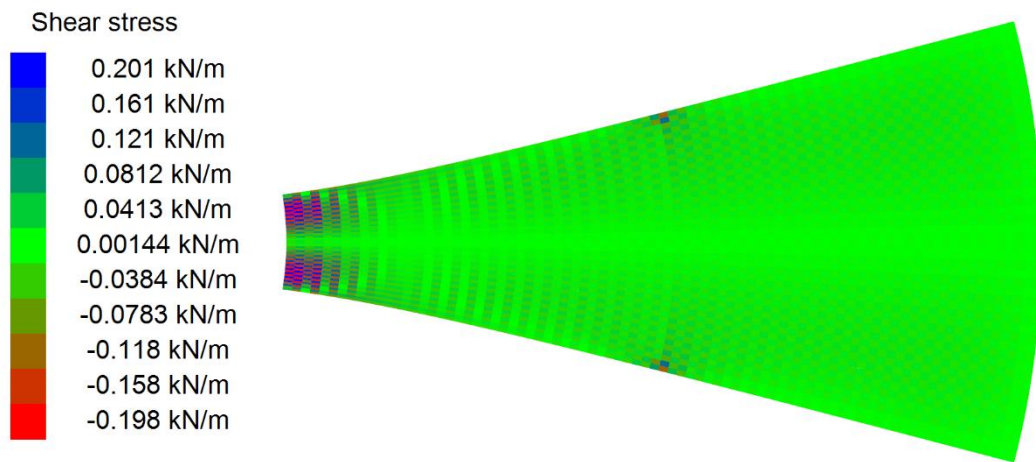


Figure 5.15 – Residual shear stresses after stress reduction and compensation, including the shear stiffness of the fabric, after flattening by direction projection

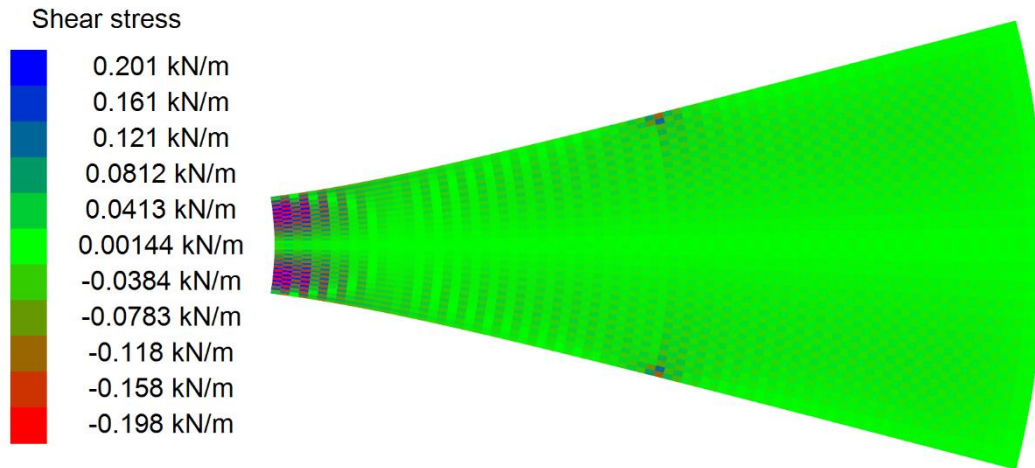


Figure 5.16 – Residual shear stresses after stress reduction and compensation, including the shear stiffness of the fabric, after flattening by unrolling with a single spine

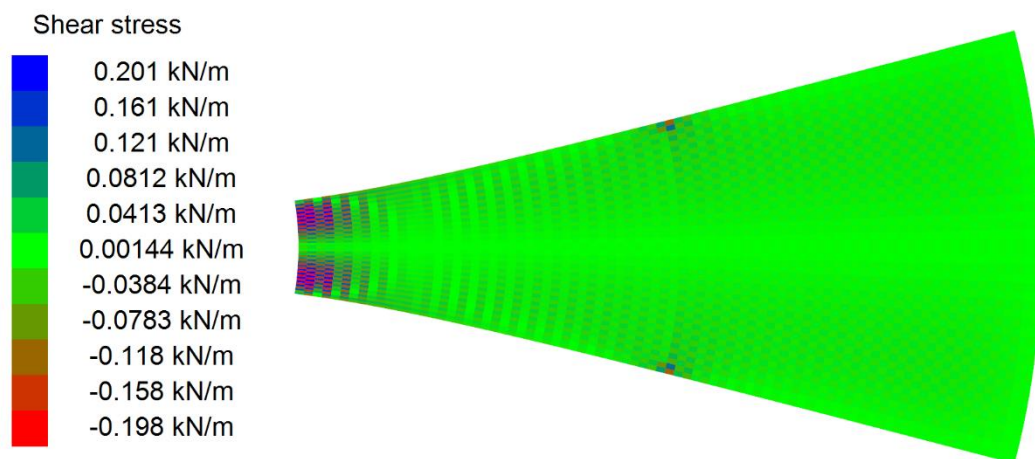


Figure 5.17 – Residual shear stresses after stress reduction and compensation, including the shear stiffness of the fabric, for flattening by unrolling with two spines

It can be seen through Figures 5.12 – 5.17 that when shear is included during stress reduction and compensation, that the dynamic relaxation analysis converges to virtually the same solution for all flattening methods. The residual axial and shear stresses are the same. In this way, for this particular example, the inclusion of shear had a stabilising effect on the analysis.

With shear included in the analysis, it is not possible to completely remove the stresses incurred by flattening. Whether the reduction of flattening stresses, and resulting residual stresses, are

sufficient must be considered in the context of the intended pre-stress. As mentioned in chapter 4, section 4.1.3, the 3D mesh is taken as the reference configuration for calculation of the element strains (and stresses), and the pre-stress is simply added to this. Thus the residual stress in the elements is the summation of any residual flattening stresses and the defined pre-stress. To give zero stress in the element, once stress-reduction has been completed, the elements must be shorter in plane than on the 3D surface, and this negative straining must balance with the intended pre-stress. This is important when considering whether the residual stresses are acceptable.

Positive residual axial stresses are observed in the warp direction, in the centre of the panel, towards the top of the panel. These stresses diminish away from the top of the panel. Positive residual stresses imply that these portions of the fabric are larger than required to give the intended pre-stress of 2 kN/m after assembly. If the residual stress is greater than the intended pre-stress, excess fabric in these areas will result in wrinkling. The greatest positive residual axial stress of 0.923 kN/m is sufficiently low, such that in comparison with the intended pre-stress of 2 kN/m, wrinkling should not occur.

Negative residual axial stresses are observed in the warp direction, along the edges of the panel, near, but not immediately adjacent to, the top of the panel. Some small areas of negative residual stress are also present in the weft direction, along the top edge of the panel. Negative residual stresses imply portions of the fabric are smaller than required to give the intended pre-stress of 2 kN/m after assembly. Thus negative residual stresses correspond to areas of the panel that will have a higher than intended stress state after assembly. If the absolute value of greatest negative residual stress, in addition to the pre-stress, is too high, failure of the fabric may occur under loading.

However, the above consideration of the residual stresses assumes that the exact reverse of these residual stresses, in addition to the intended pre-stress, will be present in the final constructed membrane. Since the structural behaviour is nonlinear, this assumption of superposition is not acceptable. Considering the stresses as above gives an indication that the cutting pattern is suitable, but simulation of the assembly of the panels is required to fully appraise the cutting pattern, as detailed in section 5.3.1.

5.2.4 Final cutting pattern shapes for the geometry from Linhard et al. [6]

The ultimate aim of the design process is the 2D geometry of the resulting cutting patterns. The cutting patterns for each flattening method, generated through stress reduction and compensation both with and without shear, are compared in the following subsections.

5.2.4.1 Cutting patterns generated without including the shear stiffness of the fabric

The first patterns examined are those generated without the inclusion of shear during stress reduction and compensation, corresponding to the stress plots shown in Figures 5.9 – 5.11. Figure 5.18 shows a comparison of the cutting patterns resulting from stress reduction and compensation without shear, for the three flattening methods.

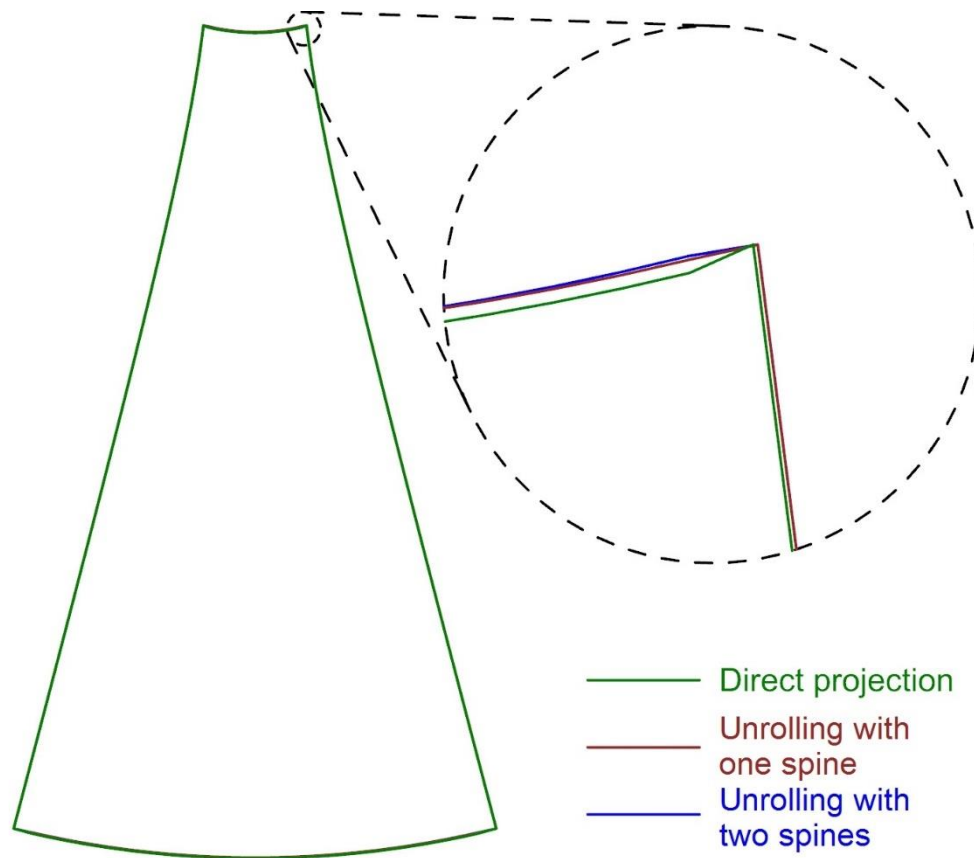


Figure 5.18 - Resultant cutting pattern boundaries for each flattening method, after stress reduction and compensation is conducted without shear

The cutting patterns shown in Figure 5.18 appear initially to be the same. On closer inspection however, it can be seen that the boundary geometry of the cutting patterns differs towards the upper corners. In particular, the cutting pattern resulting from direct projection has a sharp change in tangent along the top edge, making the pattern less suitable for cutting from architectural fabric. Less pronounced is a similar discontinuity, in a similar location, in the boundary geometry from flattening by unrolling with two spines. The case of unrolling with one spine does not show such discontinuities along the boundary geometry, resulting in the most suitable pattern.

5.2.4.2 Cutting patterns generated including the shear stiffness of the fabric

The second set of patterns examined are those resulting from stress reduction and compensation including shear, and correspond to the stress plots shown in Figures 5.12 – 5.17. Figure 5.19 shows a comparison of these cutting patterns for all three flattening methods.

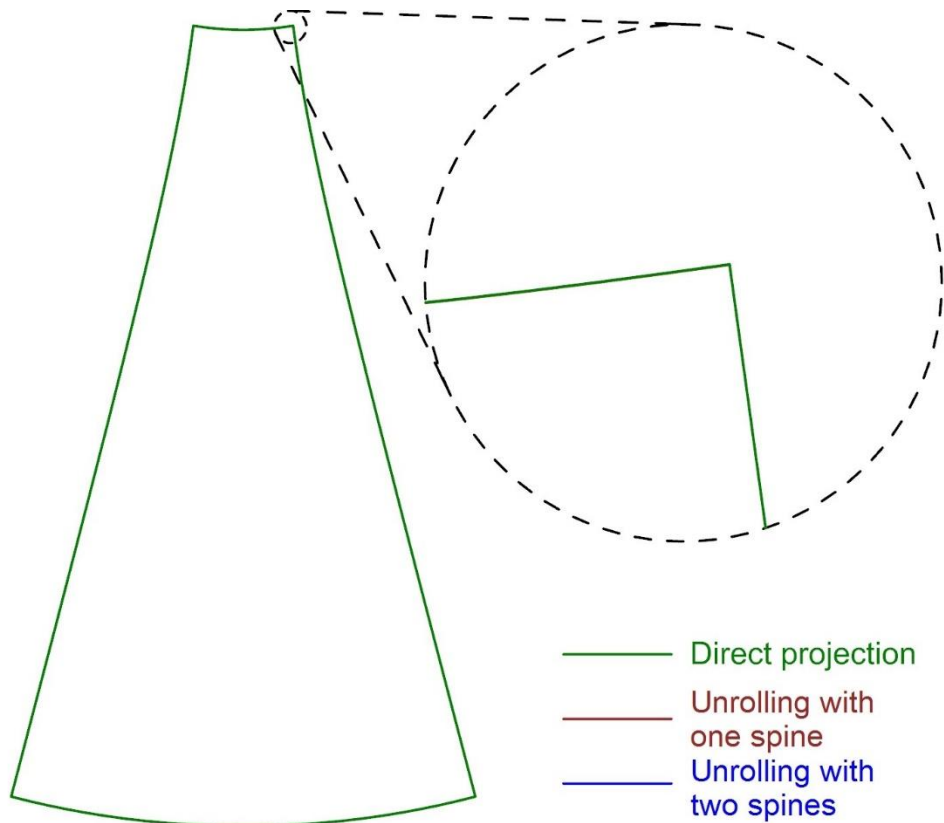


Figure 5.19 - Resultant cutting pattern boundaries for each flattening method when stress reduction and compensation is conducted with shear

As with the residual stresses after stress reduction and compensation, the final cutting patterns are virtually identical. It is not possible to distinguish the patterns for each method, even when comparing magnified sections such as the upper corners. (It is for this reason that the results from unrolling with one spine (red) and unrolling with two spines (blue) are not visible in Figure 5.19). Similar to the residual stresses, the inclusion of shear in this case has had a stabilising effect on the cutting pattern generation. Including shear during stress reduction and compensation in some ways corrects for the varying deformations incurred by different flattening methods.

5.2.4.3 Comparison of cutting patterns

Of further interest is the effect on the cutting pattern of the inclusion or exclusion of shear in the analysis, irrespective of which flattening method is used. Since unrolling with one spine gave the most suitable pattern for the analysis without shear, the cutting patterns for this method of flattening, after stress reduction and compensation with and without shear, are compared. Figure 5.20 shows the comparison between the cutting patterns generated with and without shear, for the case of unrolling with one spine.

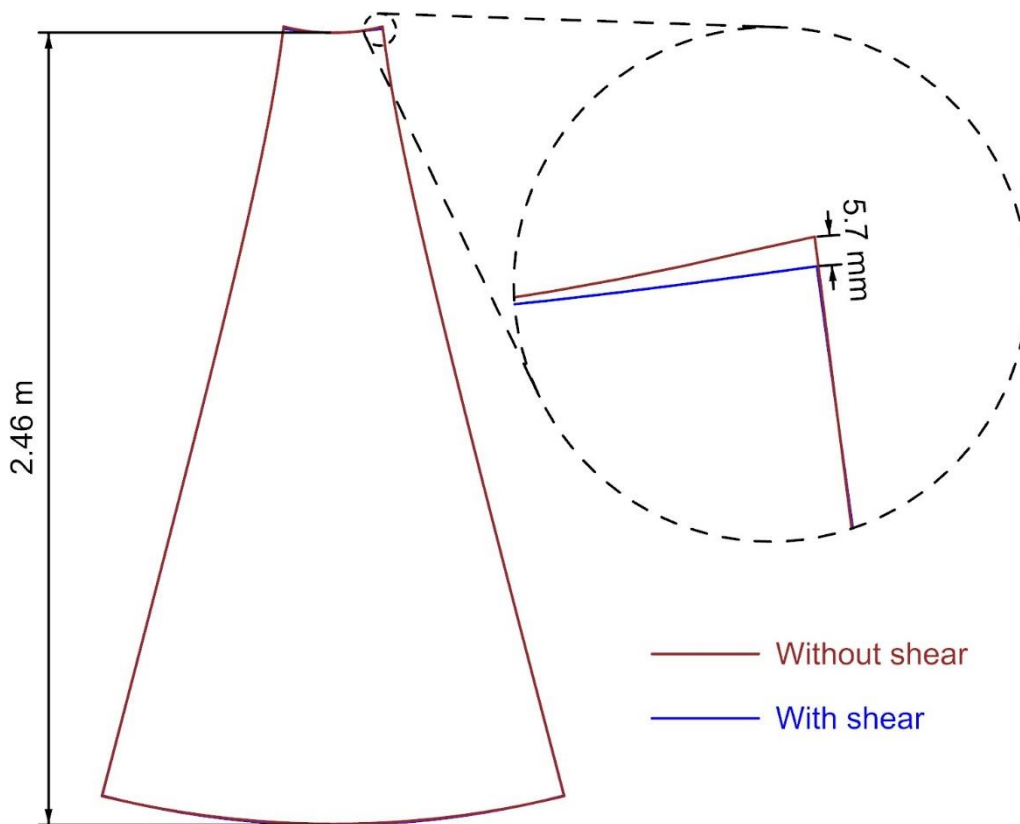


Figure 5.20 - Comparison of cutting patterns resulting from unrolling with one spine, after stress reduction and compensation is conducted with and without shear

Upon initial examination, the patterns generated with and without shear are marginally different. On closer inspection, the most important difference is the boundary geometry in the upper corners of the panel. A noticeable difference in the length of the panel in the warp direction is present. For the pattern generated including shear, less fabric is present in the upper

corners of the panel. The effect of these differences is examined further in the later sections of this chapter, when the cutting pattern is assembled.

5.2.5 Specification for the geometry from Moncrieff & Topping [4]

The second comparison is made with Moncrieff & Topping [4]. The residual stresses and cutting patterns are shown for one flattening method only. The stress reduction and compensation analyses were performed with and without shear, in fulfilment of the research objective **RO 2 (b)**. The residual stresses and cutting patterns are included for comparison with the analysis of the assembled cutting patterns later in the chapter, in sections 5.3.2 and 5.4.2.

5.2.5.1 Method used by Moncrieff & Topping [4]

The methods presented in [4] used a mixture of mechanical models. Three examples of cutting patterns were generated using three procedures: cloth unfolding, dynamic relaxation and least squares minimisation. The results presented here are done so in comparison with the third example from [4], which employed a continuum model to generate the cutting pattern, before converting the surface to tension links to perform the pattern assembly. In the third example from [4], the flattening method used geodesic lines to define the panels on the form-found surface. These panels were subsequently flattened, and the residual flattening stresses were reduced through the use of least squares minimisation. The cutting patterns generated from these steps were then re-meshed with an orthogonal mesh of line elements, and this re-meshed geometry was assembled into the final structure, and relaxed to find the final stresses and geometry.

5.2.5.2 Patterning conducted by the author

The catenoid specified in [4] had the following dimensions: upper and lower ring diameters of 3.2m and 12m respectively, and a ring separation of 2.0m. A uniform pre-stress of 3.0 kN/m was prescribed, along with a tensile stiffness of 1000 kN/m. Since no shear stiffness was given in [4],

the heuristic of $G = E/20$ was again used to estimate the shear stiffness. With a tensile stiffness of 1000 kN/m, the shear stiffness was evaluated as $G = 50$ kN/m.

The catenoid specified above was form-found and patterned using the methods outlined in chapters 3 & 4. Orthogonal re-meshing of the generated cutting patterns was included. Since the surface is rotationally symmetric, $\frac{1}{4}$ of the surface was analysed. 24 panels were used in [4], resulting in 6 panels for the $\frac{1}{4}$ surface.

For comparison with the pattern assembly results later in this chapter, a brief presentation of the residual stresses after stress reduction and compensation, and cutting patterns generated by the author for the geometry from [4] are shown in the following sections.

5.2.6 Residual stresses after stress reduction and compensation, and final cutting pattern shapes for Moncrieff & Topping [4]

Unrolling with one spine proved most suitable for the generation of the cutting patterns for the example from Linhard et al. [6]. In light of this, when generating the patterns for the example from Moncrieff & Topping [4], unrolling with one spine was used to flatten the panels before stress reduction and compensation.

Cutting patterns were generated without including shear, for direct comparison with Moncrieff & Topping [4]. Additionally, cutting patterns were generated including shear to (i) investigate the effect of including shear throughout patterning, and (ii) illustrate some conditioning factors that affect the analysis, as will be seen later in section 5.4.2.

5.2.6.1 Residual stresses without including the shear stiffness of the fabric

In the first instance, the initial cutting pattern generated through unrolling with one spine was subjected to stress reduction and compensation without including the shear stiffness of the

fabric. Figure 5.21 shows the residual axial stresses, after flattening, stress reduction and compensation, without shear, for the panel geometry from Moncrieff & Topping [4].

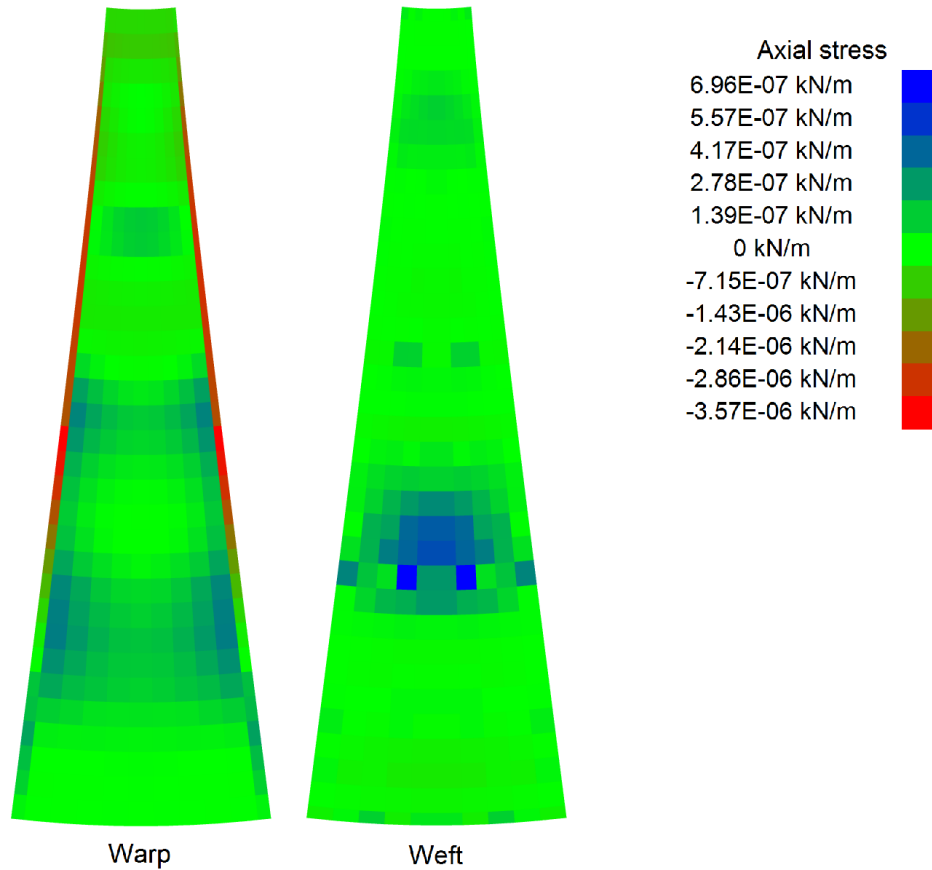


Figure 5.21 – Residual stresses after stress reduction and compensation, without including the shear stiffness of the fabric, for the geometry from Moncrieff & Topping [4]

Similar to the example based on the geometry from Linhard et al. [6] (Figures 5.9 – 5.11), the residual stresses are negligible. As mentioned in section 5.2.3.1, whilst zero residual stress is theoretically possible, it is not achievable by a numerical approach.

5.2.6.2 Residual stresses including the shear stiffness of the fabric

In the second instance, stress reduction and compensation was conducted including the shear stiffness of the fabric. Figure 5.22 shows the residual axial stresses, after flattening, stress reduction and compensation, with shear for the panel geometry from Moncrieff & Topping [4].

Figure 5.23 shows the residual shear stresses.

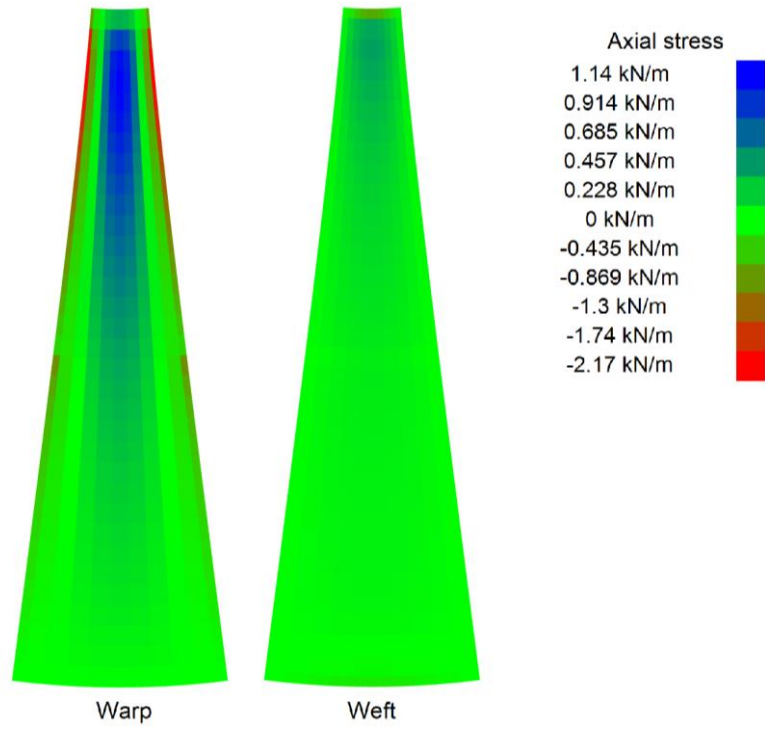


Figure 5.22 – Residual stresses after stress reduction and compensation, including the shear stiffness of the fabric, for the geometry from Moncrieff & Topping [4]

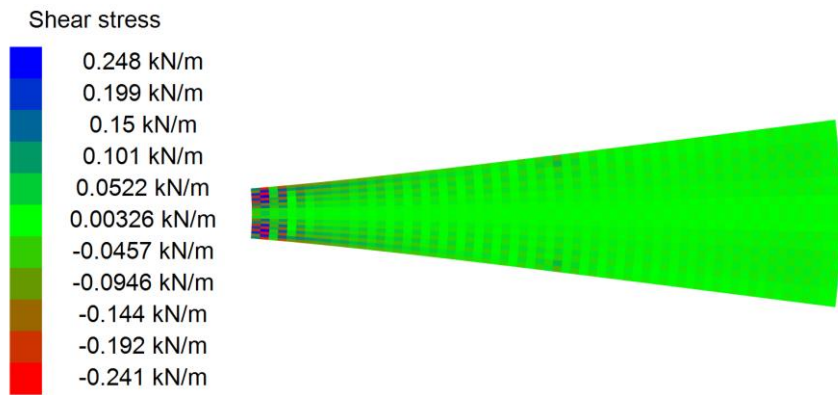


Figure 5.23 – Residual shear stresses after stress reduction and compensation, including the shear stiffness of the fabric, for the geometry from Moncrieff & Topping [4]

The pattern of residual stresses observed in Figures 5.22 & 5.23 is similar to that of the example based on the geometry from Linhard et al. [6] (Figures 5.12 – 5.17). There is an area of positive residual axial stress in the warp direction, in the centre of the panel, towards the top of the panel. These stresses diminish away from the top of the panel. Negative residual axial stresses are found at the edges of the panel, towards, but not at, the top of the panel.

Once again, since it is not possible to completely remove all flattening stresses, the suitability of the pattern must be evaluated by comparing the residual stresses to the desired pre-stress. The maximum positive residual axial stress of 1.14 kN/m, and the maximum negative residual axial stress of -2.17 kN/m are considered acceptable when compared with the intended pre-stress of 3.0 kN/m – it is not expected wrinkling or excessive overstressing will occur.

5.2.6.3 Comparison of cutting patterns

Of further interest are the cutting patterns corresponding to the above plots of stress. Figure 5.24 shows the final cutting patterns, with and without shear.

Similar to the final cutting patterns for the geometry from Linhard et al. [6], shown in Figure 5.20, the cutting patterns in Figure 5.24 are distinguishable only on closer inspection. As in Figure 5.20, the cutting pattern generated including shear is shorter in the warp direction, towards the top corners of the panel.

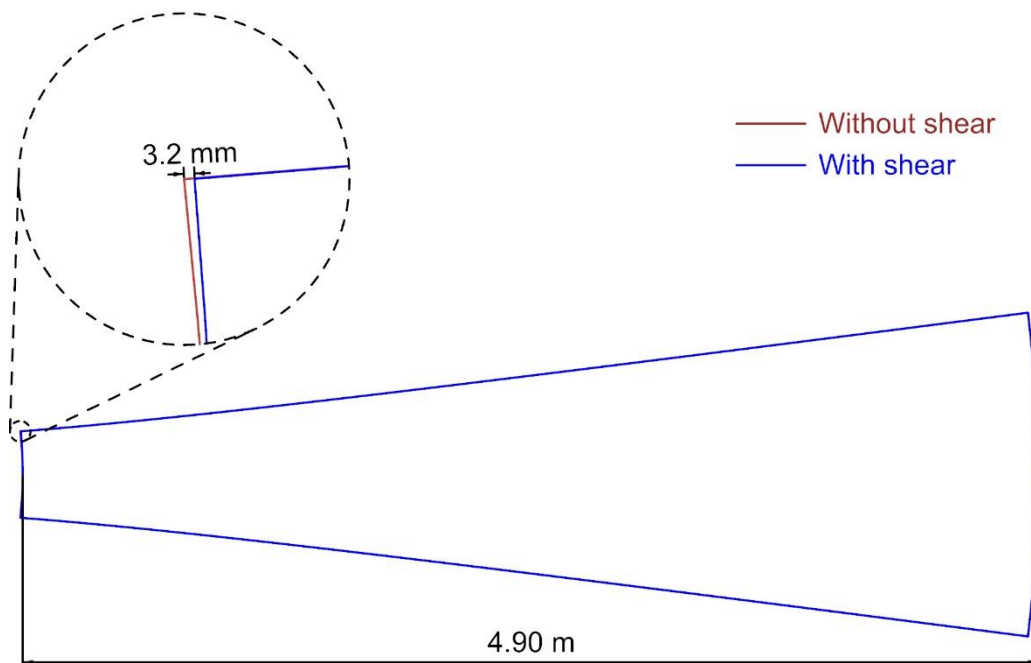


Figure 5.24 - Comparison of cutting patterns for the geometry from Moncrieff & Topping [4]

5.3 Pattern assembly results

The final step in the patterning process is the evaluation of the generated cutting patterns, and the determination of the final stress deviations. This section presents results relating to the process of cutting pattern assembly, and comparison with the examples from Linhard et al. [6], and Moncrieff & Topping [4]. These results are presented to show how the proposed model meets objectives **RO 1 (a)** & **RO 1 (b)** – the application of the discrete model, and the examination of its suitability for patterning. It is shown that the stresses resulting from the patterns achieved using the proposed patterning methodology are within the ranges reported in the original studies, indicating the suitability of the proposed discrete element model.

5.3.1 Comparison with pattern assembly results from Linhard et al. [6]

The first comparison is made with the work of Linhard et al. [6], excluding the shear stiffness of the fabric throughout the patterning process. Taking the final cutting pattern (section 5.2.4.1, for the case of unrolling with one spine) the panel was re-meshed with an orthogonal mesh, and three panels were assembled to model $\frac{1}{4}$ of the structure. The relevant material properties were:

- Tensile stiffness: $E = 220 \text{ kN/m}$
- Intended pre-stress: $\sigma_p = 2 \text{ kN/m}$

When modelling $\frac{1}{4}$ of the structure, the boundary comprises one quarter of the upper and lower ring boundaries, and two seam edges. The assembly of the three panels was oriented such that these two seam edges lie in the global XZ and YZ planes. Nodes along these seam edges were fixed in the direction perpendicular to the relevant plane. For the seam edge in the XZ plane, the nodes were fixed in the Y direction, and for the seam edge in the YZ plane, the nodes were fixed in the X direction (Figure 5.25). Nodes along the upper and lower rings were fixed in all directions.

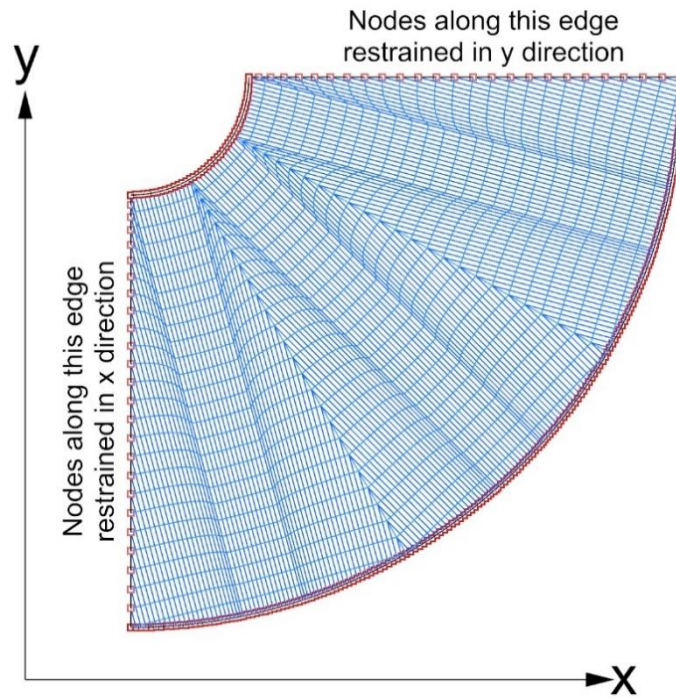


Figure 5.25 - Plan view of node restraints for the analysis of $\frac{1}{4}$ of the geometry from Linhard et al. [6]

Figures 5.26 & 5.27 show the final stress deviations for the geometry from Linhard et al. [6], after assembly and analysis, excluding shear throughout the analyses. For ease of comparison, the results from Linhard et al. [6] are reproduced in Figure 5.28.

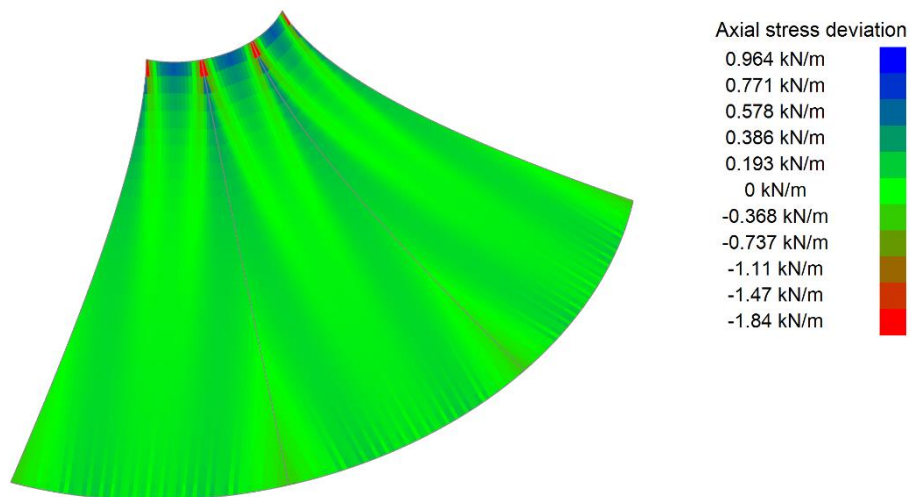


Figure 5.26 - Warp stress deviation after assembly of the cutting patterns for the geometry from Linhard et al. [6], without including shear in the analysis

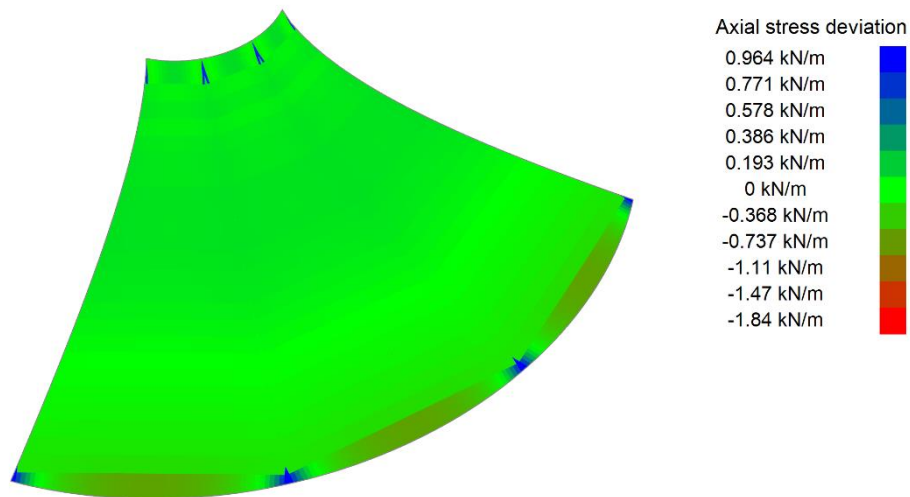


Figure 5.27 - Weft stress deviation after assembly of the cutting patterns for the geometry from Linhard et al. [6], without including shear in the analysis

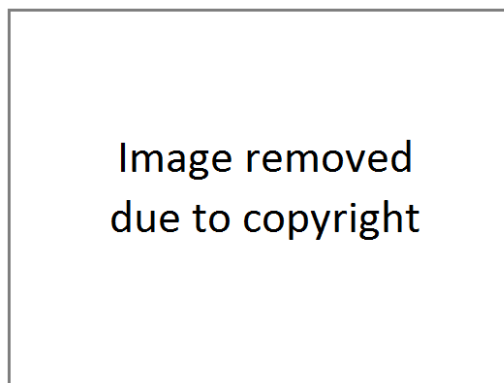


Figure 5.28 – Principal stresses after pattern assembly – reproduced from Linhard et al. [6]

The highest positive stress deviation is +0.964 kN/m, and occurs in the weft elements near the lower boundary, adjacent to the seams. There are also concentrations of higher stresses in (i) the weft elements at the intersections between the seams and the upper boundary, in (ii) the warp elements near the seams and upper boundary, but not immediately adjacent to the upper boundary, and in (iii) the warp elements near the upper boundary in the centre of the panel.

The highest negative stress deviation is -1.84 kN/m, and occurs over a very small area where the seams intersect with the upper boundary, and imply an excess of fabric in this area. Lower

stresses are also present in the weft elements next to the lower boundary, towards the centres of the panels.

With the exception of the small area of very low stress, the stress deviations are lower than in the analysis presented by Linhard et al. [6] (Figure 5.28). The greatest positive stress deviation of +0.964 kN/m corresponds to a deviation of +48.2% from the intended pre-stress. The greatest negative stress deviation of -1.84 kN/m corresponds to a deviation of -92.0% from the intended pre-stress. Principal stresses are given by Linhard et al. [6] (Figure 5.28), and the maximum and minimum deviations are +2.08 kN/m (+104%) and -0.83 kN/m (-41.5%) respectively. In Figure 5.28, higher stresses are observed towards the seams, near the upper boundary. This is a similarity in results from the two methods, and corresponds somewhat to areas of higher curvature. Lower stresses occur towards the upper boundary, in the centre of the panel.

Low stress deviations are expected for this cutting pattern, since excluding the shear stiffness of the fabric allows for an almost complete reduction of the residual stresses due to flattening for each panel. It is evident here that, as mentioned in section 5.2.3, the residual stresses after stress reduction and compensation do not manifest in the assembled geometry as their opposite stresses – i.e. a residual stress of -1 kN/m in the cutting pattern does not result in a deviation of +1 kN/m in the assembled geometry.

5.3.2 Comparison with pattern assembly results from Moncrieff & Topping [4]

The second comparison is made with the work of Moncrieff & Topping [4]. Since no shear stiffness was given in [4], the comparison is made with a shear stiffness of zero throughout the patterning processes. Taking the relevant cutting pattern from section 5.2.6, an orthogonal mesh was constructed on the panel, 6 panels were assembled, and this assembly was analysed using dynamic relaxation to give the final equilibrium position.

The deviations of the stresses from the intended pre-stress of 3.0 kN/m after re-assembly of the patterns for these geometry and material properties are shown for the warp and weft directions in Figures 5.29 and 5.30. For ease of comparison, the original results presented in [4] are included in Figure 5.31.

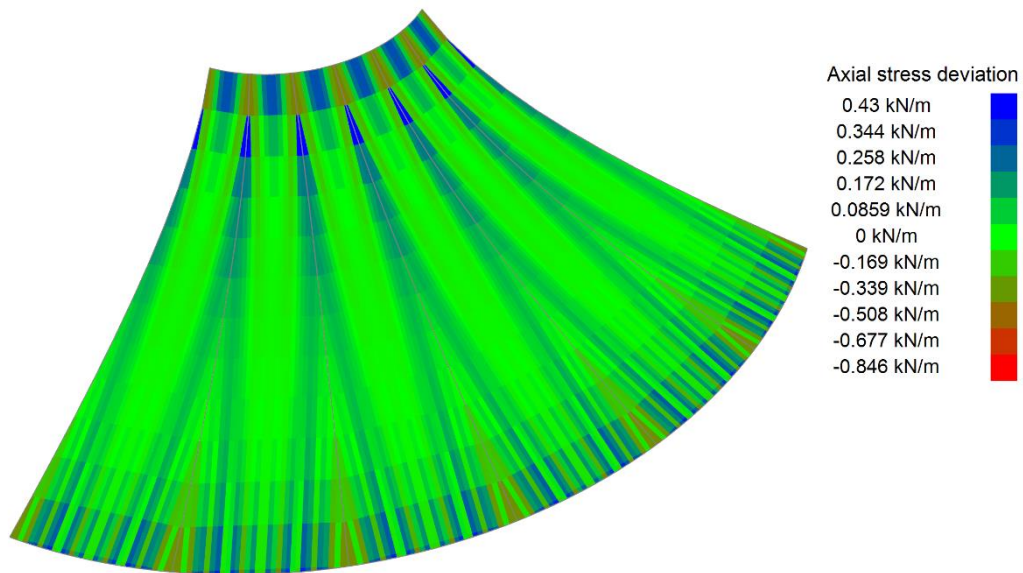


Figure 5.29 - Warp stress deviation after assembly of the cutting patterns for the geometry from Moncrieff & Topping [4], without including shear in the analysis

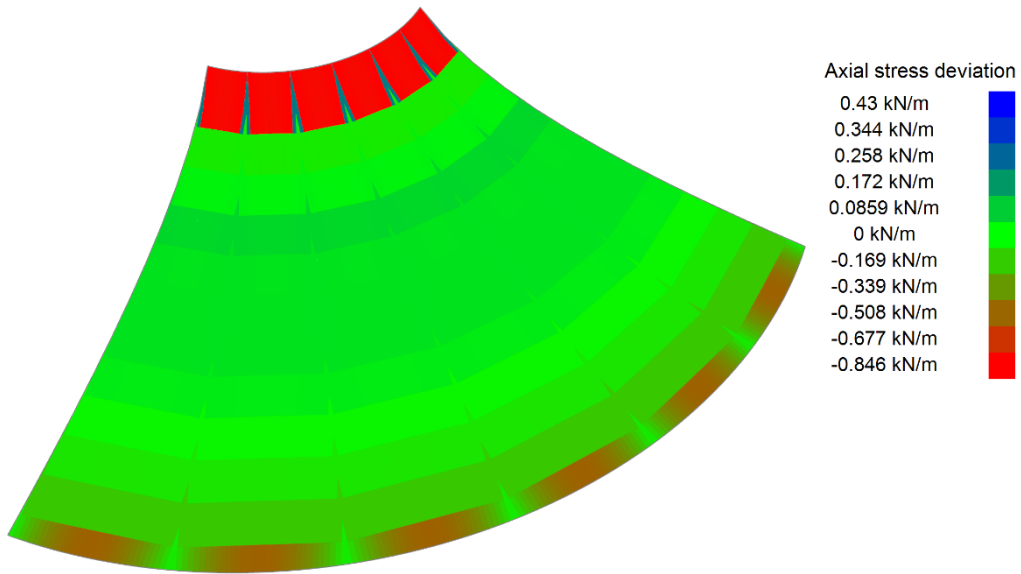


Figure 5.30 - Weft stress deviation after assembly of the cutting patterns for the geometry from Moncrieff & Topping [4], without including shear in the analysis



Figure 5.31 – Stress deviation after pattern assembly – original results from Moncrieff & Topping [4]

With reference to Figures 5.29 & 5.30, the greatest positive stress deviation is +0.43 kN/m, and occurs in the warp elements near the seams, towards, but not immediately adjacent to the upper boundary. The greatest negative stress deviation is -0.846 kN/m, and occurs in the weft elements adjacent to the upper boundary, away from the seams.

These maximum and minimum stress deviations represent deviations of +14.3% and -28.2% respectively. In [4], the maximum and minimum stress deviations were presented graphically, and thus could only be estimated. Estimating from the graphs in Figure 5.31, the maximum and minimum stress deviations were +20.0% and -18.0% respectively. Whilst the ranges of stresses are similar, in the analysis by Moncrieff & Topping [4] (Figure 5.31), greater stress deviations are seen in the main body of the panels, and not towards the boundaries, unlike in Figures 5.29 & 5.30.

The above results show that the final stresses, obtained using the proposed discrete model, for the generated cutting patterns, fall within the range of stresses quoted in published work, indicating the suitability of the discrete model and patterning method.

5.4 Conditions affecting the analyses of the pattern assembly

Further to successful implementation of the proposed discrete model, insights into patterning analyses employing discrete models were gained. The insights presented in this section are:

- (i) Including the shear stiffness of the fabric in the analysis affects both the cutting pattern (see section 5.2.4.3) and the stresses in the assembled configuration.
- (ii) To model shear in discrete models, it is necessary to include shear elements as described in chapter 3, section 3.1.2. The use of such elements requires care, due to ill-conditioning issues associated with the geometry and spacing of the mesh.
- (iii) The mesh topology has an effect on the analysis results; in particular, it is necessary to *triangulate* the mesh along the boundaries.

Insight (i) relates to research objective **RO 2 (b)**, and is not specific to discrete models.

Insights (ii) & (iii) relate to the successful implementation of the discrete model, and thus to research objective **RO 1 (c)** – the identification of conditions and guidance for successful use of discrete models.

The above insights are now demonstrated using the example catenoids from Linhard et al. [6] (section 5.2.1) and Moncrieff & Topping [4] (Section 5.2.5):

- 1) In the first analysis, the geometry from Linhard et al. [6] is revisited, and the effect of including shear throughout patterning is demonstrated.
- 2) In the second analysis, the conditioning of shear elements is explored. A re-analysis of the geometry from Moncrieff & Topping [4], this time including shear, is used to explore these conditioning issues.
- 3) In the third analysis, triangulated vs non-triangulated meshes are explored. The geometry from Linhard et al. [6] is revisited for a third time, and a non-triangulated orthogonal mesh is employed before the cutting patterns are assembled.

5.4.1 The effect of including the shear stiffness of the fabric throughout patterning

In this first analysis, the effect of including the shear stiffness of the fabric is investigated by revisiting the geometry from Linhard et al. [6]. The results presented here provide further indication that the research addresses objective **RO 2 (b)**.

As mentioned, no shear stiffness was specified in [6], so the shear stiffness was estimated as 1/20 of the tensile stiffness, in accordance with the recommendation in [15,35], giving $G = 11$ kN/m. This value of shear stiffness was used throughout flattening, stress reduction and compensation to generate the cutting pattern (see section 5.2.4.2). The shear stiffness was similarly included when re-assembling the cutting patterns, and the results are presented here.

The deviations of stresses from the intended pre-stress of 2 kN/m, after re-assembly of the patterns for these geometry and material properties, are shown for the warp and weft directions in Figures 5.32 and 5.33. The resultant shear stresses after re-assembly of the patterns are shown in Figure 5.34.

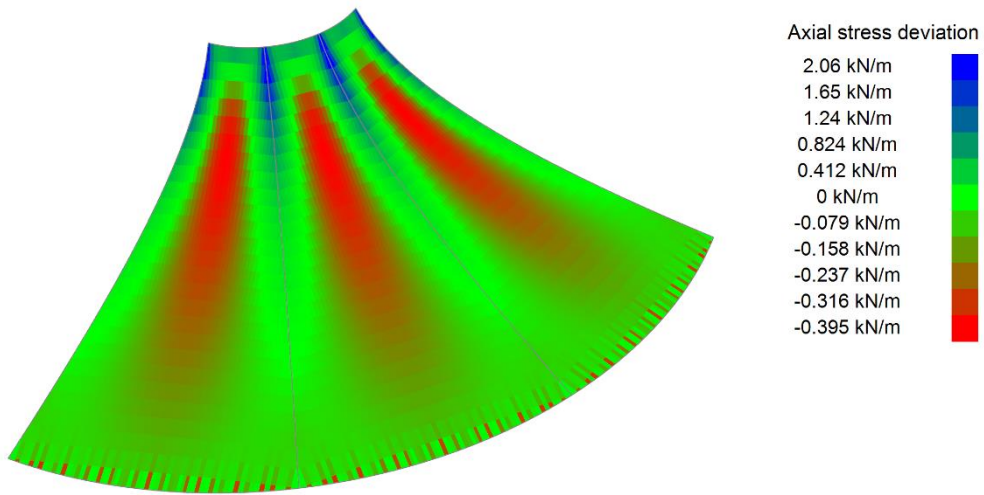


Figure 5.32 - Warp stress deviation after assembly of the cutting patterns for the geometry from Linhard et al. [6], including shear in the analysis

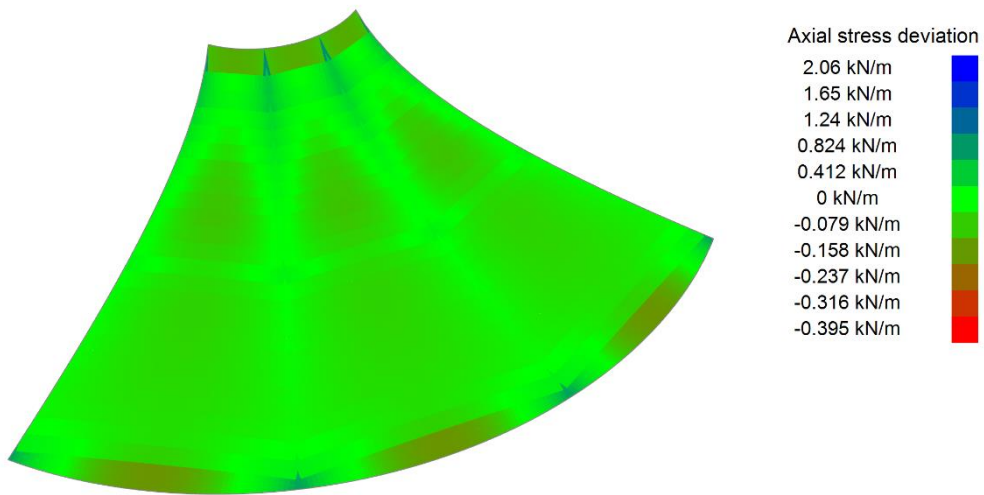


Figure 5.33 - Weft stress deviation after assembly of the cutting patterns for the geometry from Linhard et al. [6], including shear in the analysis

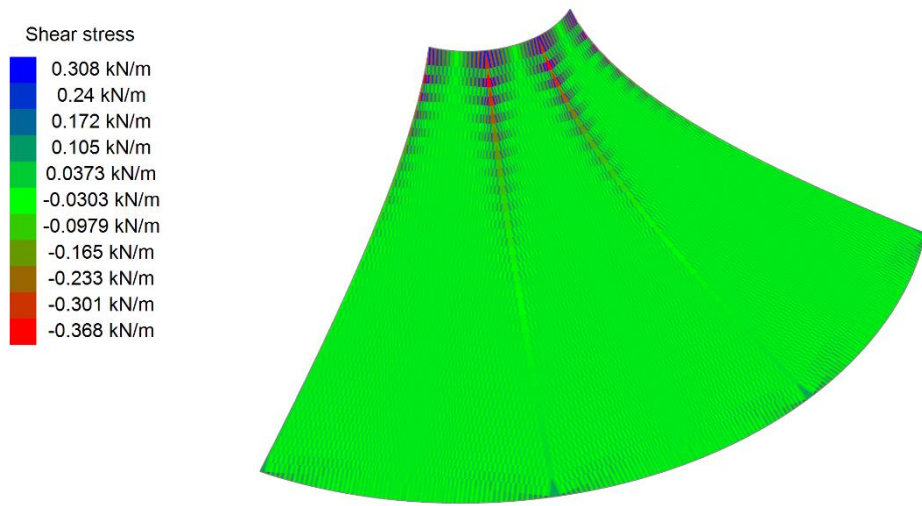


Figure 5.34 – Shear stresses after assembly of the cutting patterns for the geometry from Linhard et al. [6], including shear in the analysis

The highest positive stress deviation is +2.06 kN/m, and occurs in the warp elements near the seams, near the upper boundary. Positive stress deviations also occur in the weft elements where the seams meet the upper and lower boundaries. The highest negative stress deviation is -0.395 kN/m, and occurs in the warp elements in the panel centres. Negative stress deviations also occur in the weft elements towards the boundaries, along the centrelines of the panels.

Comparing once again with the reproduced results from Linhard et al. [6] (Figure 5.28). Similarities between the stress distributions presented in Figures 5.32 & 5.33, and Figure 5.28, can be identified. In Figure 5.28, there are concentrations of higher stresses near the seams, towards the upper boundary. These are approximately in the longer direction of the panel. In Figure 5.32, higher stresses also concentrate near the seams, towards the upper ring. In this case they are in the warp direction of the fabric, which is approximately in the longer direction of the panel. In both Figure 5.32 and 5.28, these positive stress deviations diminish away from the upper ring. In Figure 5.28, a patch of low stress is seen towards the upper boundary, in the centre of the panel. These stresses are again approximately in the longer direction of the panel. A patch of low stress is similarly seen in Figure 5.32, towards the upper boundary, though not as close

to the boundary as in Figure 5.28. These negative stress deviations occur in the warp direction, approximately in the longer direction of the panel.

Comparing the maximum and minimum deviations from Figures 5.32 & 5.33 with those of Figure 5.28 is also of interest. For Linhard et al. [6], the maximum and minimum deviations from the intended pre-stress were +2.08 kN/m (+104%) and -0.83 kN/m (-41.5%) respectively. For the analysis presented in this work, the maximum and minimum stress deviations were +2.06 kN/m (+103.00%) and -0.395 kN/m (-19.80%) respectively.

It is immediately evident from comparison between the two analyses, (excluding shear; Figures 5.26 & 5.27, and including shear; Figures 5.32 – 5.34) that including the shear stiffness of the fabric has a profound impact on the final stress distribution. In the analysis of the geometry from Linhard et al. [6], where shear was excluded (Figures 5.26 & 5.27), patches of very low stress occurred in the upper corners of the panel. These are not present in the analysis including shear (Figures 5.32 – 5.34). Looking at the comparison of the cutting patterns for these two configurations (Figure 5.20), the cutting pattern with shear has less fabric in the upper corners, supporting the implication that, in the cutting pattern without shear, there is an excess of fabric that causes the small area of very low stress after assembly. Whilst the greatest negative stress deviation is lower in the case with the shear stiffness included, the greatest positive stress deviation is higher, and these deviating stresses occur over larger areas. Whether shear is included or not, the maximum and minimum stresses in the membrane are within the range reported by Linhard et al. [6].

Of further interest in Figure 5.32 are the varying stresses in the warp elements adjacent to the bottom boundary. This variation arises due to the relative size of the shear elements either side of the row of weft elements near the bottom boundary. This effect is particularly acute in other analyses, and is discussed in detail in the next section.

5.4.2 Ill conditioning of shear elements

In the previous section, attention was drawn to the distribution of stresses in the warp elements near the bottom boundary, shown in Figure 5.32. This stress distribution results from the conditioning of the shear elements, which in turn results from the construction of the mesh. This issue relates to the successful use of the proposed discrete model, and thus contributes to the fulfilment of research objective **RO 2 (c)**. To highlight this issue, the cutting pattern for the catenoid geometry of Moncrieff & Topping [4] is re-analysed, this time including the estimated shear stiffness of $G = 50 \text{ kN/m}$ throughout the process. The final geometry, axial stress deviations and shear stresses after the analysis including shear are shown in Figures 5.35 – 5.37.

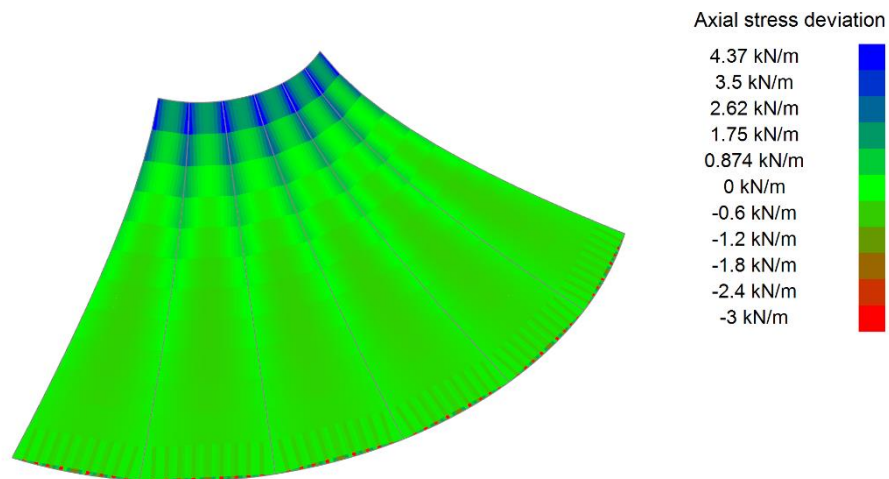


Figure 5.35 - Warp stress deviation after assembly of the cutting patterns for the geometry from Moncrieff & Topping [4], including shear in the analysis

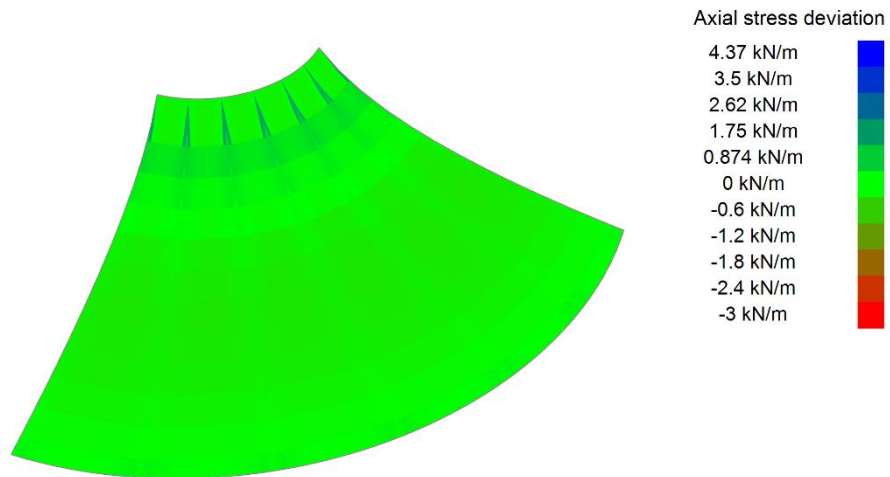


Figure 5.36 - Weft stress deviation after assembly of the cutting patterns for the geometry from Moncrieff & Topping [4], including shear in the analysis

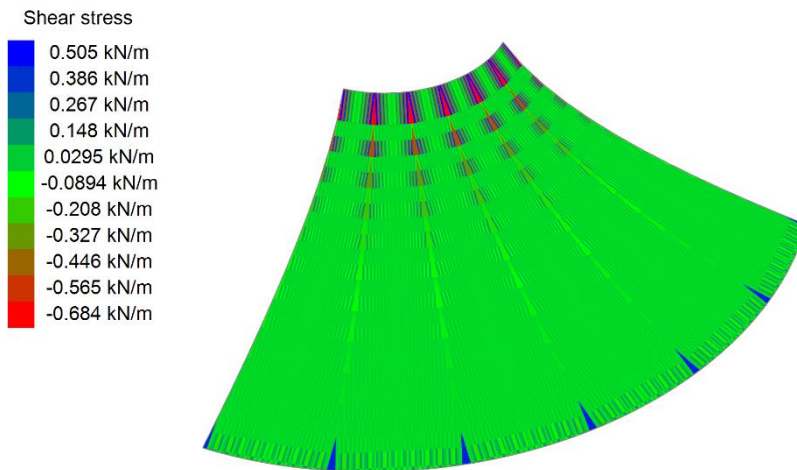


Figure 5.37 – Shear stresses after assembly of the cutting patterns for the geometry from Moncrieff & Topping [4], including shear in the analysis

It is immediately seen that the stress deviations are greater than those presented in 5.1.2. The highest positive stress deviation of +4.37 kN/m corresponds to a percentage deviation of +145.67%, and the highest negative stress deviation of -3 kN/m corresponds to a percentage deviation of -100%.

Of most interest is the location of these high negative stress deviations. They occur over very small areas, in the warp elements adjacent to the lower boundary. The distribution of stresses

in the warp elements near the boundary is similar to that seen in the analysis of the geometry from Linhard et al. [6], shown in Figure 5.32. A close up of the warp stresses in one of the panels, near the lower boundary, is shown in Figure 5.38.

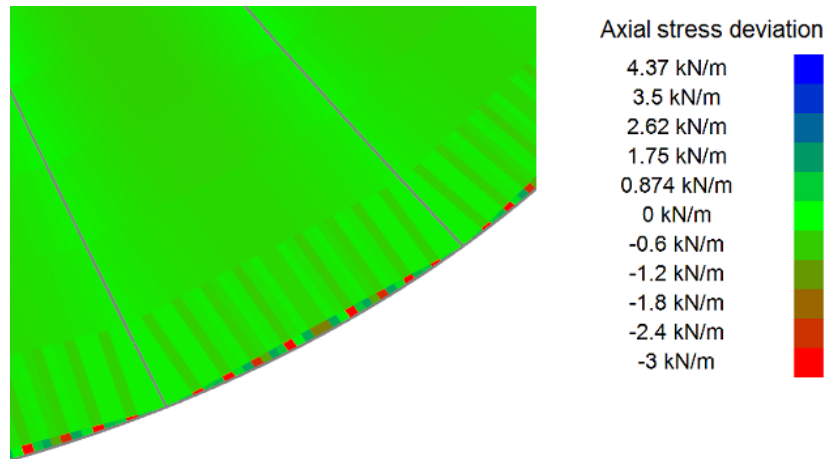


Figure 5.38 - Close up of warp stresses near lower boundary for results shown in Figures 5.35 – 5.37

The stresses in the warp elements nearest the lower boundary vary alternately across the panel – areas of higher stress occur adjacent to areas of lower stress. In the next row of warp elements, this varying stress distribution is also observed, but to a lesser extent. In the warp elements away from the lower boundary, this variation of stresses does not occur. Examining the shear stresses near these warp elements offers an explanation. A close up of the shear stresses in the panel, towards the lower boundary, is shown in Figure 5.39.

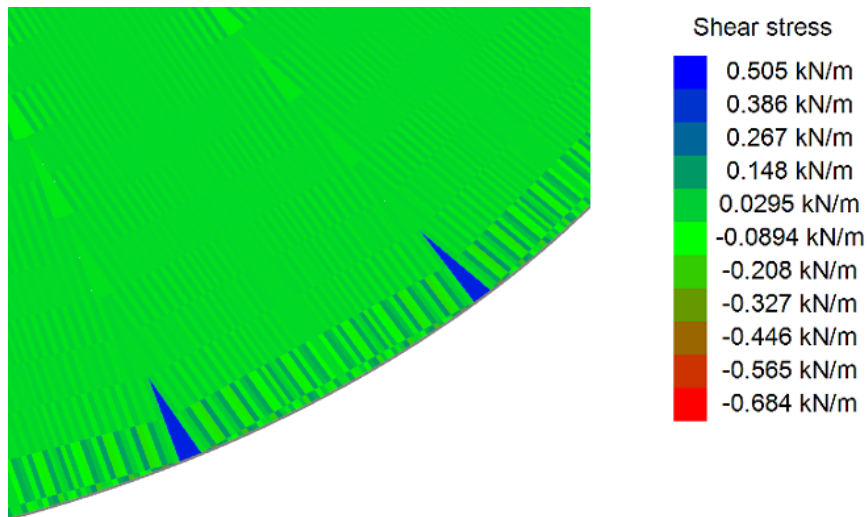


Figure 5.39 - Close up of shear stresses near lower boundary for results shown in Figures 5.35 – 5.37

Similar to the tensile stresses in the warp direction, the shear stresses vary alternately across the width of the panel. Higher shear stresses are seen adjacent to lower shear stresses.

The cause of the alternating stresses across the panel is the relative size of elements, between those elements immediately adjacent to the boundary, and those elements in the next row up from the boundary. The disparity in the length of the tensile elements can be accounted for in the calculation of element widths, and mostly affects the stresses in the other direction, i.e. a disparity in the length of warp elements affects the widths of the weft elements. However, the disparity in the size and shape of the shear elements is not so readily accounted for.

Where the geometries of different shear elements contributing to forces at the same node differ considerably, an imbalance of forces at the node results, since for a given shear stress the shape and size of the shear element affects the magnitude and direction of the calculated shear force. This concept of force imbalance is shown in Figure 5.40.

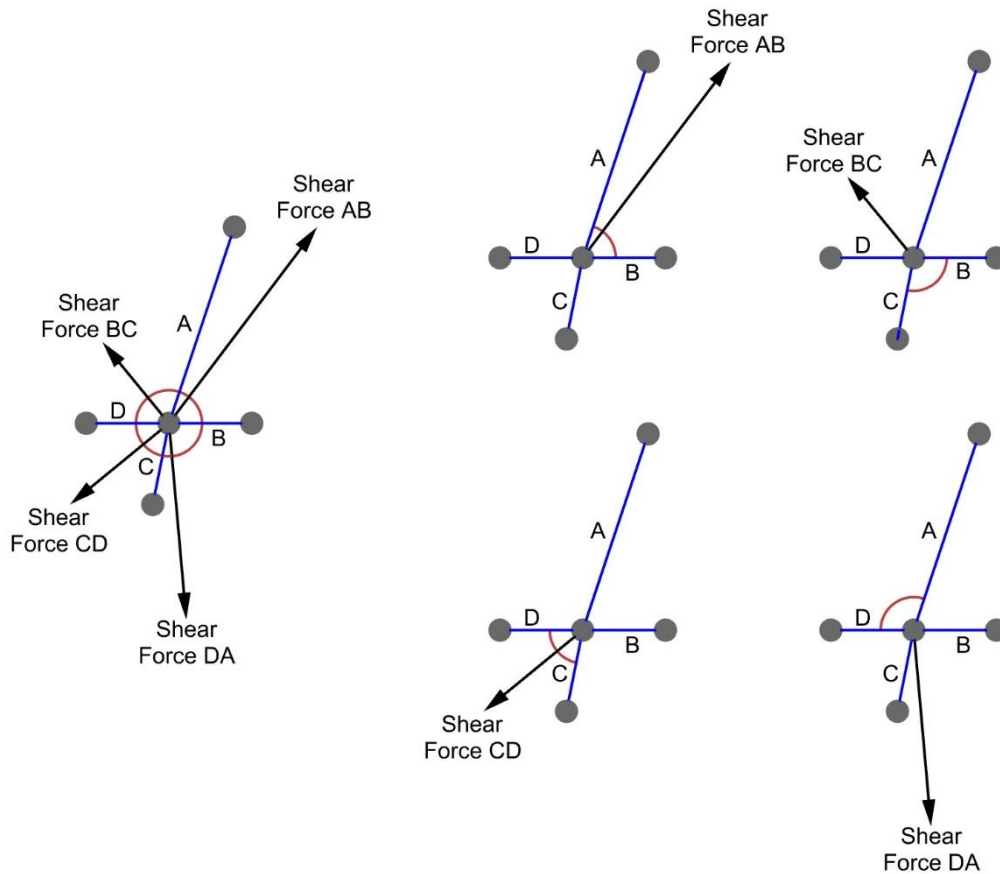


Figure 5.40 – Differing shear triangle sizes around a node and their effect on the forces apportioned to that node

In Figure 5.40, forces due to shearing will be apportioned to the central node from four shear elements. These shear elements are positioned between the tensile elements A & B, B & C, C & D and D & A, and the shear forces are calculated using the methods outlined in Chapter 3, section 3.1.2. Figure 5.40 shows the shear forces and their relative size for each shear element individually, and the cumulative effect on the central node. The forces are representative for the purposes of this example, rather than exact calculations. Because the shear elements between elements A & B and D & A are much larger than the shear elements between B & C and C & D, much larger forces are generated by these shear elements. Since element A is much larger than elements B and D, the direction of the shear forces AB and DA is affected. An imbalance of forces results.

Such an imbalance occurs for multiple nodes near the boundary, as shown in Figures 5.38 & 5.39, and means that the nodes displace disproportionately in one direction. These larger displacements result in stresses in the tensile elements around the node, affecting the forces generated in the shear elements. This can result in an accumulation of errors as a cycle of large force imbalance, and consequent changes in the tensile elements ensues.

Ensuring that the differences in shape and size of the shear elements, between different regions of the fabric, are minimised reduces the effect of this ill conditioning. It is for this reason that this ill conditioning is most noticeable when analysing the geometry from Moncrieff & Topping [4]. Employing a triangulated mesh on the slenderer panels for this analysis results in a greater difference in shear triangle sizes near the boundary.

5.4.3 Necessity for the triangulation of the mesh at the boundary

As indicated in the literature, discrete models are sensitive to their topology. The structure of the mesh has an impact on the results. The existing use of discrete models for modelling flexible materials, such as textiles, has often been restricted to rectilinear geometry. One of the contributions of the proposed discrete model, is the attempt made to model non-rectilinear shapes. This is critical for patterning, given that few structures will have cutting patterns comprising straightforward, rectilinear shapes.

As mentioned in chapter 4, section 4.2.1.2, along the boundaries of non-rectilinear shapes, the discrete mesh must be *triangulated*. This necessity for triangulation is an important insight into the behaviour and application of discrete models. This insight is presented in fulfilment of the research objective **RO 1 (c)** – the identification of conditions for successful use of discrete models in patterning.

To demonstrate the necessity for triangulation of the boundaries, the geometry from Linhard et al. [6] was re-analysed, this time, with a non-triangulated mesh. All steps were the same as in

section 5.4.1, with the exception of the orthogonal mesh, which was constructed without triangulation of the elements near the boundaries. The triangulated mesh from section 5.4.1, and the non-triangulated mesh from this analysis, are shown on the 2D cutting pattern in Figure 5.41.

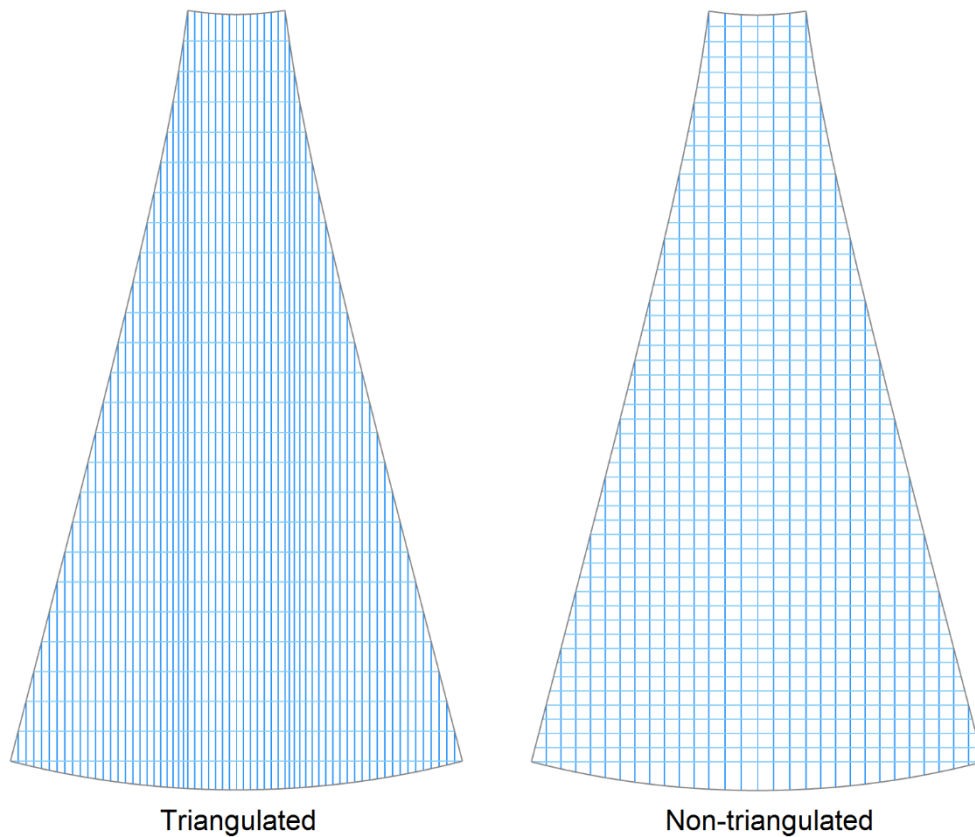


Figure 5.41 - Triangulated and non-triangulated mesh configurations for cutting patterns generated for the geometry from Linhard et al. [6], with shear included in the analysis

It is important to remember that the *triangulated mesh* is triangulated only at the boundaries, and through assembly of the panels, at the internal seam lines. Figures 5.42 & 5.43 show the final geometry and stress deviations after relaxation of the non-triangulated mesh.

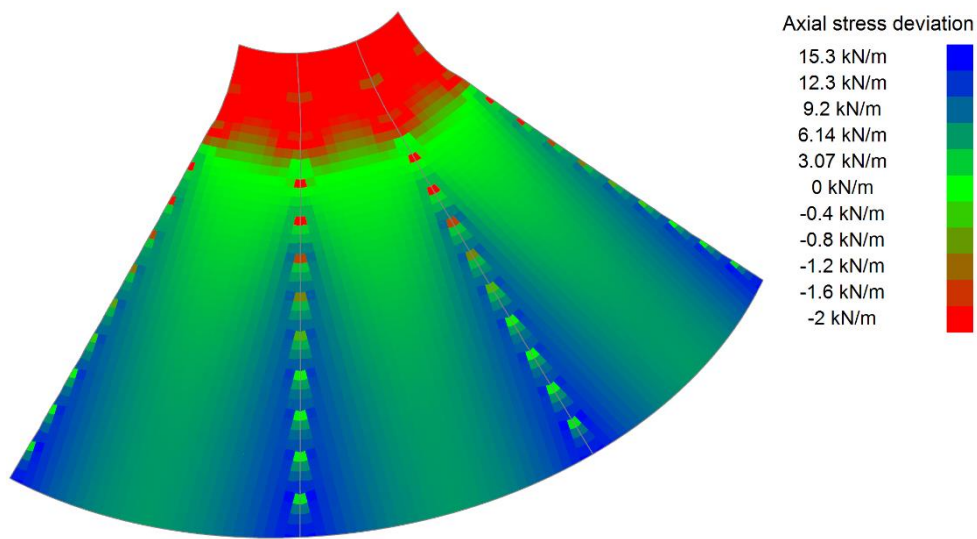


Figure 5.42 - Warp stress deviation after assembly of a non-triangulated mesh, for the geometry from Linhard et al. [6], including shear in the analysis

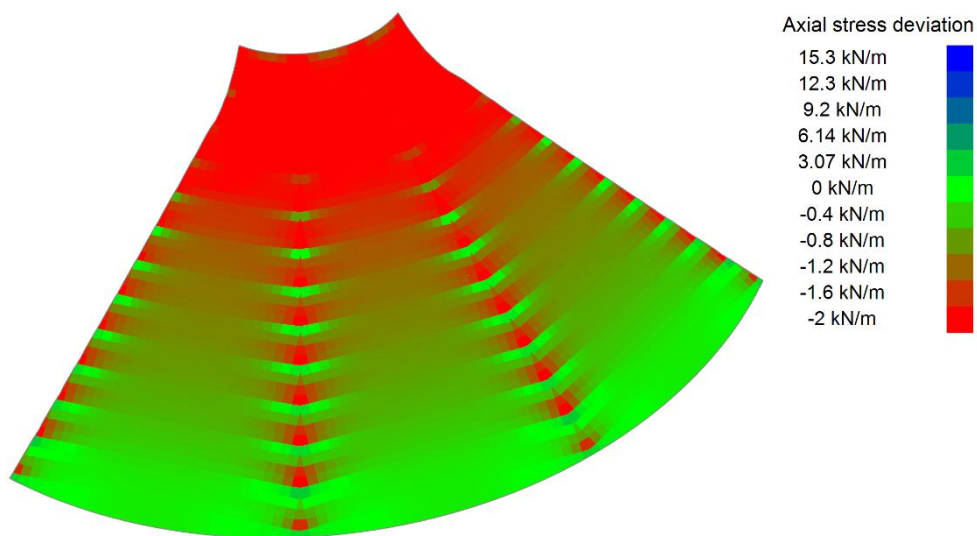


Figure 5.43 - Weft stress deviation after assembly of a non-triangulated mesh at the seam lines, for the geometry from Linhard et al. [6], including shear in the analysis

It is immediately obvious that the stress deviations are drastically higher than desired. The maximum stress deviation of + 15.3 kN/m represents a percentage deviation of +765%. The minimum stress deviation of - 2 kN/m represents a percentage deviation of -100%. This minimum stress deviation corresponds to wrinkling of the fabric due to its inability to sustain

stresses below 0. Approximately, the upper $\frac{1}{4}$ of the panel has a stress deviation of -2 kN/m (a stress of 0 kN/m).

Figures 5.42 & 5.43 illustrate that the re-meshing of the cutting pattern with a non-triangulated orthogonal mesh results in final analysis values that suggest the original cutting pattern is unsuitable. Figure 5.44 confirms further this unsuitability. In Figure 5.44, it can be seen that the final position of the seam line diverges considerably from its position in the form-found mesh (indicated by the grey line).

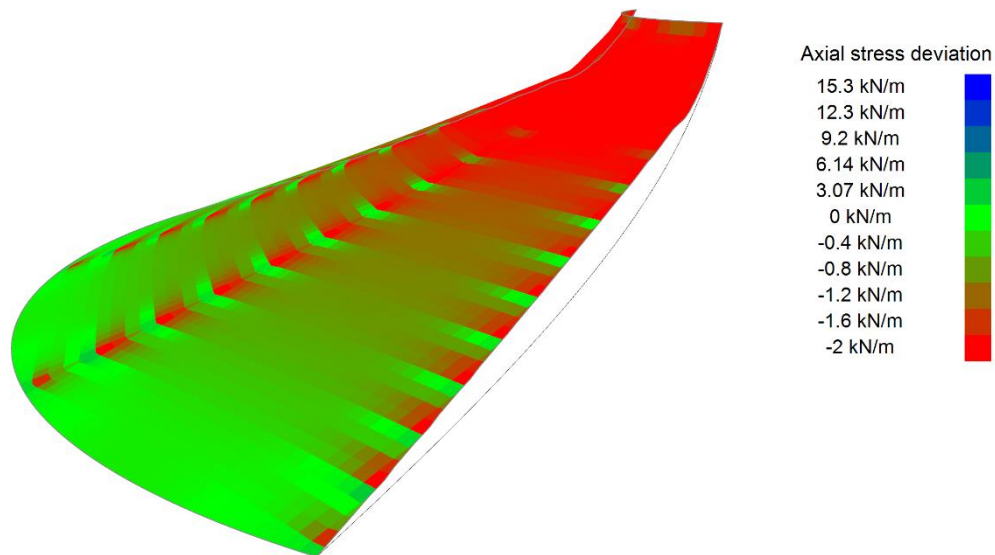


Figure 5.44 - Deviation of the boundary from its expected position, after assembly of a non-triangulated mesh, for the geometry from Linhard et al. [6], including shear in the analysis

Examining the behaviour of the mesh near the boundaries yields some insights into why non-triangulation causes issues with the convergence and final result of the analysis. Figures 5.45 & 5.46 show the reaction forces along the edge of the mesh, for both the triangulated mesh from Figures 5.32 & 5.33, and for the non-triangulated mesh from Figures 5.42 – 5.44.

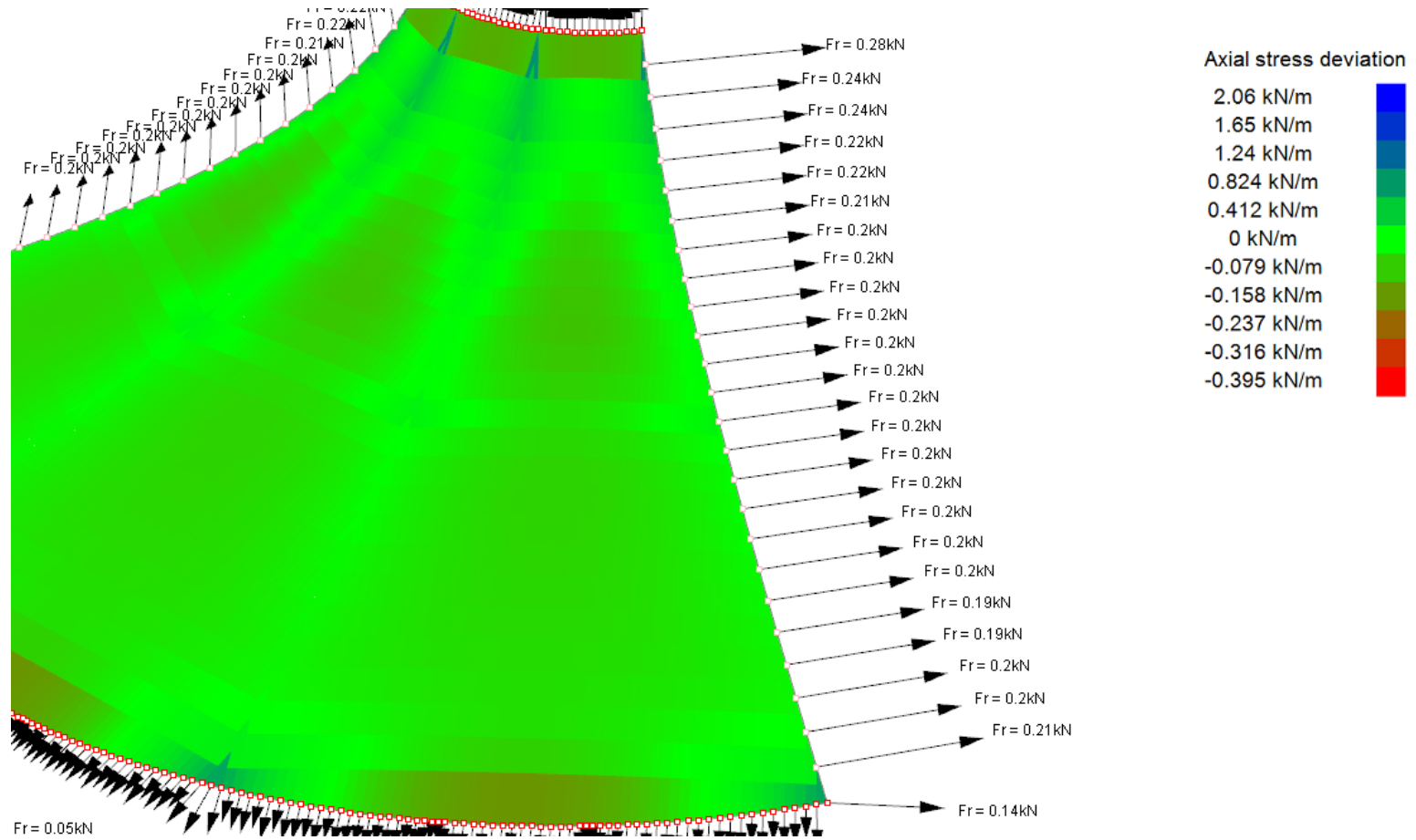


Figure 5.45 – Boundary forces after assembly of the triangulated mesh, for the geometry from Linhard et al. [6], including shear in the analysis

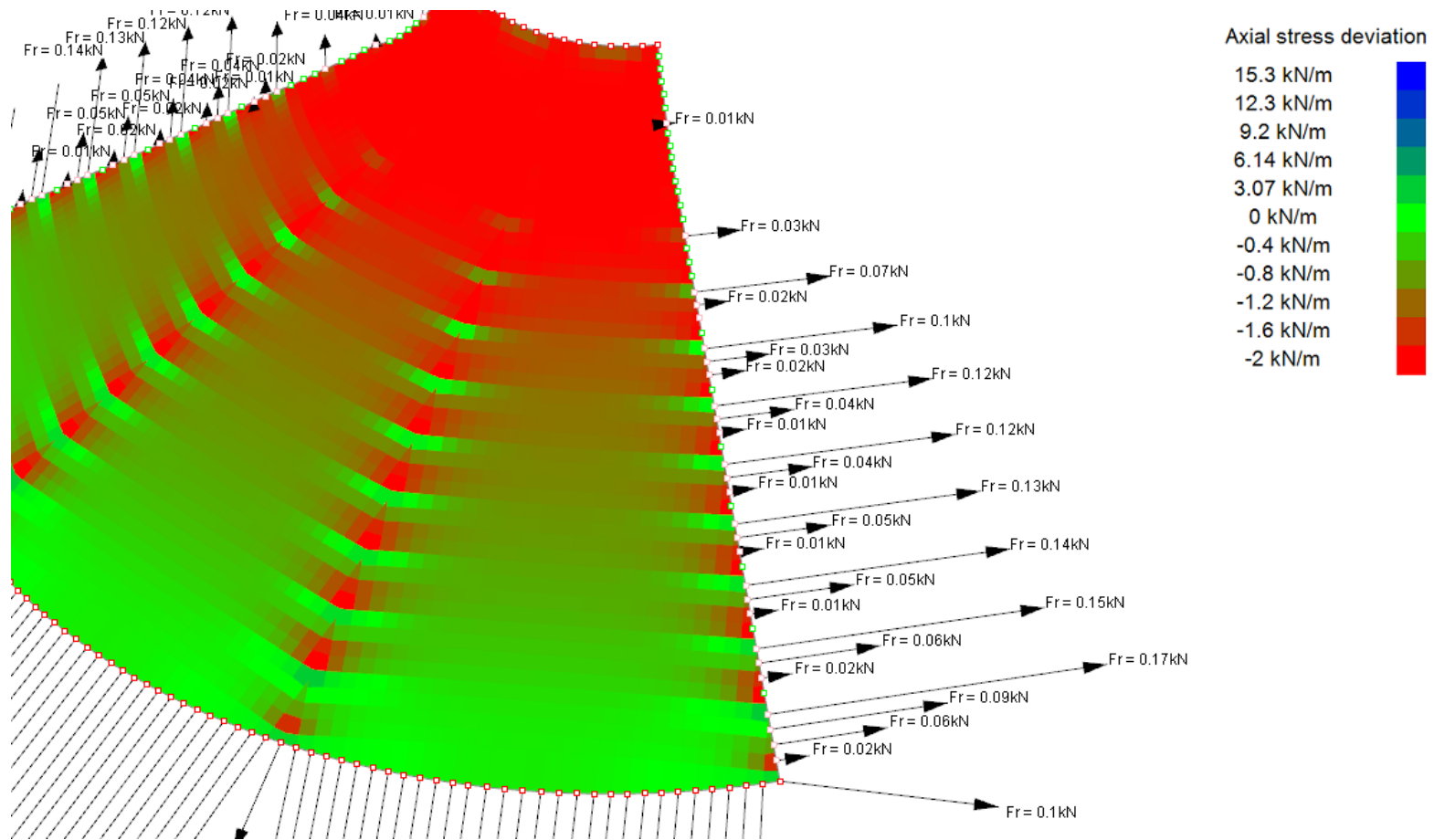


Figure 5.46 – Boundary forces after assembly of the non-triangulated mesh, for the geometry from Linhard et al. [6], including shear in the analysis

Since $\frac{1}{4}$ of the surface is modelled, the edge shown in Figures 5.45 & 5.46 corresponds to the seam line between the panels that are modelled and those that are excluded. This edge is partially restrained such that it may move only in the relevant plane – nodes are fixed in the X or Y directions (Figure 5.25), correspondingly, these nodes move only in the YZ or XZ planes respectively. The reaction forces are in the direction perpendicular to the relevant plane. Since the analysis is intended to result in a surface with a stress state near to that of the prescribed pre-stress, the reaction forces along this boundary should be near uniform, and on average over the length of the boundary, approximately equate to the prescribed pre-stress.

It is seen in Figure 5.45 that the reaction forces are mostly uniform along the partially restrained edge. In Figure 5.46 however, the edge forces are highly non-uniform. Defining the average stress perpendicular to the boundary as the average reaction force along the boundary, divided by the average edge length between nodes along the boundary, confirms the non-uniformity. For the triangulated mesh (Figure 5.45), the average reaction force is 0.21 kN, and the average edge length 0.1 m. This gives an average stress perpendicular to the boundary of 2.1 kN/m – very close to the intended pre-stress of 2 kN/m. For the non-triangulated mesh (Figure 5.46), the average reaction force is 0.032 kN, and the average edge length is 0.048 m. This gives an average stress perpendicular to the boundary of 0.67 kN/m – a greater deviation from the intended pre-stress of 2 kN/m.

This indicates that the non-triangulated mesh is unsuitable. Modelling the whole surface hides this condition of the mesh, since it is not possible to examine the interaction of forces along the seam lines. When modelling $\frac{1}{4}$ of the surface, examining the reactions along the edges (seam lines) offers an insight into how the stresses are transferred from one panel to the next.

Examining the final position of the elements near to the boundary facilitates further explanation of the issue. Figure 5.47 shows a close up view of the individual elements, near the bottom boundary of the non-triangulated mesh.

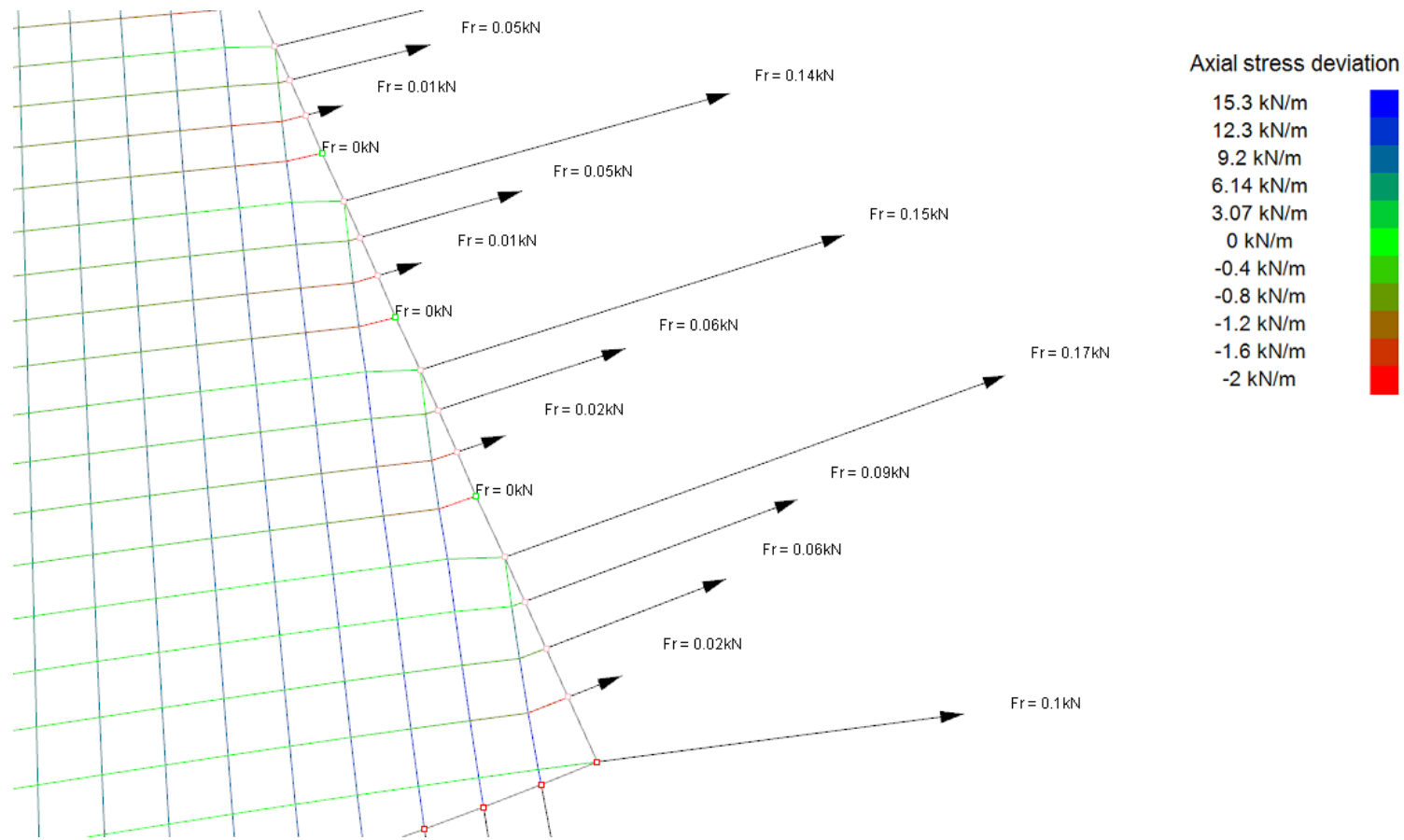


Figure 5.47 – Gross shear deformations after assembly of the non-triangulated mesh, for the geometry from Linhard et al. [6], including shear in the analysis

In Figure 5.47, the elements away from the boundary have experienced only minor shear deformation, but there are gross shear deformations between the near-boundary elements, and elements within the panel. This is corroborated when looking at the shear stresses across the surface. Figure 5.48 shows the shear stress distribution across the surface, and high shear stresses along the edges and seams can be seen.

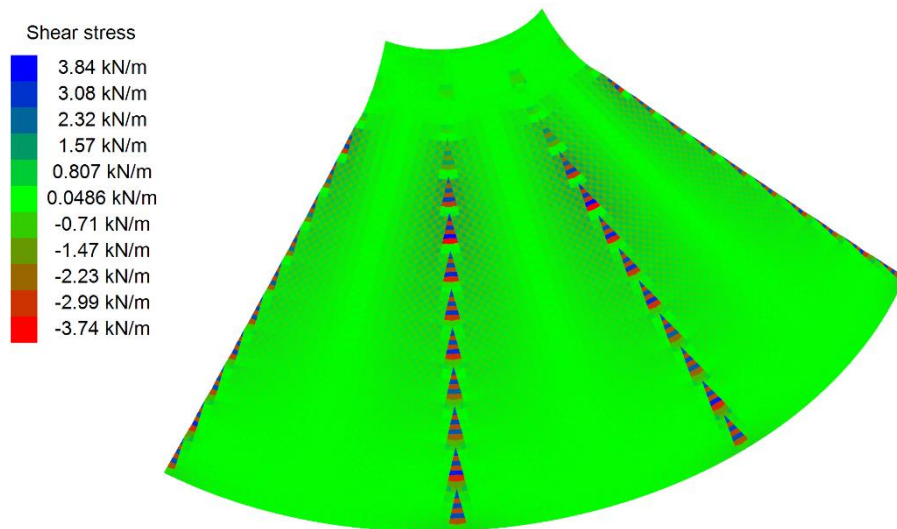


Figure 5.48 – Shear stresses after assembly of the triangulated mesh, for the geometry from Linhard et al. [6], including shear in the analysis

Referring back to Figure 5.47, the gross shear deformations can be explained by looking at the nodes along the boundary. Some of the reaction forces are approximately the same value as those in the results from the triangulated mesh, for example 0.17 kN in the non-triangulated mesh compares well with approximately 0.2 kN in the triangulated mesh. Where the reaction forces at the nodes compare well, two elements, one warp and one weft, connect to the node – the nodes have a *valency* of two as discussed in section 4.2.1.2. The reaction forces are not appropriate where the nodes are attached to only one element, and along this boundary they are attached to a weft element only. Whether one or two elements attach to a boundary node affects how the node displaces.

Figure 5.49 shows an example boundary node, in a triangulated and non-triangulated mesh.

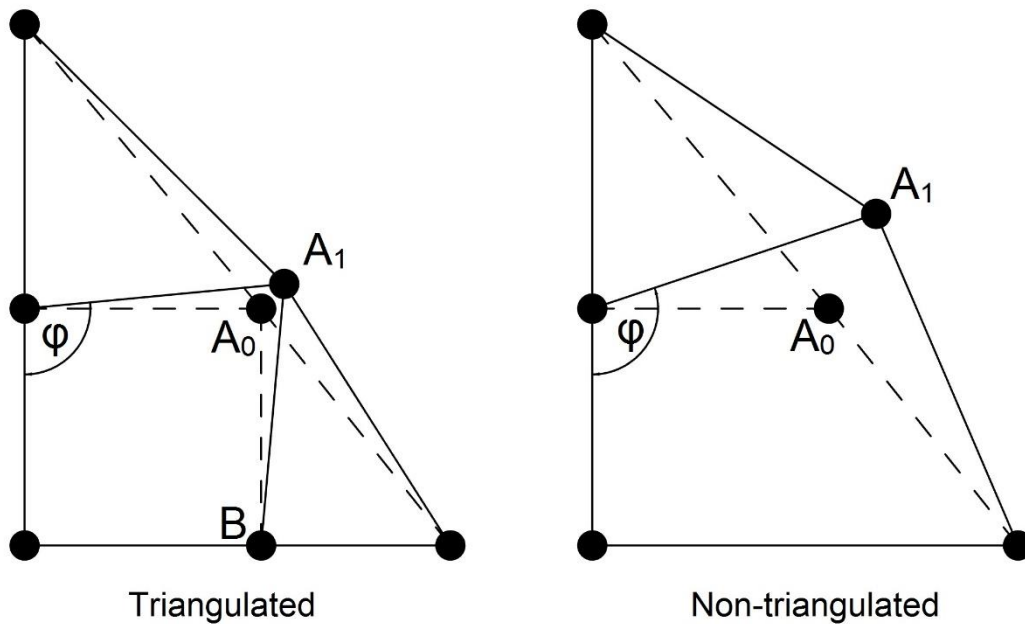


Figure 5.49 - Restriction of node movement due to connectivity of elements, and resulting control of shear deformations

In the triangulated mesh, the displacement of node A (from A_0 to A_1) is restricted by the element between nodes A and B. This has the effect of ensuring the shear strain φ , further into the membrane, is not excessive. In the non-triangulated mesh, node A may undergo large displacements, since element AB is not present. This results in a gross shear strain φ , further into the membrane. This gross shear deformation then affects the equilibrium of the internal nodes. This combination of unrestricted displacement and resulting shear deformation contributes to overall instability of the analysis, when the mesh is not triangulated along the boundary. The necessity for the mesh to be triangulated near the boundary is important for correct utilisation of discrete models, and has not been discussed in previous work.

5.5 Summary

This chapter presented results from the application of the patterning process proposed in chapter 4 and discrete model proposed in chapter 3. Results for both the determination of the cutting pattern, and for evaluating its suitability through pattern assembly were shown. Comparisons with published work showed the suitability of the proposed patterning method and discrete model, as the final stresses after pattern assembly were within the ranges reported in literature. The results presented in this chapter thus addressed both main research objectives: **RO 1**: the development, application and examination of a discrete model, and **RO 2**: the advancement of the computational process of patterning.

For pattern assembly, it was first shown that the patterning method is suitable, by comparison with the work of Linhard et al. [6], and Moncrieff & Topping [4]. Further to this, it was shown that the assembly of the cutting patterns and subsequent equilibrium analysis is dependent on a number of factors: (i) the inclusion of shear stiffness throughout the analysis, (ii) the conditioning of shear elements, and (iii) the triangulation of the mesh at the panel boundaries. These factors were explored through further analyses based on the geometries from Linhard et al. [6] and Moncrieff & Topping [4].

6 Summary, conclusions and future work

6.1 Summary of thesis

The work presented in chapters 2 – 5 was undertaken to address the research objectives: **RO 1** – the development, application and examination of a discrete model, and **RO 2** – the advancement of the computational process of patterning, as stated in chapter 1.

The literature review presented in chapter 2 examined the process of patterning of tensile fabric structures, and highlighted the criticality of weave shear. Various numerical models were discussed, which included continuum and discrete approaches. The continuum approaches included expressions of geometric nonlinearity through the inclusion of higher order terms or the use of Green's strain, and constitutive relationships such as Saint-Venant Kirchoff models or those derived from a unit cell approach. These continuum models were variously implemented using finite element methods. The discrete approaches included particle-spring and spring-mass systems from fields such as cloth animation and non-architectural textiles, and discrete element models used to model engineering fabrics. The specific nature of patterning was shown to justify the need for a discrete model.

A discrete model was proposed, and detailed in chapter 3. The proposed model was developed to accommodate large displacements, both axial and in shear, and irregular, non-rectilinear geometries. Solution by the dynamic relaxation method was presented.

The proposed patterning method, presented in chapter 4, expanded on the majority of existing methods with the introduction of geometric flattening methods and orthogonal re-meshing of the panel, prior to assembly of the cutting pattern.

Chapter 5 presented the application of the proposed discrete model to patterning. Comparisons with two published works were included for the proposed patterning method. It was shown that

the proposed discrete model and patterning method give results within the expected range of stress deviation (deviation from the assumed design pre-stress), indicating the suitability of the discrete model, and that geometric flattening methods can be used to reduce distortions in the planar cutting pattern before stress reduction and compensation.

6.2 Conclusions

Through successful completion of the research, a number of conclusions, pertaining to the numerical analysis of tensile fabric structures at the patterning stage, were reached:

1. Shear of the weave is an important phenomenon in the design of tensile fabric structures, and is particularly relevant at the patterning stage. The existing numerical models, derived from continuum assumptions, and which ignore this phenomenon, are potentially inaccurate because of this. The effect of weave shear is most important for structures with higher curvature. Thus to design structures of increasing complexity and architectural ambition, this effect must be modelled.
2. Discrete models offer an excellent alternative to existing numerical models, but none of the discrete models available at present are individually suitable for the modelling of tensile fabric structures.
3. The previously ignored area of advanced flattening methods has an effect on the cutting patterns generated through flattening, stress reduction and compensation.
4. The shear stiffness of the fabric is important and should be included in analyses.

The proposed discrete model for patterning accommodates these important features of the numerical modelling of tensile fabric structures. The results presented in chapter 5 show that the model is suitable for modelling the fabric during patterning, and offers advantages over the existing models, none of which offer all of the following:

1. The proposed model accommodates weave shear for irregular geometries. Modelling of complex surface shapes without omission of such important mechanical behaviour is thus possible.
2. Geometric nonlinearity is handled in a straightforward manner through the use of dynamic relaxation and formulation of the fabric mechanical response in local coordinates.
3. The model uses common material properties such as Young's modulus and Shear modulus, rather than properties specific to fabrics, allowing straightforward integration into, and comparison with, existing methods of analysis.

The successful implementation of the discrete model shows the discrete models can accommodate the phenomenon of weave shear, and the conclusions outlined previously illustrate that doing so is critical for successful analysis of tensile fabric structures.

Further elaboration of the conclusions presented above, is now provided through conclusions specific to the research objectives.

The development and application of a discrete model for patterning (**RO 1**) represents the main contribution of this work, and has led to the following conclusions:

1. The proposed discrete model is suitable for patterning, giving, for the assembly of the cutting pattern, residual stresses within the ranges reported in literature. The proposed model reflects the directions of the fabric warp and weft, and thus accommodates weave shear, offering an advantage over traditional continuum models **[RO 1 (a) & RO 1 (b)]**.
2. Use of the discrete model when assembling the generated cutting patterns offers a more representative description of the surface via orthogonal re-meshing.
3. The shear elements proposed by the author in chapter 3 are a necessary inclusion to model the shear stiffness of the fabric in a discrete model environment; they are capable of

accommodating irregular geometry, something not attempted in previously published work **[RO 1 & RO 2 (b)]**.

Successful use of the proposed discrete model is dependent on the topology and geometry of the constructed mesh. Some further conclusions of this research are therefore related to the use of the discrete model:

4. Careful construction of the mesh is required when modelling irregular geometry with shear elements. Otherwise, ill conditioning can occur due to disparities in the size and shape of the shear elements **[RO 1 (c)]**.
5. Triangulation of the mesh at the boundary must be enforced to model non-rectilinear geometries; otherwise, ill conditioning will occur. This is a necessity for fabric structures patterning since the cutting pattern edges are not rectilinear **[RO 1 (c)]**.

Further to the development and application of the discrete model, conclusions pertaining to patterning as a computational process were drawn from this research **(RO 2)**. In the context of generating the cutting pattern, the methods presented in chapter 4, and explored in chapter 5, gave rise to the following conclusions:

6. The proposed patterning method results in cutting patterns that, when assembled, give stresses within the expected ranges, as reported in literature **[RO 2]**.
7. The method of flattening can have an effect on the ultimate cutting pattern, though only for the case where the shear stiffness of the fabric is not considered. It was shown that different flattening methods 'favour' axial or shear deformation more than others. Unrolling with one spine offered the best compromise for minimising axial distortions without incurring excessive shear deformation **[RO 2 (a)]**.
8. Exclusion of the shear stiffness of the fabric during stress reduction and compensation facilitates the generation of effectively zero-distortion patterns, since without the shear

stiffness, only axial stresses affect the stress reduction and compensation, and it is possible to achieve negligibly low axial stresses. In this case different patterns are achieved depending on the flattening method used – the shear distortions incurred by each flattening method differ, and the stress reduction and compensation process does not reduce these distortions directly **[RO 2 (a) & (b)]**.

9. Inclusion of the shear stiffness of the fabric during stress reduction and compensation gives patterns with the same residual stresses, whichever flattening method is used. In this way, the shear stiffness ‘corrects’ for the differing distortions incurred by different flattening methods, and has a stabilising effect on the stress reduction and compensation process **[RO 2 (b)]**.
10. Inclusion of the shear stiffness during the analysis has a marked effect on the cutting pattern and final stress distribution in the assembled membrane. This is particularly relevant when considering that the shear stiffness of architectural fabrics is low, and thus frequently ignored. On this basis, the author of this work advocates the inclusion of shear stiffness throughout the analysis and design of tensile fabric structures **[RO 2 (b)]**.

6.2.1 Limitations of the work

It is at this point relevant to state the limitations of the work detailed in this thesis.

Limitations of the proposed discrete element model

1. Out-of-plane deformation is ignored in the proposed discrete model. This is consistent with the expected behaviour of architectural fabrics and tensile fabric membranes. This is however an important limitation in the context of shear modelling, where it more difficult to differentiate between in-plane and out-of-plane deformations. The proposed model ignores the effects of bending and twisting of the fabric, and this is considered acceptable since the resistance of fabrics to these types of deformations is very low. Shear strains are

measured between two elements (which by default lie in their own plane), which is intended to ensure that inadvertent and incorrect shear strains, due to out-of-plane deformations, are not introduced.

2. Constitutive relationships are limited to a linear relationship between stress and strain. This is considered acceptable given that the stresses during patterning are low, and low stresses for architectural fabrics correspond to portions of the stress-strain behaviour which may be idealised as linear.
3. To ensure an accurate analysis, careful construction of the mesh is required. Re-meshing, based on the criteria outlined in chapters 4 & 5, for example ensuring triangulation of the boundary, may be required to obtain an accurate solution. Re-meshing may increase computation times. Accurate modelling of the boundary conditions where triangulation occurs may also be challenging.

Limitations of the research overall

4. Comparison of the discrete model and patterning method was limited to tensile fabric structures which are the shape of a Catenoid. The model has not been tested on structures supported by cables.
5. Validation of the discrete model is limited to comparison with published work and existing numerical methods.

6.3 Future work and implications for engineering practice

This work has presented the use of a discrete model for patterning that includes axial and shear forces in the fabric. Further testing is required to validate the proposed discrete element model, and where necessary improve it by, for example, overcoming errors associated with shear element conditioning. In addition to this, elements of the patterning method may yet be improved. A number of suggestions for future work are thus made:

1. Further validation of the discrete model is required. Comparison with additional computational results, and where possible, experimental results, merits further study.
2. The proposed shear elements are simple, but suffer from ill conditioning when the mesh is not carefully constructed, particularly when the geometry of potential cutting patterns becomes more complex. Developing the shear model further, and expanding on the conditions for successful analyses would be valuable.
3. The existing model is limited to the use of a linear constitutive relationship. Expanding the model to include nonlinear material behaviour would be of value. This could be achieved through formulating the constitutive response as a function of the element strain, and through the use of nonlinear stress-strain curves available in literature. Achieving modelling of nonlinear material behaviour would allow large strain analysis to be conducted.
4. Use of the discrete model when generating the cutting pattern is limited by assumptions concerning the topology and direction of the mesh on the form-found surface. Orthogonal meshing of the planar cutting pattern was included to give a more accurate representation of the fibre directions. The topology of an orthogonally meshed panel (Figure 6.1 (b)) differs from the topology of the mesh used for flattening (Figure 6.1 (a)). The 'correct' mesh topology on the form-found panel should represent that of the orthogonally meshed panel. The proposed meshing, flattening and stress reduction algorithms (chapter 4) are limited to meshes which are, topologically, a rectilinear grid (Figure 6.1 (a)). However, to construct an orthogonal mesh on the planar cutting pattern, the mesh must have a non-rectilinear topology (Figure 6.1 (b)). It is this non-rectilinear topology that should be reflected in the mesh used to conduct flattening and stress reduction in the first place. Figure 6.1 compares the two mesh topologies.

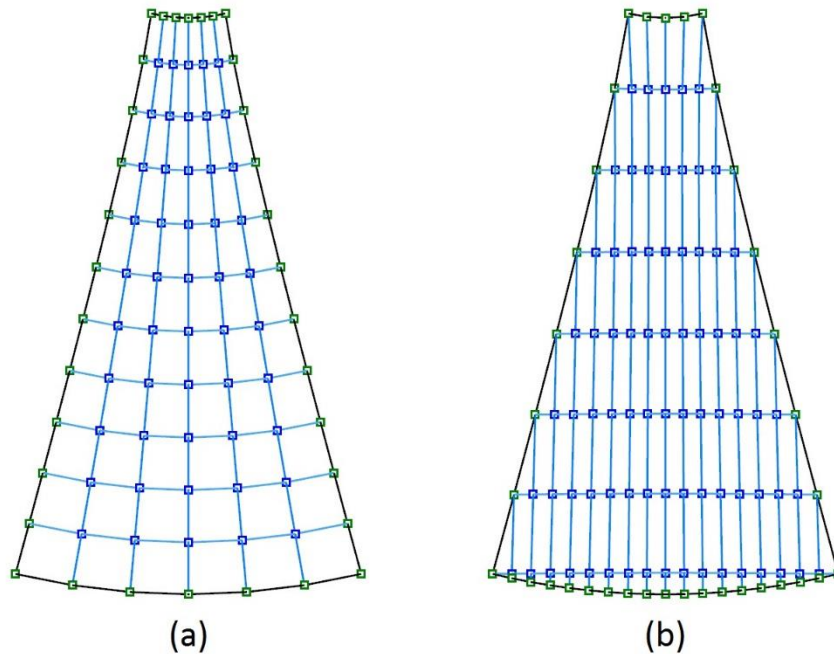


Figure 6.1 - 3D form-found panel with two different meshes – (a) current, rectilinear mesh, (b) suggested, non-rectilinear mesh

Methods for achieving successful cutting pattern generation with meshes of such topology merits further study.

5. For successful use of the discrete model, the condition of triangulation of the mesh near the boundary may limit the scope of the analysis, dependent on the structure being modelled, or cause issues for users when it is not enforced. Improving the model such that the quality of the mesh has less of an effect on the analysis would be valuable.
6. On the basis of conclusions 7, 8 & 9, a flattening method that gives the engineer control over the trade-off between axial and shear deformation would be desirable, and would allow direct manipulation of the cutting pattern in view of the residual stresses.

In addition to the recommendations for further work, the implications of the research for engineering practice are now discussed. Existing methods of analysis do not incorporate shear of the weave, as this phenomenon has not, until now, been explored.

In light of this new knowledge, engineering judgement must be used when designing tensile structures – is a proposed structure of sufficiently low curvature that weave shear is not significant, or is further, detailed analysis required? Would a less conservative, and therefore more economic design, be achieved by a more detailed analysis that includes modelling of weave shear?

For structures where the architectural ambition leads to greater geometric complexity, a discrete model, such as the one proposed, should be considered when conducting the structural analysis and design. Careful use of the discrete model, including awareness of the conditions highlighted in this research, and good engineering judgment, must be exercised throughout.

7 References

- [1] Gosling PD, Bridgens BN, Zhang L. Adoption of a reliability approach for membrane structure analysis. *Struct Saf* 2013;40:39–50. doi:10.1016/j.strusafe.2012.09.002.
- [2] Lewis W. Understanding novel structures through form-finding. *Proc ICE - Civ Eng* 2005;158:178–85.
- [3] Bletzinger K-U, Linhard J, Wüchner R. Advanced Numerical Methods for the Form Finding and Patterning of Membrane Structures. In: De Mattos Pimenta P, Wriggers P, editors. *New Trends Thin Struct. Formul. Optim. Coupled Probl.*, vol. 519, SpringerWienNewYork; 2010, p. 133–54. doi:10.1007/978-3-7091-0231-2.
- [4] Moncrieff E, Topping BHV. Computer methods for the generation of membrane cutting patterns. *Comput Struct* 1990;37:441–50.
- [5] Brew JS, Lewis WJ. Spline-based and stress-monitored patterning of fabric structures. *Comput Struct* 2013;119:203–14.
- [6] Linhard J, Wüchner R, Bletzinger K-U. Introducing Cutting Patterns in Form Finding and Structural Analysis. In: Oñate E, Kröplin B, editors. *Text. Compos. Inflatable Struct. II*, vol. 8, Springer; 2008, p. 69–84. doi:10.1007/978-1-4020-6856-0.
- [7] Seidel M. *Tensile Surface Structures: A Practical Guide to Cable and Membrane Construction*. Ernst & Sohn, Verlag für Architektur und technische Wissenschaften GmbH & Co. KG; 2009. doi:10.1002/9783433600269.refs.
- [8] Kreysig E. *Differential Geometry*. Dover Publications, Inc.; 1991.
- [9] Fomenko AT, Tuzhilin AA. *Elements of the Geometry and Topology of Minimal Surfaces in Three-Dimensional Space*. Providence, R.I.: American Mathematical Society; 1991.

- [10] Bletzinger K-U, Wüchner R, Daoud F, Camprubí N. Computational methods for form finding and optimization of shells and membranes. *Comput Methods Appl Mech Eng* 2005;194:3438–52. doi:10.1016/j.cma.2004.12.026.
- [11] Houtman R, Werkman H. Detailing and Connections. In: Forster B, Mollaert M, editors. *Eur. Des. Guid. Tensile Surf. Struct., TensiNet*; 2004, p. 147–76.
- [12] Lewis W. Architectural fabrics. In: Forde M, editor. *ICE Man. Constr. Mater.*, London: Thomas Telford Limited; 2009, p. 873–85. doi:10.1680/mocm.35973.0873.
- [13] Blum R, Bögner H, Némóz G. Material Properties and Testing. In: Forster B, Mollaert M, editors. *Eur. Des. Guid. Tensile Surf. Struct., TensiNet*; 2004, p. 219–42.
- [14] Balz M, Dencher M. Design Loading Conditions. In: Forster B, Mollaert M, editors. *Eur. Des. Guid. Tensile Surf. Struct., TensiNet*; 2004, p. 191–204.
- [15] Barnes M, Gründig L, Moncrieff E. Form-finding, load analysis and patterning. In: Forster B, Mollaert M, editors. *Eur. Des. Guid. Tensile Surf. Struct., TensiNet*; 2004, p. 205–18.
- [16] Wagner R. Basics in tension structures. *Int J Sp Struct* 2009;24:223–31. doi:10.1260/026635109789968218.
- [17] Colman AG, Bridgens BN, Gosling PD, Jou G-T, Hsu X-Y. Shear behaviour of architectural fabrics subjected to biaxial tensile loads. *Compos Part A Appl Sci Manuf* 2014;66:163–74. doi:10.1016/j.compositesa.2014.07.015.
- [18] Wagner R. On the Design Process of Tensile Structures. In: Oñate E, Kröplin B, editors. *Text. Compos. Inflatable Struct.*, Springer; 2005, p. 1–16.
- [19] Jackson AL, Bridgens BN, Gosling PD. A new biaxial and shear protocol for architectural fabrics. In: Domingo A, Lazaro C, editors. *Proc. Int. Assoc. Shell Spat. Struct. Symp.* 2009,

- Val., Valencia: 2009, p. 2167–79.
- [20] Moncrieff E. Systems for Lightweight Structure Design: the State-of-the-Art and Current Developments. In: Oñate E, Kroplin B, editors. Text. Compos. Inflatable Struct., Springer; 2005, p. 17–28.
- [21] Gale S, Lewis WJ. Patterning of tensile fabric structures with a discrete element model using dynamic relaxation. *Comput Struct* 2016;169:112–21. doi:10.1016/j.compstruc.2016.03.005.
- [22] Gale S, Lewis WJ. Computational patterning methods for tensioned fabric structures. Use of a discrete element model. *Proc. Int. Assoc. Shell Spat. Struct. Symp.* 2015, Amsterdam, Amsterdam: 2015.
- [23] Floater MS, Hormann K. Surface Parameterization: a Tutorial and Survey. In: Dodgson N, Floater MS, Sabin M, editors. *Adv. Multiresolution Geom. Model.*, Springer-Verlag Berlin Heidelberg; 2005, p. 157–86.
- [24] Lewis WJ. *Tension Structures: Form and Behaviour*. Thomas Telford Publishing; 2003.
- [25] Lewis WJ. Modeling of fabric structures and associated design issues. *J Archit Eng* 2013;19:81–8.
- [26] Kim J-Y, Lee J-B. A new technique for optimum cutting pattern generation of membrane structures. *Eng Struct* 2002;24:745–56.
- [27] Ströbel D, Gründig L, Singer P. Selected Examples for the Optimization of Cutting Patterns for Textile Membranes. In: Bletzinger K-U, Kröplin B, Oñate E, editors. *VI Int. Conf. Text. Compos. Inflatable Struct. Struct. Membr.* 2013, Munich: International Center for Numerical Methods in Engineering; 2013, p. 258–67.

- [28] Gründig L, Moncrieff E, Singer P, Ströbel D. High-performance cutting pattern generation of architectural textile structures. In: Papadrakakis E, editor. IASS-IACM 2000 Fourth Int. Colloquium Comput. Shell Spat. Struct., Chania-Crete: 2000.
- [29] Pargana JB, Lloyd-Smith D, Izzuddin BA. Fully integrated design and analysis of Tensioned Fabric Structures: Finite elements and case studies. *Eng Struct* 2010;32:1054–68. doi:10.1016/j.engstruct.2009.12.032.
- [30] Punurai W, Tongpool W, Morales JH. Implementation of genetic algorithm for optimum cutting pattern generation of wrinkle free finishing membrane structures. *Finite Elem Anal Des* 2012;58:84–90. doi:10.1016/j.finel.2012.04.008.
- [31] Oden JT, Sato T. Finite strains and displacements of elastic membranes by the finite element method. *Int J Solids Struct* 1967;3:471–88.
- [32] Tayeb F, Lefevre B, Baverel O, Caron J, DU Peloux L. Design and realisation of composite gridshell structures. *J Int Assoc Shell Spat Struct* 2015;56:49–59.
- [33] Aono M, Breen DE, Wozny MJ. Fitting a woven-cloth model to a curved surface: mapping algorithms. *Comput Aided Des* 1994;26:278–92.
- [34] Aono M, Breen DE, Wozny MJ. Modeling methods for the design of 3D broadcloth composite parts. *Comput Aided Des* 2001;33:989–1007. doi:10.1016/S0010-4485(00)00135-4.
- [35] Bridgens B, Birchall M. Form and function: The significance of material properties in the design of tensile fabric structures. *Eng Struct* 2012;44:1–12. doi:10.1016/j.engstruct.2012.05.044.
- [36] Ashby MF, Jones DRH. *Engineering materials 1: an introduction to properties, applications and design*. 4th ed. Butterworth-Heinemann; 2011.

- [37] Bridgens BN, Gosling PD, Birchall MJS. Membrane material behaviour: concepts, practice and developments. *Struct Eng* 2004;82:28–33.
- [38] Chou PC, Pagano NJ. *Elasticity: Tensor, Dyadic, and Engineering Approaches*. Dover Publications, Inc.; 1992.
- [39] Tabarrok B, Qin Z. An Integrated Finite Element Procedure for Computer Modelling of Tension Structures. *Sci Iran* 1995;2:29–39.
- [40] Tabarrok B, Qin Z. Nonlinear analysis of tension structures. *Comput Struct* 1992;45:973–84.
- [41] Philipp B, Dieringer F, Wüchner R, Bletzinger K-U. Form-finding and structural analysis for the design of hybrid structures. *J Int Assoc Shell Spat Struct* 2015;56:17–24.
- [42] Belytschko T, Liu WK, Moran B. *Nonlinear Finite Elements for Continua and Structures*. John Wiley & Sons Ltd.; 2000.
- [43] Bonet J, Wood RD. *Nonlinear Continuum Mechanics for Finite Element Analysis*. 2nd ed. Cambridge University Press; 2008.
- [44] Gil AJ. Structural analysis of prestressed Saint Venant–Kirchhoff hyperelastic membranes subjected to moderate strains. *Comput Struct* 2006;84:1012–28. doi:10.1016/j.compstruc.2006.02.009.
- [45] Gil AJ. F.E.M. for Prestressed Saint Venant-Kirchhoff Hyperelastic Membranes. In: Oñate E, Kroplin B, editors. *Text. Compos. Inflatable Struct.*, Springer; 2005, p. 123–42. doi:10.1007/1-4020-3317-6_8.
- [46] Pargana JB, Lloyd-Smith D, Izzuddin BA. Advanced material model for coated fabrics used in tensioned fabric structures. *Eng Struct* 2007;29:1323–36.

doi:10.1016/j.engstruct.2006.09.001.

- [47] Kato S, Yoshino T, Minami H. Formulation of constitutive equations for fabric membranes based on the concept of fabric lattice model. *Eng Struct* 1999;21:691–708. doi:10.1016/S0141-0296(98)00024-8.
- [48] Wakefield DS. Engineering analysis of tension structures: theory and practice. *Eng Struct* 1999;21:680–90. doi:10.1016/S0141-0296(98)00023-6.
- [49] Breen DE, House DH, Getto PH. A physically-based particle model of woven cloth. *Vis Comput* 1992;8:264–77. doi:10.1007/BF01897114.
- [50] Eischen JW, Bigliani R. Continuum versus Particle Representations. In: House DH, Breen DE, editors. *Cloth Model. Animat.*, A. K. Peters Publishing; 2000, p. 79–122.
- [51] Dai X, Li Y, Zhang X. Simulating Anisotropic Woven Fabric Deformation with a New Particle Model. *Text Res J* 2003;73:1091–9. doi:10.1177/004051750307301211.
- [52] Etmuss O, Gross J, Strasser W. Deriving a Particle System from Continuum Mechanics for the Animation of Deformable Objects. *IEEE Trans Vis Comput Graph* 2003;9:538–50. doi:10.1109/TVCG.2003.1260747.
- [53] Breen DE, House DH, Wozny MJ. A Particle-Based Model for Simulating the Draping Behavior of Woven Cloth. *Text Res J* 1994;64:663–85. doi:10.1177/004051759406401106.
- [54] Provot X. Deformation Constraints in a Mass Spring Model to Describe Rigid Cloth Behavior. *Proc Graph Interface* 1995:147–54. doi:10.1.1.84.1732.
- [55] Zhou C, Jin X, Wang CCL. Shear buckling and dynamic bending in cloth simulation. *Comput Animat Virtual Worlds* 2008;19:493–503. doi:10.1002/cav.

- [56] Fan J, Wang Q, Chen S-F, Yuen MMF, Chan CC. A Spring-Mass Model-based Approach for Warping Cloth Patterns on 3D Objects. *J Vis Comput Animat* 1998;9:215–27.
- [57] Wang CCL, Tang K, Yeung BML. Freeform surface flattening based on fitting a woven mesh model. *Comput Des* 2005;37:799–814. doi:10.1016/j.cad.2004.09.009.
- [58] Ballhause D, König M, Kröplin B. Modelling Fabric-Reinforced Membranes with the Discrete Element Method. In: Oñate E, Kröplin B, editors. *Text. Compos. Inflatable Struct. II*, Springer; 2008, p. 51–67.
- [59] Van Gelder A. Approximate Simulation of Elastic Membranes by Triangulated Spring Meshes. *J Graph Tools* 1998;3:21–42. doi:10.1080/10867651.1998.10487490.
- [60] Kot M, Nagahashi H, Szymczak P. Elastic moduli of simple mass spring models. *Vis Comput* 2015;31:1339–50. doi:10.1007/s00371-014-1015-5.
- [61] Barnes MR. Form finding and Analysis of Tension Structures by Dynamic Relaxation. *Int J Sp Struct* 1999;14:89–104.
- [62] <http://www.rhino3d.com/>. Accessed 29/05/2014 n.d. <http://www.rhino3d.com/> (accessed May 29, 2014).
- [63] RhinoMembrane - Form-Finder plugin for RhinoCeros. <http://www.ixforten.com/rhinomembrane.htm>. Accessed: 29/05/2014 n.d. <http://www.ixforten.com/rhinomembrane.htm> (accessed May 29, 2014).
- [64] <http://math.stackexchange.com/questions/1236211/finding-a-point-a-certain-distance-away-from-2-points>. Accessed 22/04/2016 n.d. <http://math.stackexchange.com/questions/1236211/finding-a-point-a-certain-distance-away-from-2-points>.

- [65] Tayeb F, Baverel O, Caron J, DU Peloux L. Construction of gridshells composed of elastically bent elements and covered by a stretched three-dimensional membrane. In: Bletzinger K-U, Kröplin B, Oñate E, editors. VI Int. Conf. Text. Compos. Inflatable Struct. Struct. Membr. 2013, 2013, p. 27–38.
- [66] Bridgens B, Gosling P, Jou G-T, Hsu X-Y. Inter-laboratory comparison of biaxial tests for architectural textiles. *J Text Inst* 2012;103:706–18. doi:10.1080/00405000.2011.602824.